CHAPTER 25 ■ CORONARY ARTERY ANOMALIES AND DISEASE

SETH KLIGERMAN

Noninvasive imaging of the coronary arteries can be obtained through various modalities including ultrasound (echocardiography), CT, and MRI. While echocardiography is a useful tool to rapidly assess systolic and diastolic myocardial function and complications of myocardial infarct, its ability to directly assess the coronary arteries is limited. Due to its excellent spatial resolution as low as 0.5 mm and temporal resolution as low as 66 ms, cardiac CTA has become the primary tool to directly visualize the anatomy as well as congenital and acquired anomalies of the coronary arteries. While cardiac MRI can be used to assess the coronary arteries, its strength lies in its ability to assess for myocardial damage after infarction and to guide therapy.

CORONARY ARTERY ANATOMY

The coronary arteries course through the epicardial fat to supply oxygenated blood to the myocardium. Coronary artery anatomy is highly variable, and the size and distribution of the coronary arteries vary from person to person. Given this, it is important to distinguish normal variant anatomy from congenital abnormalities. It is also imperative to distinguish between benign congenital anomalies and ones that can compromise myocardial blood flow with subsequent myocardial ischemia, infarction, or sudden cardiac death.

Left Main Coronary Artery

The coronary arteries arise from the sinuses of Valsalva, which are three anatomic outpouchings in the ascending aorta. The left main coronary artery and right coronary artery (RCA) arise from the left and right sinuses, respectively (Fig. 25.1). No coronary artery should arise from the noncoronary sinus, which is directed posteriorly toward the interatrial septum.

After its origin from the left sinus of Valsalva, the left main coronary artery courses laterally to the left before dividing. It is usually the largest coronary artery but is of variable length. In most people, the left main coronary artery bifurcates into an anteriorly directed left anterior descending coronary artery (LAD) and a posteriorly directed left circumflex coronary artery (LCx) (Fig. 25.2). In approximately 20% to 30% of patients, the left main coronary artery trifurcates with a ramus intermedius branch arising between the LAD and LCx (Fig. 25.3).

Left Anterior Descending Coronary Artery

The LAD is usually a large vessel that runs along the anterior surface of the left ventricle (LV) (Fig. 25.4). The LAD can be of variable length but usually wraps around the left ventricular apex before terminating. The LAD is divided into three portions, proximal, mid, and distal (Fig. 25.5). The proximal

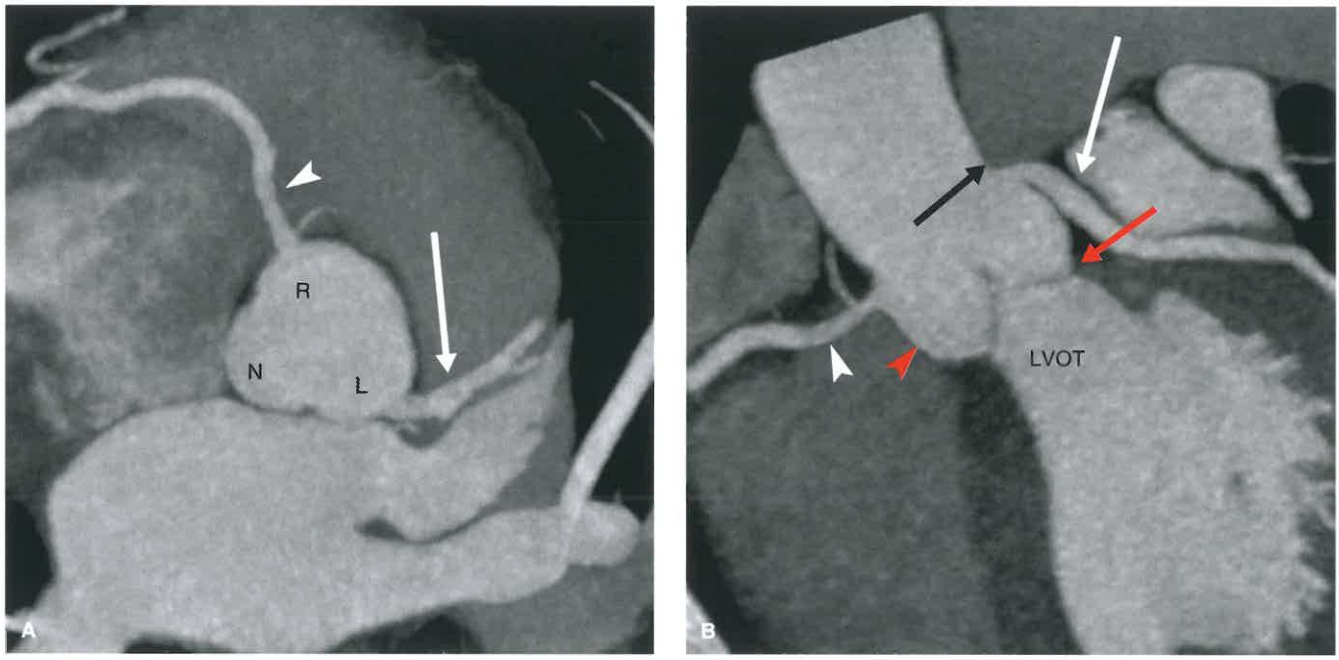

FIGURE 25.1. **Normal Coronary Ostial Anatomy. A:** A 7-mm thick MIP image transverse to the aortic sinus from a coronary CTA shows the left (*L*), right (*R*), and noncoronary (*N*) sinuses. The left main coronary artery (*white arrow*) and right coronary artery (*white arrowhead*) arise normally from the left and right coronary sinuses, respectively. **B:** Coronal oblique 5-mm thick MIP image through the left ventricular outflow tract (*LVOT*) shows that the ostia for the left main (*white arrow*) and right (*white arrowhead*) coronary arteries originate from the aortic root between the level of the sinuses of Valsalva (*red arrowhead*) and sinotubular junction (*black arrow*). The aortic valve leaflets attach at the annulus (*red arrow*) which separates the LVOT from the aortic root.

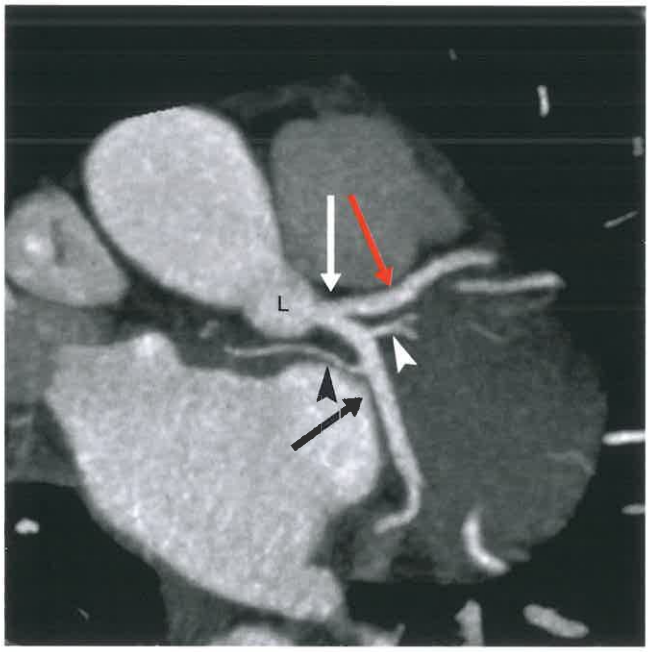

FIGURE 25.2. **Normal Anatomy of the Left Main Coronary Artery.** Double oblique multiplanar reformat shows the left main coronary artery (*white arrow*) arises from the left sinus of Valsalva (*L*). In this patient, the left main is only 4 mm long before bifurcating into left anterior descending (LAD, *red arrow*) and left circumflex (LCx) coronary arteries (*black arrow*). The sinoatrial (SA) nodal branch artery arises from the left circumflex (*black arrowhead*) which occurs in about one-third of patients. An early first obtuse marginal branch is also seen (*white arrowhead*). The left main coronary artery can vary in length from a few millimeters to a few centimeters.

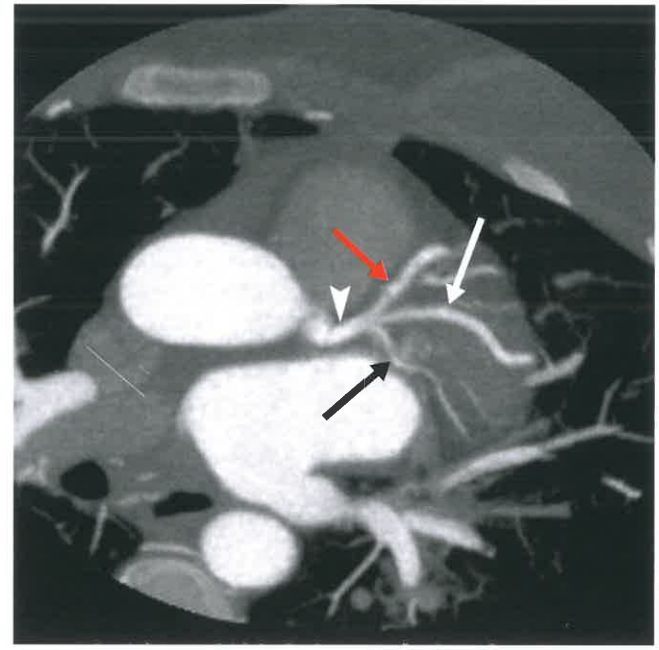

FIGURE 25.3. **Ramus Intermedius.** Axial oblique 4-mm thick MIP image through the left main coronary artery (*white arrowhead*) shows that the vessel trifurcates into the left anterior descending (*red arrow*), left circumflex (*black arrow*), and ramus intermedius branches (*white arrow*). A ramus intermedius is present in 20–30% of the population and may be a diminutive vessel, or as in this case, a large caliber vessel.

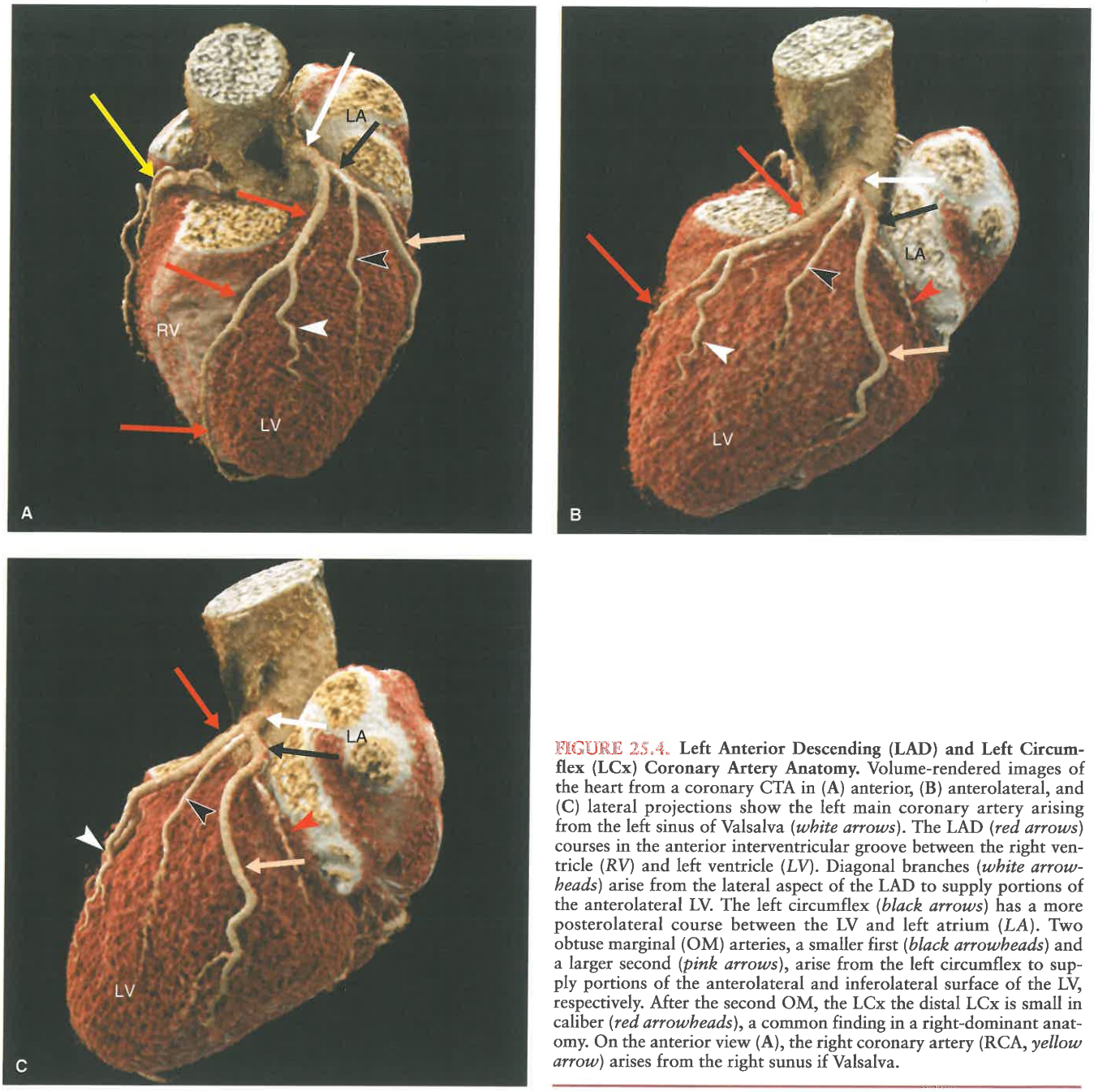

FIGURE 25.4. **Left Anterior Descending (LAD) and Left Circumflex (LCx) Coronary Artery Anatomy.** Volume-rendered images of the heart from a coronary CTA in (**A**) anterior, (**B**) anterolateral, and (**C**) lateral projections show the left main coronary artery arising from the left sinus of Valsalva (*white arrows*). The LAD (*red arrows*) courses in the anterior interventricular groove between the right ventricle (*RV*) and left ventricle (*LV*). Diagonal branches (*white arrowheads*) arise from the lateral aspect of the LAD to supply portions of the anterolateral LV. The left circumflex (*black arrows*) has a more posterolateral course between the LV and left atrium (*LA*). Two obtuse marginal (OM) arteries, a smaller first (*black arrowheads*) and a larger second (*pink arrows*), arise from the left circumflex to supply portions of the anterolateral and inferolateral surface of the LV, respectively. After the second OM, the LCx the distal LCx is small in caliber (*red arrowheads*), a common finding in a right-dominant anatomy. On the anterior view (**A**), the right coronary artery (RCA, *yellow arrow*) arises from the right sunus if Valsalva.

LAD extends from its origin to the ostium of the first large septal branch or diagonal branch, whichever arises first. The mid-LAD extends from end of the proximal LAD to one-half the distance to the LV apex, and the distal LAD is defined as the end of the mid-LAD to its termination.

The LAD gives rise to both septal branches and diagonal branches (Figs. 25.4 and 25.6). While smaller than the LAD itself, the diagonal and septal branches are needed to supply oxygenated blood to the anterolateral and anteroseptal LV myocardium, respectively. Numerous small septal branches arise from the inferomedial aspect of the LAD and dive into the anterior portion of the interventricular septum. The diagonal branches arise from the lateral aspect of the LAD and course over the anterolateral aspect of the LV. Although the number varies, most patients have between two and four diagonals.

Left Circumflex Coronary Artery

At the bifurcations of the left main, the LCx courses posterolaterally between the LV and left atrium (Fig. 25.2). The LCx gives rise to obtuse marginal (OM) vessels that supply oxygenated blood to the inferolateral aspect of the LV (Fig. 25.4). Blood supply to the anterolateral aspect of the LV at the base and mid-cavity level can occur via the OM or diagonal vessels, depending on the patient's anatomy. The size and number of OM branches vary, but most patients have at least two visible OM vessels. Once the LCx reaches the inferolateral aspect of the left atrioventricular (AV) groove and begins to wrap around the inferior aspect of the LV, it is usually a diminutive vessel since most people are right dominant. However, in patients who have left or codominant circulation (representing approximately 10%

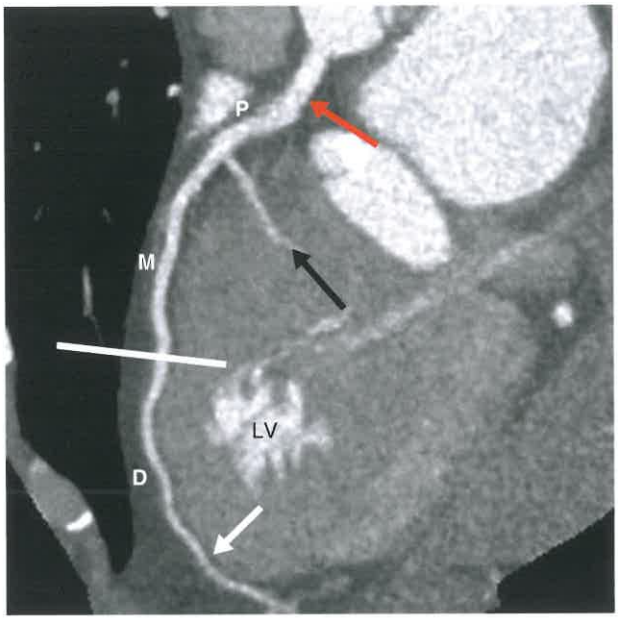

FIGURE 25.5. **Left Anterior Descending (LAD) Coronary Artery Segmentation.** Curved MPR of LAD (*red arrow*) shows the vessel coursing over the anterior wall of the left ventricle (*LV*). The proximal LAD extends from the origin of the LAD to the ostium of the first large septal (*black arrow*) or diagonal vessel, whichever arises first. To divide the mid and distal LAD, a line is drawn at the mid-way point (*white line*) between the end of the proximal LAD (*white arrow*) and LV apex (*white arrow*). The mid-LAD (*M*) extends from the end of the proximal LAD (*P*) to this line and the distal LAD (*D*) is defined as the end of the mid-LAD to the termination of the LAD. The LCx is not visualized in this plane.

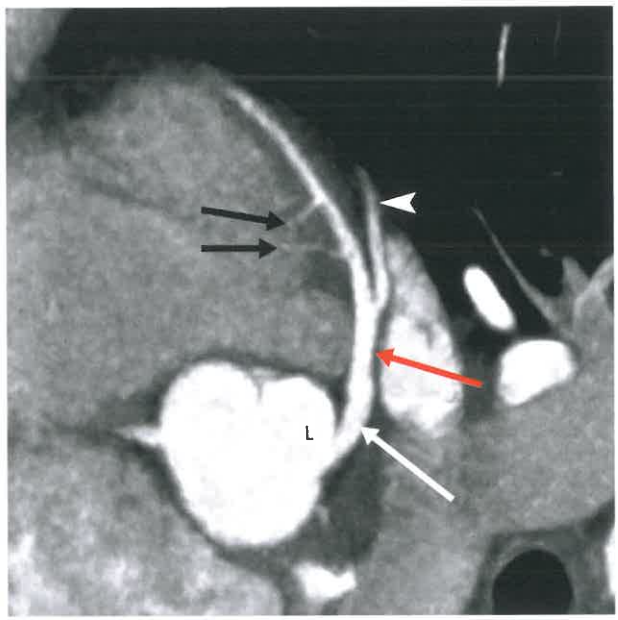

FIGURE 25.6. **Septal and Diagonal Branches of the Left Anterior Descending (LAD) Coronary Artery.** Double oblique 3-mm thick MIP image shows the left main coronary artery (*white arrow*) arising from the left sinus of Valsalva (*L*). The left main bifurcates into the LAD (*red arrow*) and LCx (not seen). The branches of the LAD that extend laterally to supply portions of the anterolateral wall of the left ventricle are called diagonal branches (*white arrowhead*). The septal branches (*black arrows*) are more numerous but small in size. They supply the anteroseptal portion of the left ventricle.

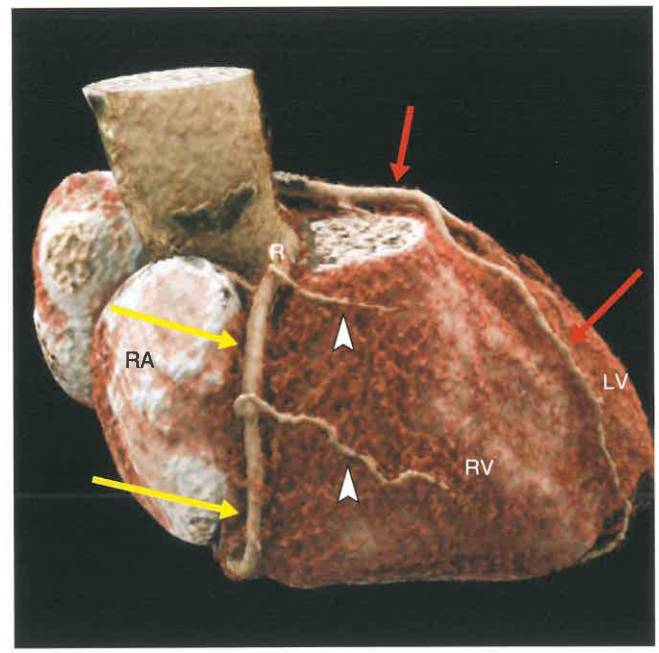

FIGURE 25.7. **Right Coronary Artery Anatomy.** Right lateral volume-rendered image from a coronary CTA shows the right coronary artery (RCA, *yellow arrows*) arising from the right sinus of Valsalva (*R*). The RCA courses in the right atrioventricular groove between the right atrium (*RA*) and right ventricle (*RV*). Acute marginal branches (*white arrowheads*) arise anteriorly and supply to the anterior free wall of the RV. The LAD (*red arrows*) can be seen coursing over the anterior wall of the left ventricle (*LV*).

and 20% of the population, respectively), the distal LCx will be larger in size (Fig. 25.7).

Ramus Intermedius

In approximately 20% to 30% of patients, the left main coronary artery will trifurcate into the LAD, LCx, and a middle branch called the ramus intermedius or intermediate branch (Fig. 25.3). This branch can vary in size and distribution; in some patients, it courses anterolaterally in a distribution similar to a diagonal branch, while in other cases it courses more posteriorly in a distribution similar to an OM branch.

Right Coronary Artery

The RCA arises from the anterior-facing right sinus of Valsalva (Figs. 25.1 and 25.7). Since approximately 70% of patients are right dominant, the RCA is a large vessel that courses anteriorly in the right AV groove and gives rise to the posterior descending artery (PDA) and posterior left ventricular (PLV) branches (Figs. 25.7 and 25.8). The RCA is divided into three territories (Fig. 25.9). The proximal RCA is defined as the ostium of the RCA to one-half the distance to the acute margin of the heart. The mid-RCA is defined as the end of the proximal RCA to the acute margin of the heart, and the distal RCA is defined as the end of the mid-RCA to the origin of the PDA.

As the RCA courses in the right AV groove, acute marginal branches arise from the RCA and course anteriorly and extend to the anterior surface of the right ventricle (Fig. 25.7). In right-dominant patients, the distal RCA will divide into two branches along the undersurface of the heart, the PDA and PLV (Fig. 25.8).

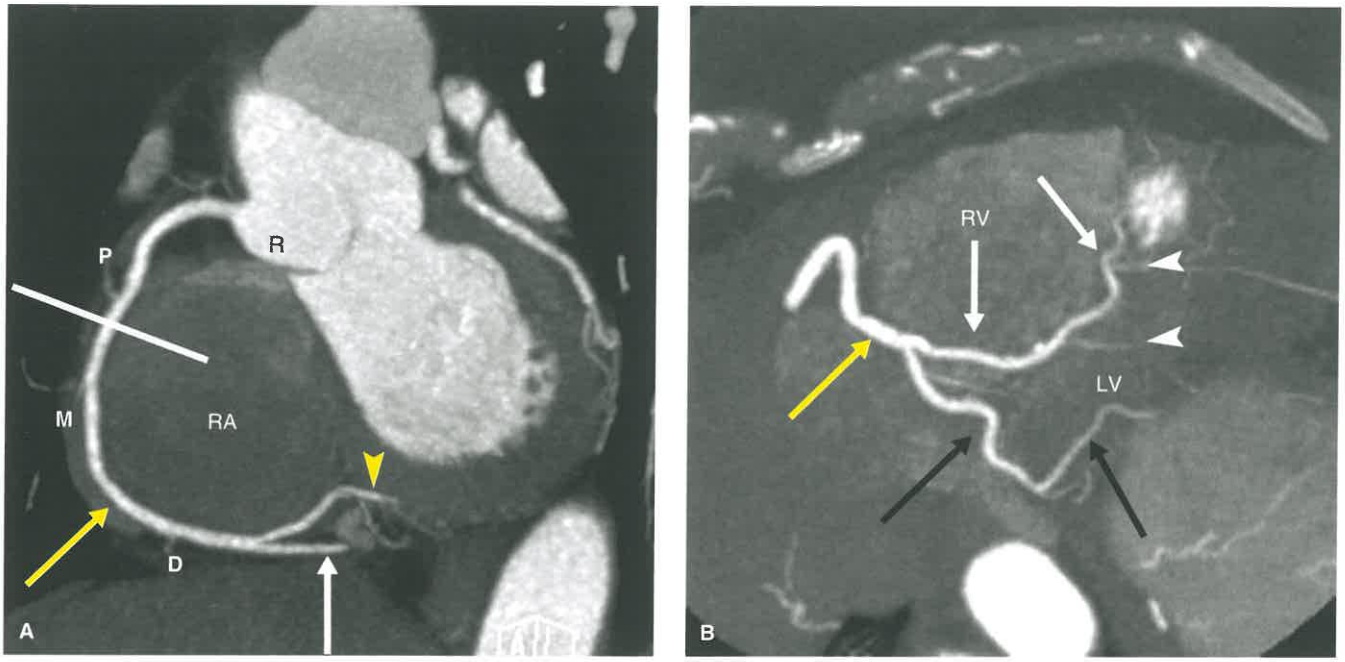

FIGURE 25.8. **Right Coronary Artery (RCA) Anatomy. A:** "C-view" of RCA as it courses in the right atrioventricular groove between the right atrium (*RA*) and right ventricle (not visualized in this plane) shows its division into three territories. The proximal RCA (*P*) is defined as the ostium from the right sinus (*R*) to one-half the distance (*white line*) to the acute margin, or angle, of the heart (*yellow arrow*). The mid-RCA (*M*) is defined as the end of the proximal RCA to the acute margin of the heart. The distal RCA (*D*) is defined as the end of the mid-RCA to the origin of the posterior descending artery (PDA, *white arrow*). The posterior left ventricular branch (PLV, *yellow arrowhead*) courses over the PDA. **B:** Distal RCA anatomy (*yellow arrow*) is often best seen on an inferior view of the heart. The distal RCA divides into the PDA (*white arrows*) and the PLV (*black arrows*). The PDA courses in the inferior interventricular groove between the inferior surface of the left ventricle (*LV*) and right ventricle (*RV*) and gives rise to small septal branches that supply the inferoseptal segments (*white arrowheads*). The PLV (*black arrow*) supplies the inferior and inferolateral portions of the left ventricular base. The size and extent of the PDA and PLV greatly vary depending on dominance and size of the LAD and LCx, both of which were relatively small in this patient. This patient is right heart dominant with a single PDA arising from the RCA, as seen in 70% of the population.

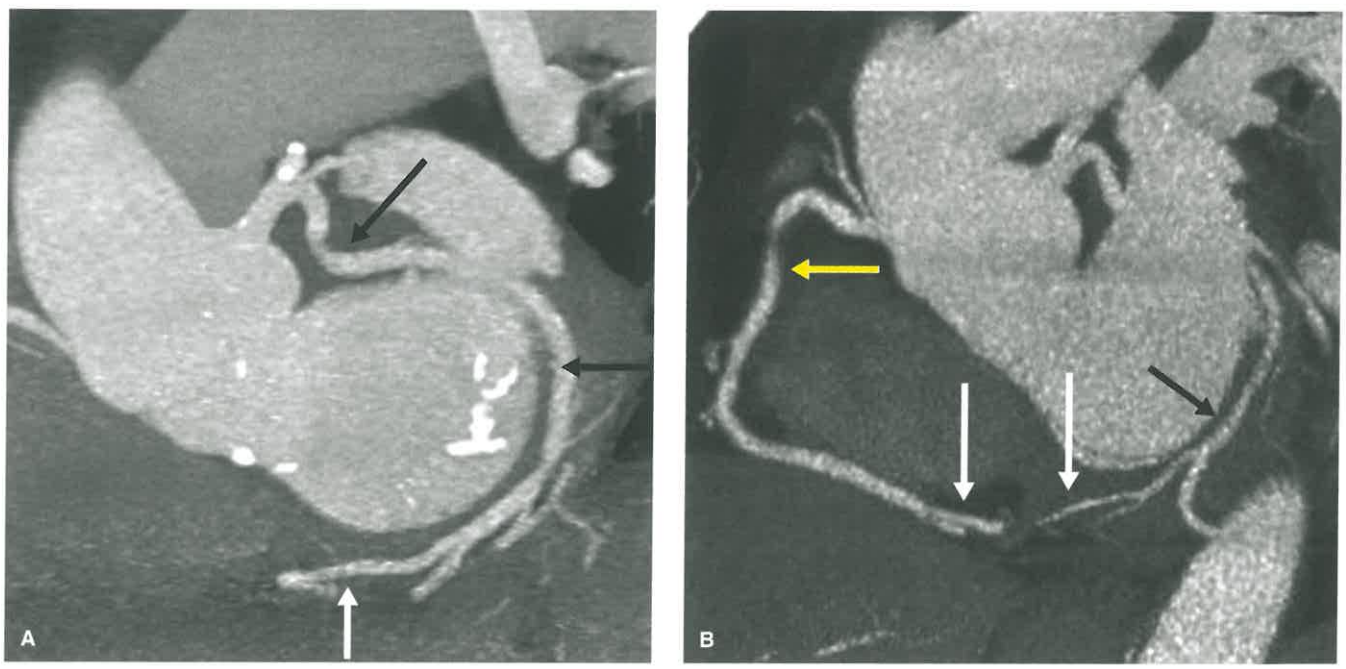

FIGURE 25.9. **Left Dominance and Codominance. A:** Coronal oblique MIP image shows a large LCx (*black arrows*) giving rise to the PDA (*white arrow*) denoting a left-dominant system. The RCA, which is not visualized, was small in size. **B:** Coronal oblique MIP in another patient shows two PDAs (*white arrows*), one arising from the RCA (*yellow arrow*) and the other arising from the LCx (*black arrow*) consistent with a codominant system.

Posterior Descending Artery

In the majority of patients, the PDA arises from the RCA and thus they are considered right dominant (Fig. 25.8). In approximately 10% of patients, the PDA arises from the left circumflex, and the patient is considered left dominant (Fig. 25.9A). In the remainder of patients, both the RCA and LCx give rise to a PDA branch, and these patients are often considered balanced or codominant (Fig. 25.9B).

Whichever vessel gives rise to the PDA, the vessel courses in the posterior interventricular sulcus to supply the inferior wall of the LV (Fig. 25.8). Like the LAD, the PDA gives rise to septal branches that supply the inferolateral aspect of the left ventricular septum. The PDA is of variable size and length. In patients with a smaller LAD, the PDA tends to be a larger artery and vice versa (Fig. 25.8).

Posterior Left Ventricular Branch

Arising from the distal RCA, the posterior left ventricular branch (PLV), also called the PLB, course laterally and extends along the posterior AV groove between the inferior aspect of the left atrium and LV (Fig. 25.8). It is of variable size and length. Depending on the patient's anatomy, in right-dominant patients either the PLV or LCx can supply the inferolateral wall at the base of the heart.

Conus Branch

The conus branch is usually the first branch of the RCA, although it can have a separate origin from the right coronary sinus in 17% to 50% of patients (Fig. 25.10). The conus branch extends anteriorly to supply blood to the right ventricular outflow tract (RVOT) or conus. In some instances, the conus acts as a collateral pathway for blood flow to the LAD, and this circuit is often referred to as the arterial circle of Vieussens.

Sinoatrial Nodal Branch

The sinoatrial (SA) nodal branch is a small vessel that most often originates from the RCA (Fig. 25.14) but arises from the LCx in about one-third of patients (Fig. 25.2). Less commonly, the SA branch can arise from the left main coronary artery, directly from the aorta (Fig. 25.11), or there may be two SA arteries supplied by both the LCx and RCA. Depending on its origin, the SA nodal branch courses posteriorly (RCA origin) or medially (LCx origin) and terminates in the region of the SA node located along the posterior aspect of where the superior vena cava enters the right atrium. It is important not to mistake this normal vessel for an anomalous coronary artery.

Atrioventricular Nodal Branch

In most patients, the AV nodal branch arises from the very distal "U-shaped" aspect of the distal RCA as it courses superior to the PDA. It is a small vessel that courses superiorly toward the posterior annulus of the mitral valve (Fig. 25.12).

CORONARY ARTERY ANOMALIES

Occurring in between 0.5% and 1.5% of the population, coronary artery anomalies are frequently encountered on cardiac CT. While many of these anomalies have little clinical

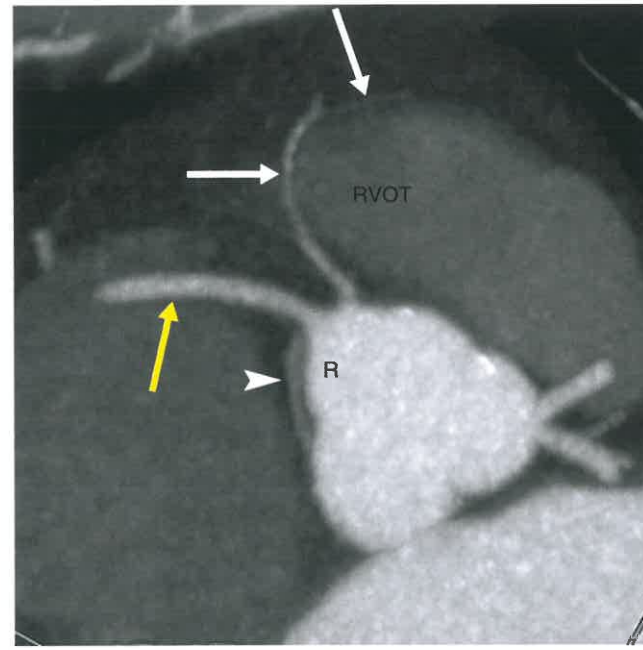

FIGURE 25.10. **Anatomy of the Conus Artery.** Axial oblique MIP image shows the RCA (*yellow arrow*) arising from the right sinus of Valsalva (*R*). The conus branch (*white arrows*) usually is the first vessel to arise from the very proximal RCA; however, in this case, it arises directly from the right aortic sinus which is a common benign anatomic variant. The conus courses superiorly and anteriorly to supply the right ventricular outflow tract (*RVOT*) and is an important pathway for collateralization. The sinoatrial nodal branch (*white arrowhead*) arises from the proximal RCA and is partially visualized as it courses posteriorly.

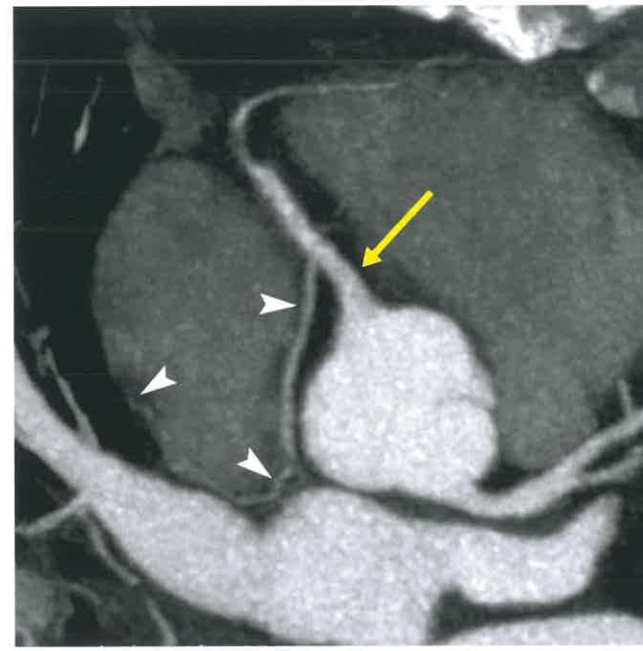

FIGURE 25.11. **Sinoatrial (SA) Nodal Branch Anatomy.** Curved multiplanar reformat image shows the SA branch (*white arrowheads*) arising from the proximal RCA (*yellow arrow*) and coursing posteriorly to end between left atrium (LA) and superior portion of the right atrium. The SA branch most commonly arises from the RCA but can originate from the LCx (Fig. 25.2). In rare instances, both the RCA and LCx give rise to separate SA nodal branches.

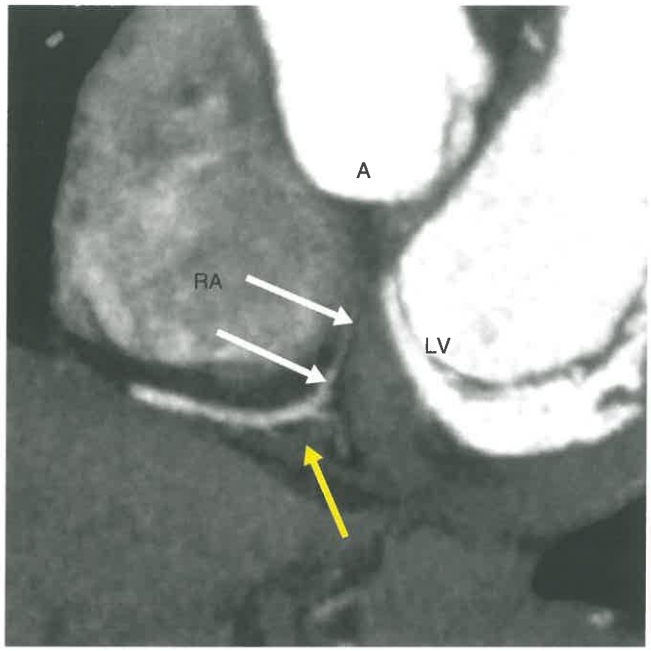

FIGURE 25.12. **Atrioventricular (AV) Nodal Branch Anatomy.** Coronal oblique MPR image shows the AV nodal branch (*white arrows*) arising from the distal right coronary artery *(yellow arrow)*. The AV nodal branch extends superiorly between the right atrium (*RA*) and left ventricle (*LV*) toward the aortic root (*A*).

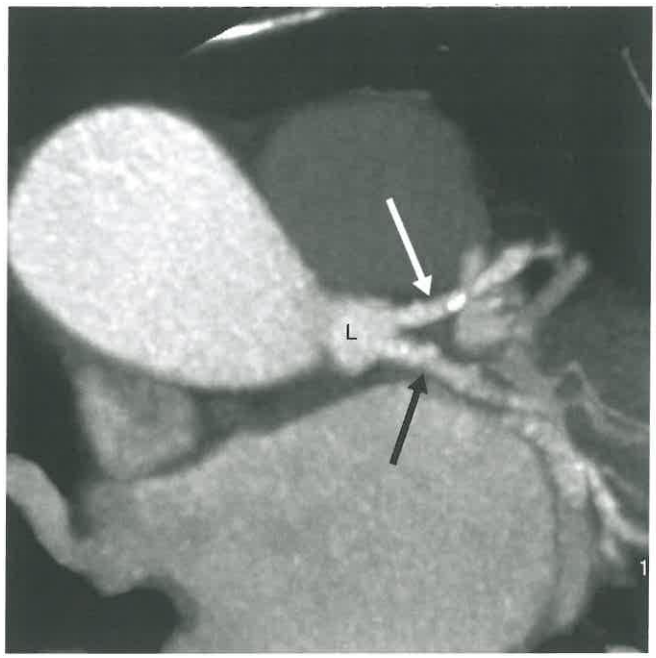

FIGURE 25.13. **Absent Left Main Coronary Artery.** Axial oblique image from a coronary CTA shows complete absence of the left main coronary artery. The left anterior descending (*white arrow*) and left circumflex (*black arrow*) coronary arteries arise directly from the left sinus of Valsalva (*L*). This is a rare but benign congenital variant.

significance, anomalous coronary anatomy can lead to sudden cardiac death. Some of these anomalies can lead to symptoms and thus be the reason for the study; however, they are often clinically silent and are frequently an incidental finding. It is also important to remember that although anomalous coronary anatomy is best visualized with electrocardiography (ECG)-gated CT angiography, the improved temporal resolution of modern scanners often allows for a basic assessment of coronary artery origins and course on nongated thoracic CT scans.

There are many ways to subdivide these anomalies. One of the more commonly used methods is to divide them based on anomalous origin, course, and termination. No matter how one chooses to classify these anomalies, it is important to recognize that even though many of the anomalies are benign, others can lead to a reduction in coronary blood flow and major adverse cardiac events (MACEs).

ABNORMALITIES IN ORIGIN

There are numerous congenital coronary artery anomalies associated with an anomalous origin. While it may be an isolated finding, in some instances, such as in patients with a single coronary artery, multiple anomalies or origin and course may coexist. These anomalies include absence of the left main coronary artery, anomalous location of the coronary ostium outside the aortic root, and anomalous origin of the coronary ostium from the incorrect sinus.

Abnormalities in Origin, Benign

Absence of the Left Main Coronary Artery. Absence of the left main coronary artery is a benign variant that occurs in approximately 0.4% to 2% of the population. In this situation, the LAD and LCx have independent origins from the left sinus of Valsalva (Fig. 25.13).

Anomalous Origin of the Coronary Arteries Outside of the Aortic Root. In certain instances, the coronary arteries may arise from a location outside of the sinuses. While some of these anomalies may be potentially malignant, as discussed later, many are benign. A high origin of a coronary artery occurs when its ostium is located 1 cm or greater above the sinotubular junction. This most commonly affects the RCA (Fig. 25.14). Although this origin is benign, its location could lead to accidental injury during surgical manipulation of the ascending aorta.

Retroaortic. In a retroaortic course, the anomalous coronary artery arises from the opposite sinus and courses posteriorly between the aorta and left atrium. This most commonly occurs when the LCx or left main coronary artery arises from the right sinus of Valsalva, either directly from the aorta or from the proximal RCA (Fig. 25.15A). In rare instances, the RCA can arise from the left sinus with a retroaortic course (Fig. 25.15B). While these are benign anomalies, they can be inadvertently injured during aortic valve or annular surgery.

Anterior to Pulmonary Outflow Tract (Prepulmonic or Precardiac). A prepulmonic course occurs when an anomalous coronary artery courses anterior to the RVOT (Fig. 25.16). Most commonly, this abnormality involves the LAD or left main coronary artery. This prepulmonic vessel often arises directly from the proximal RCA in the setting of a single coronary artery (Fig. 25.17). If the LAD has a prepulmonic course, the LCx may have a retroaortic course or can arise directly from the left sinus. In addition, the anomaly may be accompanied by a small anomalous septal branch arising from the right cusp to supply the basilar septum. Less commonly, the RCA may have a prepulmonic course, usually in the setting of a single left coronary artery.

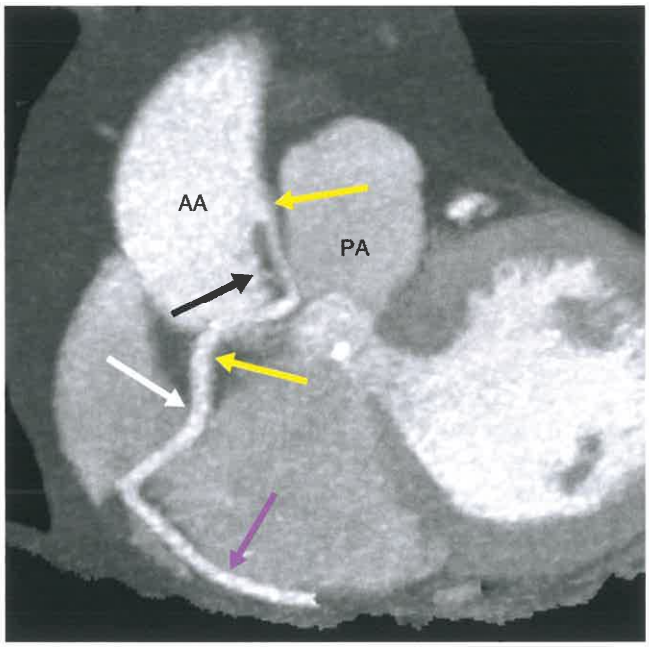

FIGURE 25.14. **High Origin of the Right Coronary Artery (RCA).** Sagittal oblique MIP image shows the RCA (*yellow arrows*) arising from the ascending aorta (*AA*) and coursing inferiorly between the aorta and pulmonary artery (*PA*) before entering the AV groove (*white arrow*). A high origin, which is a benign anomaly, occurs when a coronary artery ostium is located greater than 1 cm above the sinotubular junction (*black arrow*). This most commonly affects the RCA.

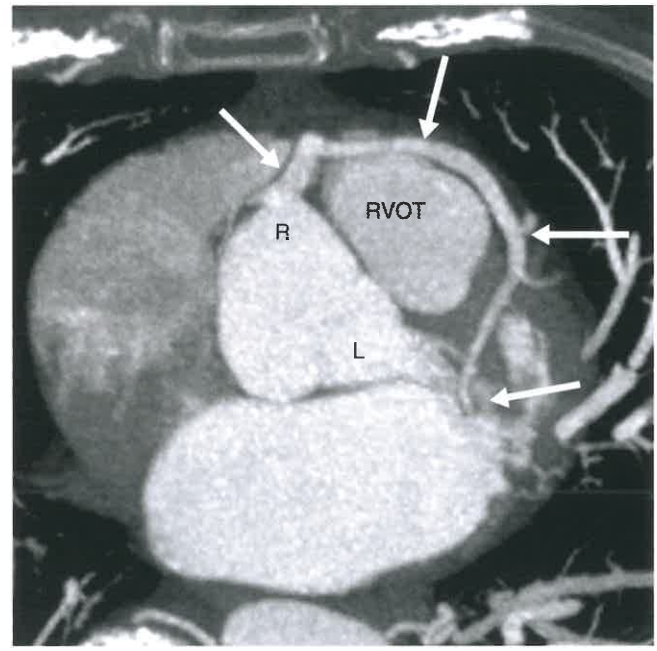

FIGURE 25.16. **Prepulmonic Course.** Axial oblique image from a coronary CTA shows that the left main coronary artery (*white arrows*) arises from the right sinus of Valsalva (*R*) and courses anteriorly around the right ventricular outflow tract (*RVOT*), consistent with a prepulmonic or precardiac course. No coronary artery arises from the left sinus of Valsalva (*L*). This is a benign anomaly.

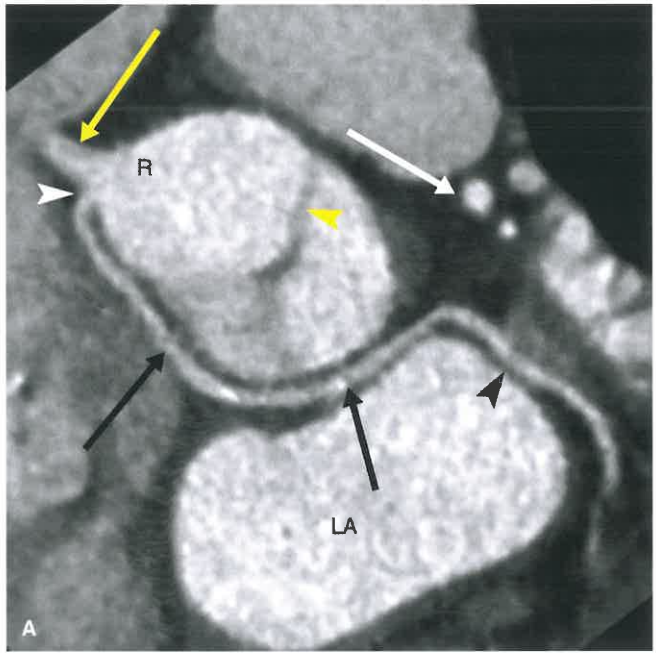

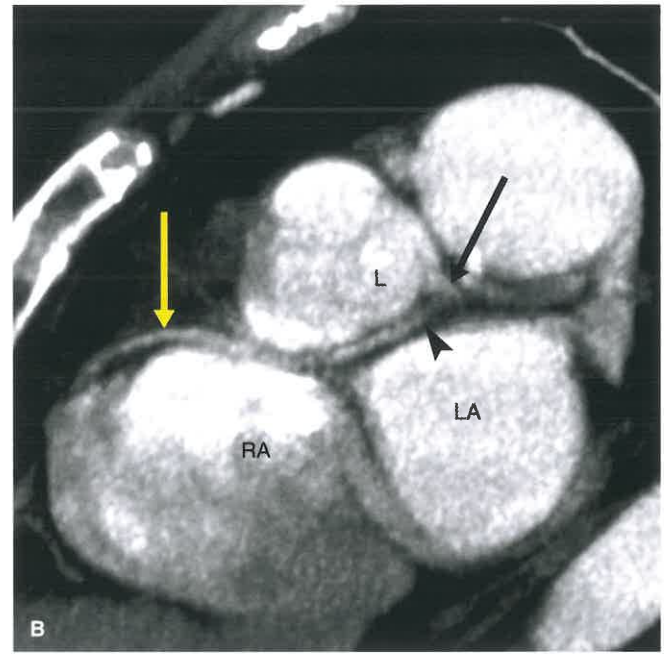

FIGURE 25.15. **Retroaortic Course. A:** Axial oblique image through the aortic root from a coronary CTA in a 47-year-old man shows that the origin of the LCx (*white arrowhead*) is from the right coronary sinus (*R*). The LCx then courses posteriorly (*black arrows*) between the aortic root and left atrium (*LA*) before entering its normal territory (*black arrowheads*). The LCx has a separate ostium from the RCA (*yellow arrow*). The LAD (*white arrow*) originated from the left coronary sinus. Incidental note is made of a bicuspid aortic valve (*yellow arrowhead*). **B:** Sagittal oblique image from a coronary CTA in a 9-year-old child shows ostium of the RCA (*black arrow*) arising from the left sinus (*L*) and coursing posteriorly between the left atrium and aortic root (*black arrowhead*) before entering the right atrioventricular groove (*yellow arrow*). While the LCx anomaly is not uncommon, a retroaortic course of the RCA is extremely rare. Both are benign courses.

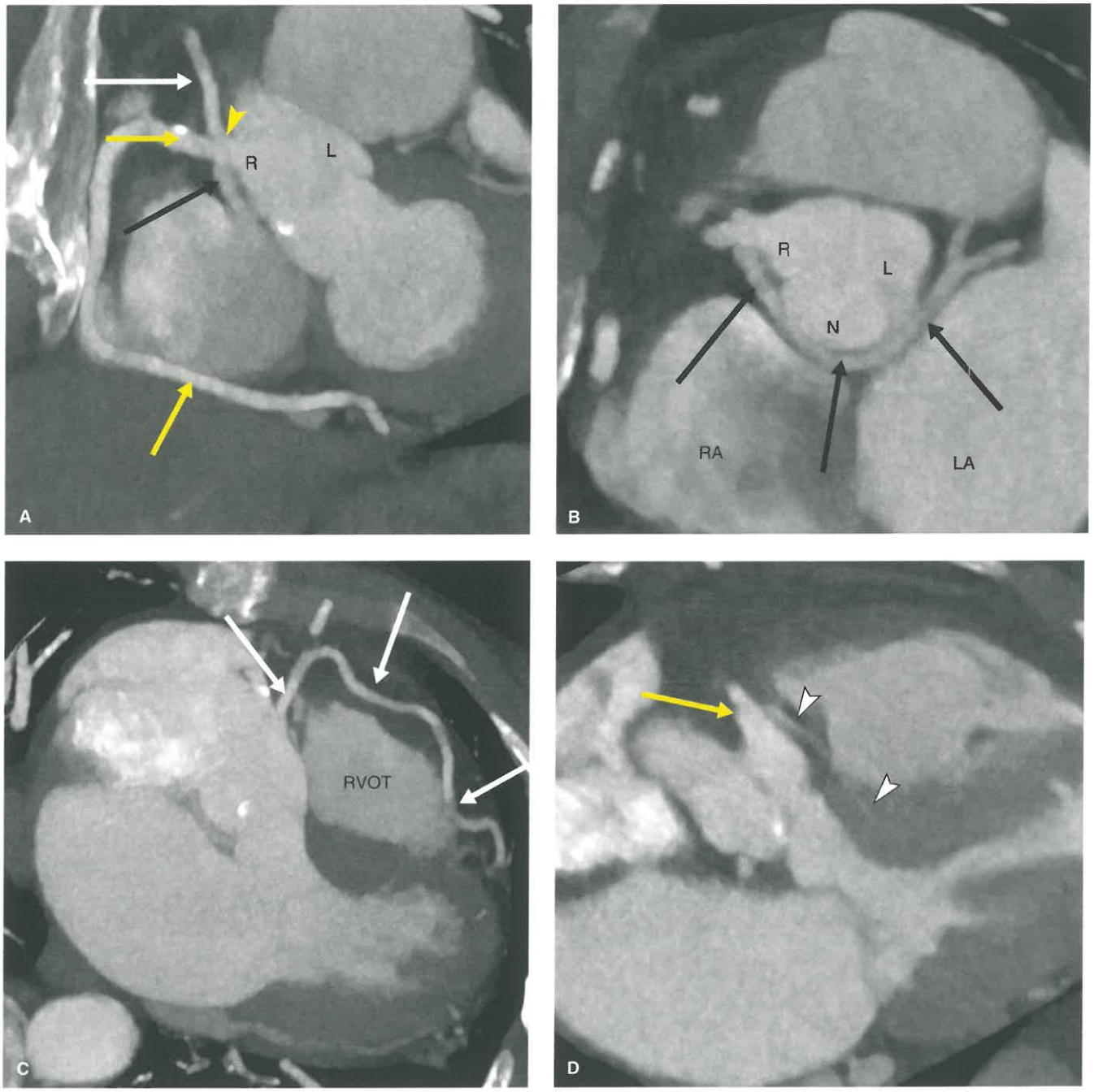

FIGURE 25.17. **Incidental Discovery of a Single Right Coronary Artery in a 54-Year-Old Woman With Atypical Chest Pain. A:** C-view of the RCA shows a single right coronary artery (*yellow arrowhead*) arising from the right sinus (*R*) and trifurcating into the RCA (*yellow arrows*), with large branches extending both superiorly (*white arrow*) and inferiorly (*black arrow*). Except for mild atherosclerotic disease, the RCA is otherwise normal. No coronary artery arises from the left sinus (*L*). **B:** Coronal oblique MIP shows that the inferiorly directed artery in **A** (*black arrow*) represents a retroaortic LCx (*black arrows*) coursing posteriorly between the right atrium (*RA*), left atrium (*LA*), and noncoronary sinus (*N*). **C:** Axial oblique MIP image shows that the superiorly directed artery in A (*white arrow*) is a prepulmonic LAD (*white arrows*) which courses around the right ventricular outflow tract (*RVOT*). **D:** In addition to these three larger vessels, axial oblique MIP shows a very small anomalous septal branch (*white arrowheads*) originating from the proximal RCA (*yellow arrow*) to supply basilar septum. In this instance of a single coronary artery, all of the anomalous courses are benign. However, there are numerous configurations of single coronary arteries which can have both benign and potentially malignant configurations.

Septal (Intramyocardial) Course. A septal course usually involves the LAD arising from the right coronary sinus (Figs. 25.17D and 25.18). It is important to recognize the inferomedial course of the vessel that dives into the proximal aspect of the left ventricular septum as this distinguishes this benign course from the potentially malignant interarterial course discussed below. Although it can rarely be associated with myocardial ischemia, in most instances it is benign.

Noncoronary Sinus. Origin from the noncoronary sinus is an extremely rare anomaly. This can occur with the RCA or left

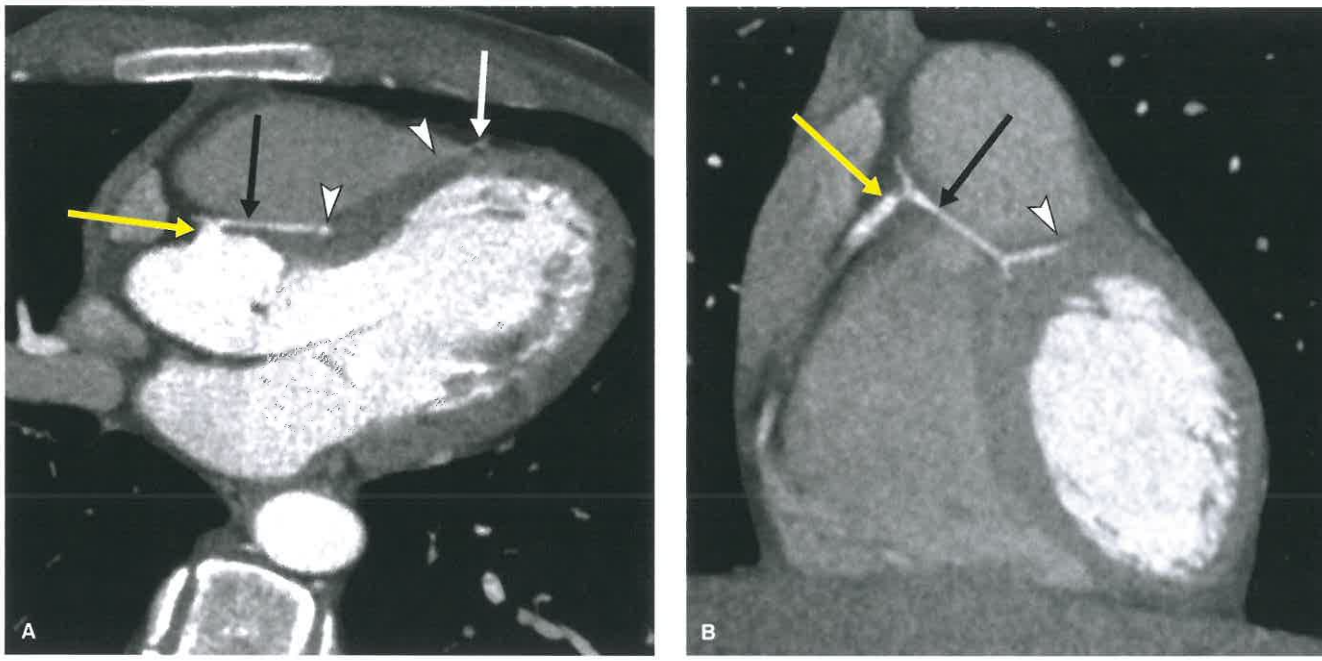

FIGURE 25.18. **Septal Course of the Left Anterior Descending Coronary Artery (LAD). A:** Axial oblique and **(B)** coronal oblique images from a coronary CTA show the LAD arising from the proximal RCA (*yellow arrows*) and coursing inferiorly and medially (*black arrows*) before diving into the interventricular septum (*white arrowheads*). The proximal and mid LAD (*white arrowheads*) run in the wall of the left ventricle consistent with a long-segment myocardial bridge. The distal LAD (*white arrow*) reenters its normal location in the epicardial fat. This benign course needs to be delineated from the potentially malignant interarterial course where the coronary artery crosses directly between the main pulmonary artery and aorta and does not have the inferiorly directed course as seen in this case.

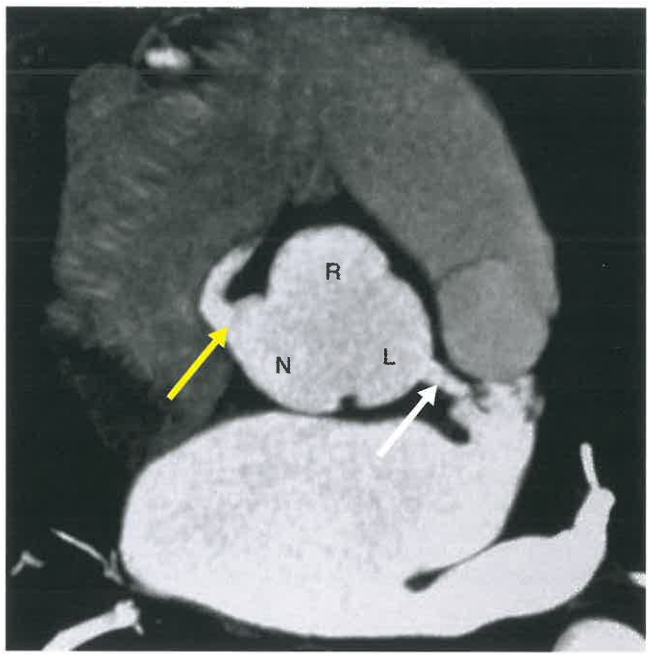

FIGURE 25.19. Maximum-intensity projection image through the sinuses of Valsalva in a 43-year-old woman with atypical chest pain shows the RCA (*yellow arrow*) arising from the noncoronary sinus (*N*). The left main (*white arrow*) arises from the left sinus (*L*). No coronary artery arises from the right sinus (*R*). A coronary artery arising from the noncoronary sinus is an extremely rare anomaly. (Courtesy of Jacobo Kirsch, MD.)

main coronary artery (Fig. 25.19). Although there is little information on this anomaly given its rarity, it is often considered a benign anomaly.

Abnormalities in Origin, Possibly Malignant

Interarterial Course. With an interarterial course, a coronary artery arises from the opposite sinus and courses medially between the aorta and pulmonary artery. This can involve the RCA (Fig. 25.20), left main (Fig. 25.21), or LAD. Unlike the retroaortic or septal course, an interarterial course, especially when involving the left main or LAD, can lead to myocardial ischemia, infarction, and sudden cardiac death. The cause of this is believed to be multifactorial. When the artery courses medially, it can experience extrinsic compression between the aorta and pulmonary artery. Compression can worsen during exercise due to physiologic dilation of the aorta and pulmonary artery at a time when myocardial oxygen demand increases. Proximal compression can also occur as the vessel passes through the aortic wall, which is termed an *intramural course*. The intramural course can be of various lengths and is often identified on imaging by soft tissue attenuation surrounding the proximal coronary artery. As it courses through the wall of the aorta, the narrowed vessel has an ovoid shape with an increased height/width ratio (Figs. 25.20 and 25.21). In addition, the coronary artery ostium is often dysplastic and "slit like," further reducing blood flow into the vessel. Lastly, the proximal vessel can have a tangential course with an acute angulation that leads to a further reduction in blood flow.

An interarterial course of the RCA is more common than those involving the left system. In patients with an interarterial RCA, a higher incidence of symptoms and adverse cardiac events has been reported in those with a more superior course

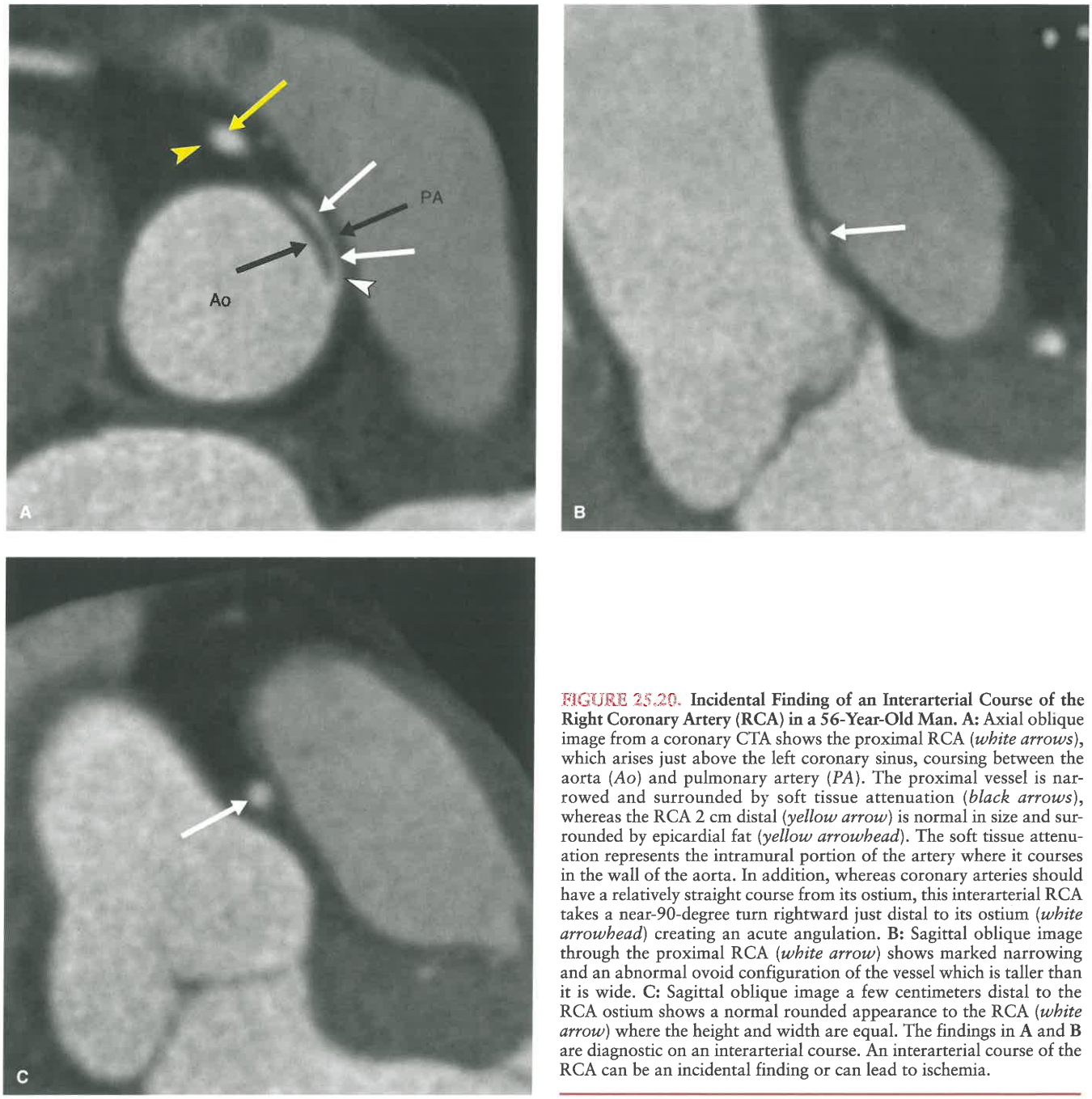

FIGURE 25.20. **Incidental Finding of an Interarterial Course of the Right Coronary Artery (RCA) in a 56-Year-Old Man. A:** Axial oblique image from a coronary CTA shows the proximal RCA (*white arrows*), which arises just above the left coronary sinus, coursing between the aorta (*Ao*) and pulmonary artery (*PA*). The proximal vessel is narrowed and surrounded by soft tissue attenuation (*black arrows*), whereas the RCA 2 cm distal (*yellow arrow*) is normal in size and surrounded by epicardial fat (*yellow arrowhead*). The soft tissue attenuation represents the intramural portion of the artery where it courses in the wall of the aorta. In addition, whereas coronary arteries should have a relatively straight course from its ostium, this interarterial RCA takes a near-90-degree turn rightward just distal to its ostium (*white arrowhead*) creating an acute angulation. **B:** Sagittal oblique image through the proximal RCA (*white arrow*) shows marked narrowing and an abnormal ovoid configuration of the vessel which is taller than it is wide. **C:** Sagittal oblique image a few centimeters distal to the RCA ostium shows a normal rounded appearance to the RCA (*white arrow*) where the height and width are equal. The findings in **A** and **B** are diagnostic on an interarterial course. An interarterial course of the RCA can be an incidental finding or can lead to ischemia.

of the interarterial vessel (between the aorta and pulmonary artery) as compared to those with a more inferior course (between the aorta and right ventricular outflow tract). However, in most patients, an interarterial course of the RCA is an incidental finding which does not cause ischemia. When an interarterial course of an RCA is identified, surgical correction is recommended if the patient has chest pain, ischemia, syncope, presyncope, or LV dysfunction in the appropriate vascular territory. Asymptomatic adults often undergo a stress test to determine whether there is inducible ischemia in the affected vascular distribution. If ischemia is absent on stress testing, many currently favor no intervention. However, practices vary depending on the patient's age and the specific institution.

Compared to the RCA, an interarterial course of the LAD or left main has a higher association with myocardial ischemia and sudden cardiac death. Surgical correction is recommended in most cases even if the finding is incidental. This can occur via various techniques including unroofing, reimplantation, or bypass.

Anomalous Origin of the Left Main Coronary Artery From the Pulmonary Artery. Anomalous origin of the left main coronary artery from the pulmonary artery (ALCAPA), or Bland–Garland–White syndrome, is a rare congenital anomaly with an estimated incidence of 1/300,000 live births. In utero, admixture of blood and high pulmonary pressures allow for adequate perfusion of the left main coronary artery. In the neonatal period, pulmonary pressures remain high enough to allow for adequate perfusion of the left main coronary artery with pulmonary arterial blood. However, during the first few months of life, pulmonary artery pressures begin to decrease. Once this occurs, the timing of symptoms depends on the presence or

FIGURE 25.21. **Interarterial Course of the Left Main Coronary Artery in a 14-Year-Old Boy Who Presented to the Emergency Department after Cardiac Arrest while Playing Basketball. A:** Axial oblique image from a coronary CTA shows the left main coronary artery (*white arrow*), which arises above the right coronary sinus, coursing between the aorta (*Ao*) and pulmonary artery (*PA*). The proximal vessel is severely narrowed. **B:** Sagittal oblique image through the proximal left main near the ostium shows severe narrowing of the LM (*white arrow*), which has an ovoid shape as it courses between the aorta and pulmonary artery. The vessel measures 2 × 1 mm in diameter. **C:** Sagittal oblique image 1 cm distal to the ostium; the LM has a more normal rounded shape and size (*white arrow*), measuring 4 × 4 mm. A 5-mm intramural course of the proximal left main was confirmed at surgery. Interarterial course of the left main or LAD is less common than that of the RCA but has a much high incidence of sudden cardiac death.

absence of collaterals. In the absence of adequate collaterals, the decrease in pulmonary pressures leads to inadequate blood flow from the PA into the left main coronary artery. This can lead to myocardial ischemia, infarct, and cardiac death in 90% of infants in the first year of life (Fig. 25.22). However, if robust RCA collaterals are present, high pressure systemic blood from the RCA will flow retrograde into the left main distribution and ultimately into the main pulmonary artery due to lower pulmonary pressures. This retrograde blood flow from the RCA to the left main and into the main pulmonary artery creates a physiologic state akin to a fistula (Fig. 25.23). Due to preferential flow into the lower-pressure PA and not the microcirculation, capillary hypoperfusion may lead to chronic subendocardial ischemia. Patients with this pattern of ALCAPA often present in their third or fourth decade of life with subacute symptoms such as angina, dyspnea, palpitations, and fatigue. While some patients with ALCAPA may be asymptomatically discovered in their eighth decade of life, ventricular arrhythmia and sudden death are still common in this population.

Single Coronary Artery. With a single coronary artery, all coronary artery branches arise from a single vessel which can have various benign or potentially malignant anomalous courses (Fig. 25.17). A single RCA is more common than left.

Ostial Atresia. Ostial atresia is an extremely rare abnormality where the ostium of the RCA or left main does not develop (Fig. 25.24). It more commonly affects the left main coronary artery ostium than the RCA ostium. While the ostium is atretic, just distal to the atretic segment normal coronary artery anatomy is present. This anomaly is often associated with sudden cardiac death in newborns but patients can survive into adulthood if collateral pathways between the opposite coronary circulation exist.

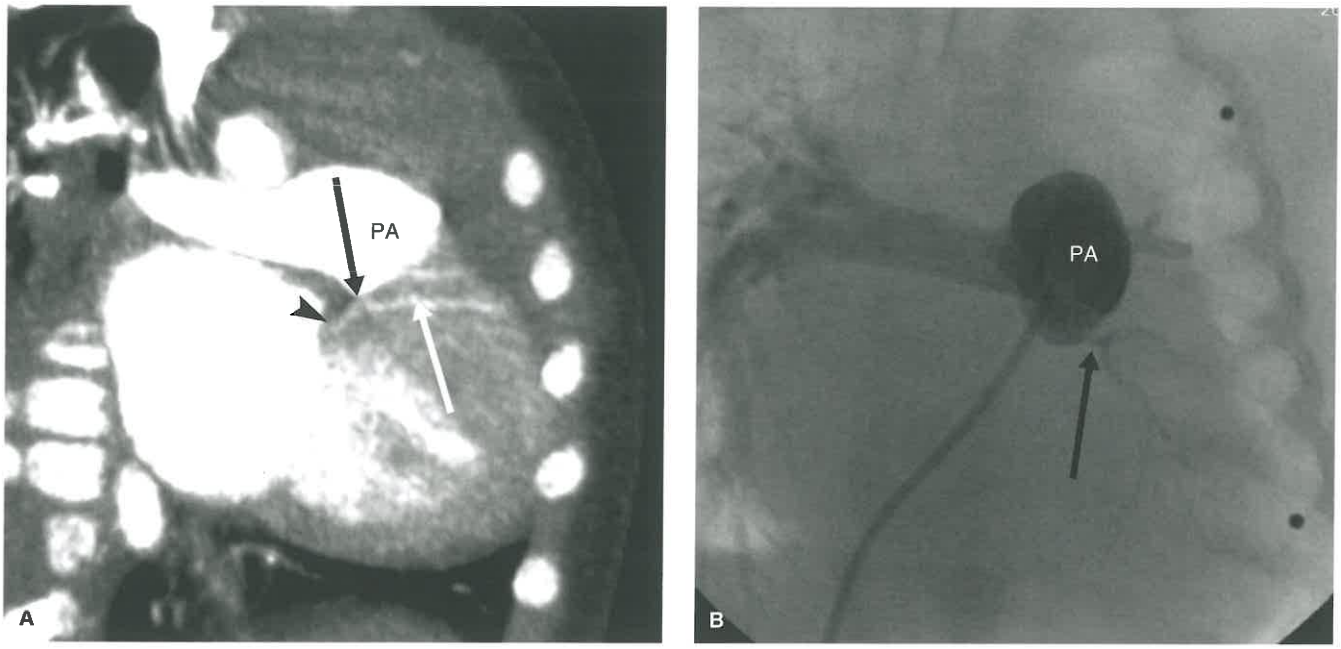

FIGURE 25.22. **Anomalous Origin of the Left Main Coronary Artery From the Pulmonary Artery (ALCAPA) in an 8-Week-Old Infant With Poor Feeding, Lethargy, and Irritability. A:** Sagittal oblique image from a CTA shows the left main coronary artery (*black arrow*) arising from the pulmonary artery (*PA*) with subsequent bifurcation into the LAD (*white arrow*) and LCx (*black arrowhead*). **B:** Anterior image from catheter angiography confirms the presence of ALCAPA with the left main (*black arrow*) arising from the PA.

ABNORMALITIES IN COURSE

Myocardial Bridging

An intramyocardial course of a coronary artery, **or myocardial bridging,** is a common incidental finding and has been reported in up to 58% of patients undergoing coronary CTA and in up to 86% of autopsies. Bridging most often involves the mid-LAD where a band of myocardial tissue extends around the vessel (Fig. 25.25). The depth and length of the bridged segment can vary significantly from a few millimeters to a few centimeters. While the vessel is compressed during systole, this rarely leads to symptoms as the coronary

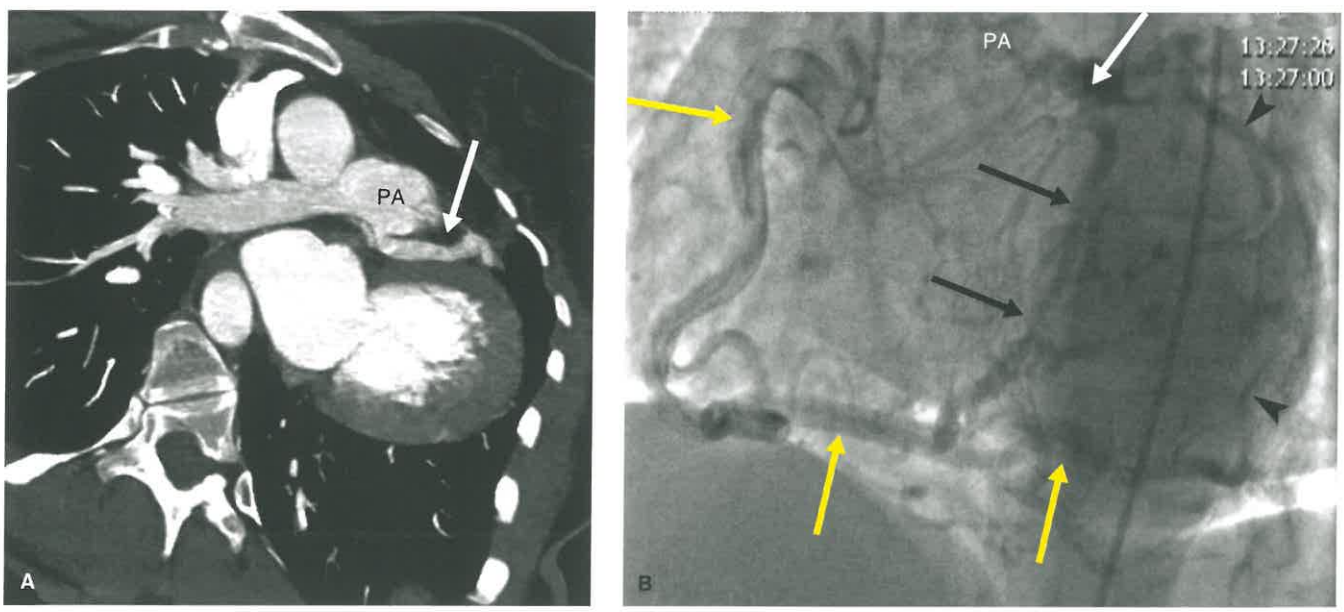

FIGURE 25.23. **Anomalous Origin of the Left Main Coronary Artery From the Pulmonary Artery (ALCAPA) in a 50-Year-Old Woman With Chest Pain. A:** Coronal oblique image of the left main coronary artery from a gated CTA of the chest shows a dilated left main coronary artery (*white arrow*) arising from the pulmonary artery (*PA*), consistent with ALCAPA. **B:** Coronary angiogram with a right coronary artery (RCA) injection shows a diffusely dilated RCA and associated branches (*yellow arrows*). Flow from these dilated vessels fills the left circumflex (*black arrowheads*), left anterior descending (*black arrows*), and left main (*white arrow*) via retrograde flow. The blood then drains into the pulmonary artery (*PA*) creating a large fistula. Due to the presence of collateral circulation, the patient was able to survive into adulthood with this congenital abnormality.

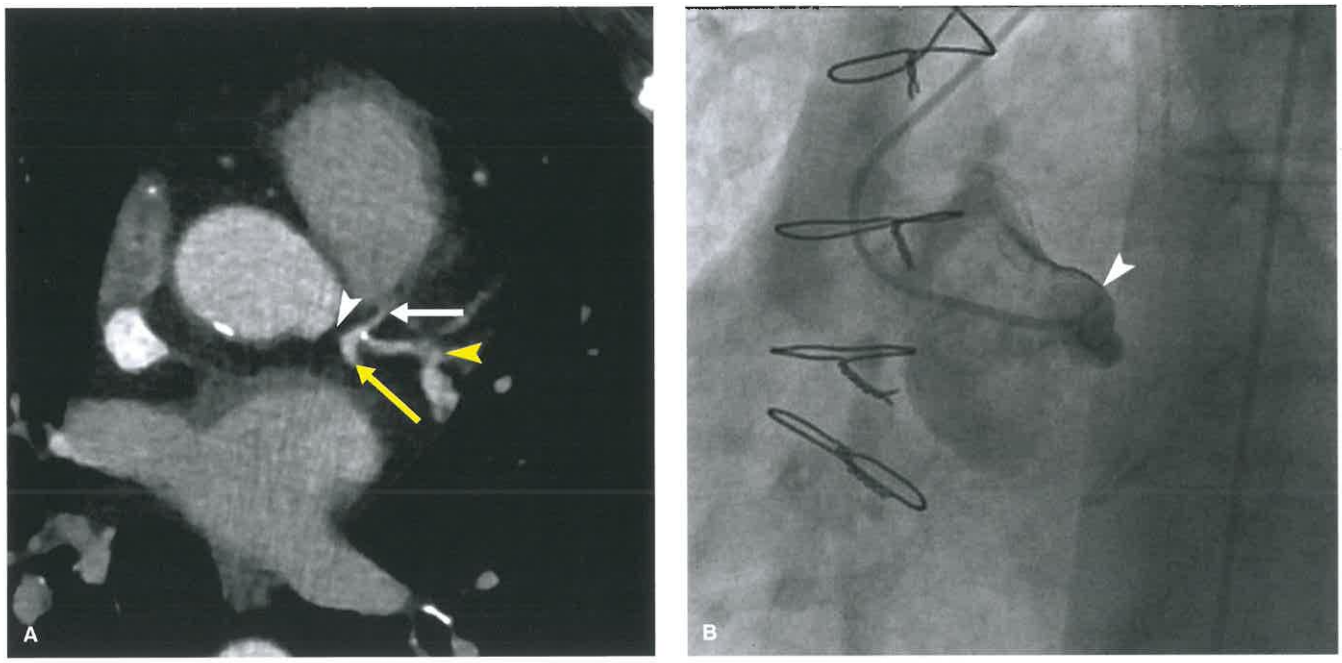

FIGURE 25.24. **Ostial Atresia in a 51-Year-Old Woman. A:** Axial oblique MPR through the expected location of the left main coronary artery shows complete absence of the vessel (*white arrowhead*). The left main distal to the atresia can be seen trifurcating into the LAD (*white arrow*), ramus intermedius (*yellow arrowhead*), and LCx (*yellow arrow*). The patient underwent coronary artery bypass surgery when she was 15 for surgically proven left main ostial atresia. **B:** Still image from a coronary angiogram with injection in the expected location of the left main ostium shows no hint of ostial development (*white arrowhead*).

arteries fill during diastole. Although the vast majority of myocardial bridges are an incidental finding on coronary CTA, myocardial bridges can lead to angina and ischemia through various mechanisms including phasic systolic vessel compression, persistent diastolic lumen diameter reduction, increased blood flow velocities, retrograde systolic flow, and reduced coronary flow reserve. In addition, there is an increased incidence of coronary artery atherosclerotic disease

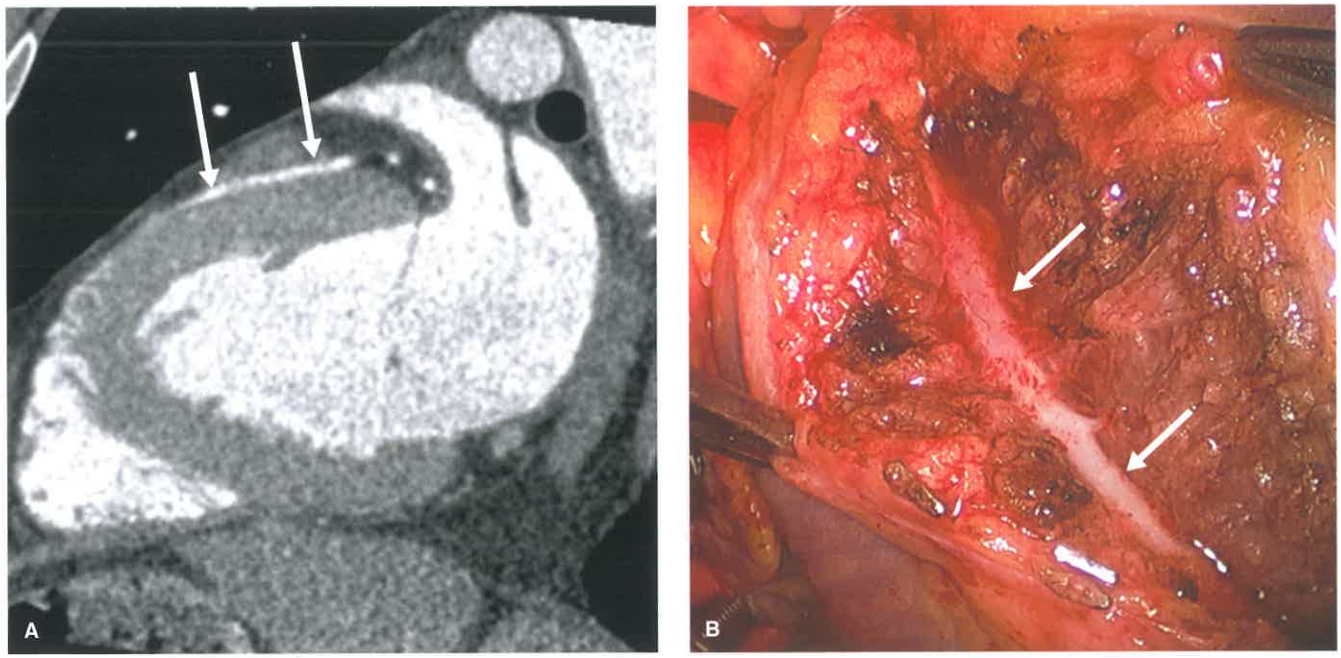

FIGURE 25.25. **Myocardial Bridging in a 22-Year-Old Man With Repeated Visits to the Emergency Department for Chest Pain. A:** Sagittal oblique image from a coronary CTA shows the mid-LAD diving into the left ventricular myocardium (*white arrows*), consistent with a 38-mm myocardial bridge which measured 8 mm in depth. No other abnormalities were found, and stress imaging showed no abnormality. Although this is a common incidental finding and of little clinical significance in the majority of patients, due to his repeated symptoms and lack of other explanation for pain, the patient elected to undergo surgery. **B:** Surgical image during myotomy shows the mid-LAD surrounded by myocardium (*white arrow*). Two months after surgery, the patient returned to the emergency department with chest pain similar to that experienced prior to surgery.

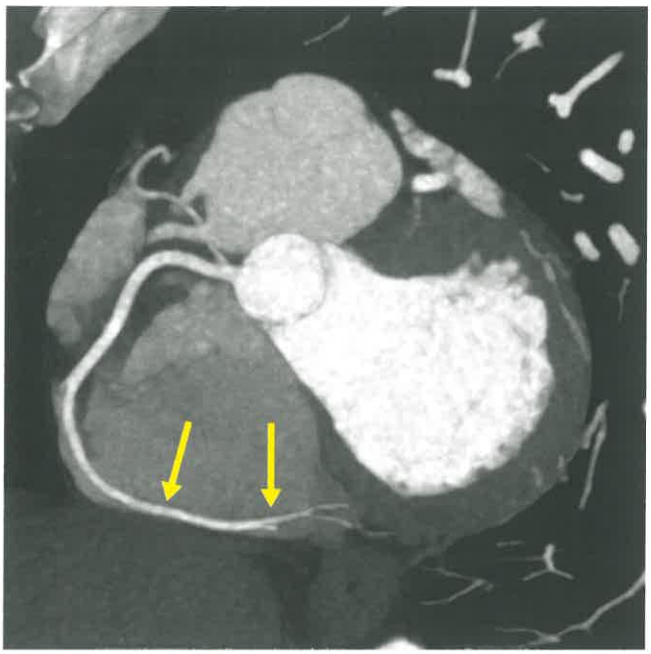

FIGURE 25.26. **Intracavitary Course of the RCA in a 40-Year-Old Man Presenting to the Emergency Department With Chest Pain.** C-view of the RCA (*yellow arrows*) shows the distal RCA coursing within the right atrium. This is a benign course, although the vessel could be theoretically injured during various forms of intervention.

proximal to the bridge, although the bridged segment is typically free of disease. Although there are no definitive imaging findings to distinguish between incidental and symptomatic bridges, deep bridges are more likely to be symptomatic.

Intracavitary Course

Compared to myocardial bridging, an intracavitary course of the coronary artery, where the vessel dives into a cardiac chamber, is relatively rare. In most reported instances, this involves the RCA extending into the right atrium (Fig. 25.26). In one large autopsy series of 331 patients, this abnormal course was seen in 1.8%. However, in a retrospective review of over 9,284 coronary CTAs, the anomaly was seen in only 0.15% of the studies. This anomalous course should not cause any symptoms in relation to compression, but the vessel could be inadvertently injured during right heart cannulation, instrumentation, ablation therapy, or even central line placement.

Split (Double) Coronary Artery

A split or double coronary artery is an extremely rare anomaly. In most instances, there is one coronary artery arising from the sinus of Valsalva, which then divides in its proximal portion into two parallel coronary arteries that mirror their courses. Since in most cases there is a single ostium, many have preferred to use the term "split" to describe this anomaly (Fig. 25.27A). In rarer instances, there is a true "double" or duplicate coronary artery where each has an independent origin from the aortic sinus with near-parallel courses (Fig. 25.27B). In general, this is a benign anomaly.

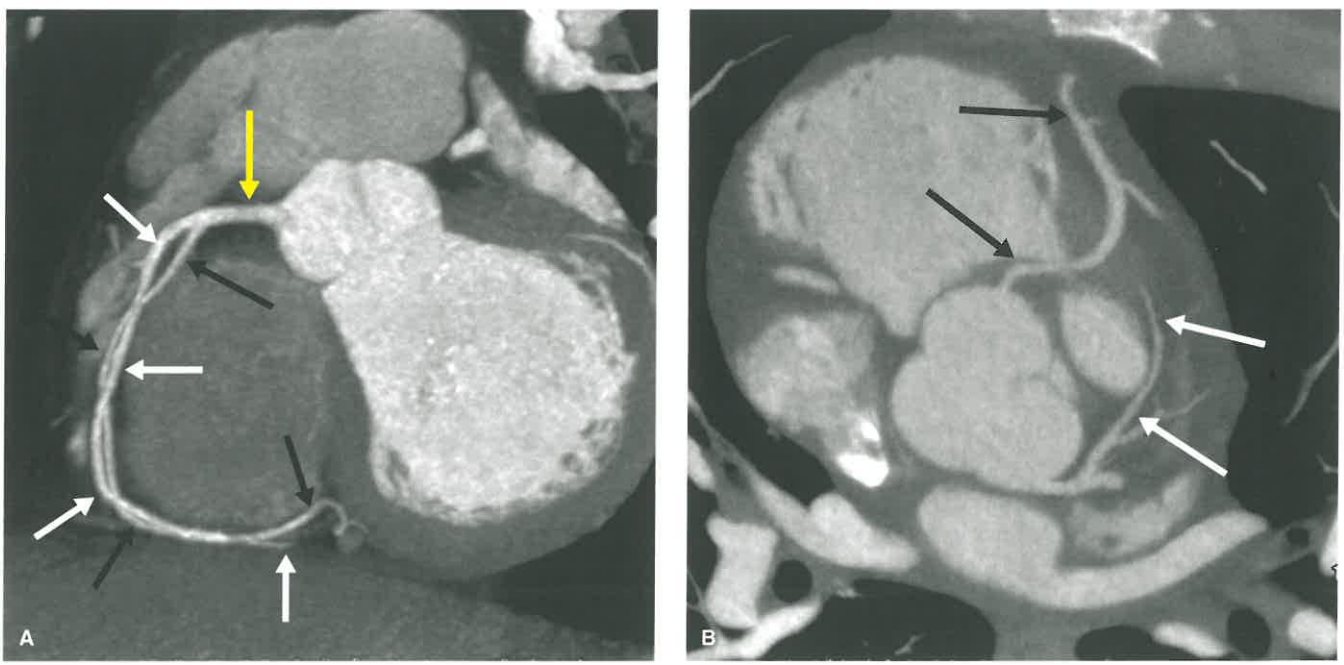

FIGURE 25.27. **Incidental Findings of Extranumerary Coronary Arteries in Two Patients Presenting to the Emergency Department With Chest Pain. A:** A 6-mm MIP C-view of the RCA in a 38-year-old man shows a single RCA proximally (*yellow arrow*), although a few centimeters distal to its origin, the vessel splits in two. The larger vessel (*white arrows*) gives rise to various acute marginal (AM) branches and continues distally as the PDA. The smaller vessel (*black arrows*) does not give rise to any AM branches and continues as the PLV. **B:** Dual left anterior descending (LAD) coronary artery in a 30-year-old man. Axial oblique MIP shows two LAD vessels. The first is a smaller LAD arising from the left main coronary artery which supplies the proximal LAD territory (*white arrows*). The second is a larger LAD arising from the right coronary sinus and supplying the mid and distal LAD territory through a septal course (*black arrows*). These are both benign anomalies.

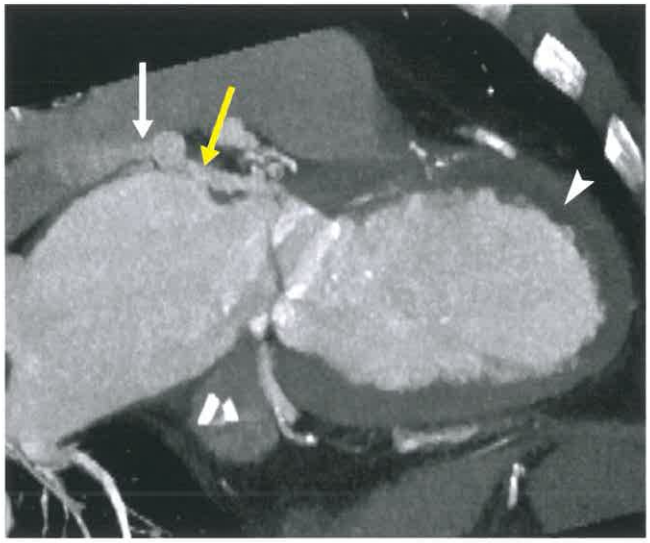

FIGURE 25.28. **Coronary Artery Fistula.** Sagittal oblique multiplanar reformat from a retrospectively gated coronary CTA showed diffuse tortuosity and dilation of the LCx (*yellow arrow*), a portion of which drains into the left pulmonary artery (*white arrow*). The LAD territory shows subendocardial hypoperfusion (*white arrowhead*).

ABNORMALITIES IN TERMINATION

Coronary Fistula

Coronary artery fistulas may be acquired but are most often congenital. Fistulas can involve either the left or right coronary systems, and the literature varies on which distribution is most common. No matter which coronary artery is involved, drainage is most commonly to the right side (from the coronary sinus to the pulmonary artery) and physiologically acts like a left-to-right shunt. In nearly all cases, the involved coronary artery is markedly dilated and tortuous and such a finding on CT should lead to suspicion of a fistula (Fig. 25.28; Video 25.1). Although a fistula can be incidentally found, patients often present with congestive heart failure due to long-standing shunt, ischemia due to a steal phenomenon (preferential flow of blood through lower-pressure fistula instead of through higher-pressure capillary bed), or endocarditis.

CORONARY ARTERY DISEASE

Coronary artery disease (CAD) is the leading cause of mortality of both men and women in the western world. One of the most common indications for coronary CTA is for the assessment of CAD. The excellent spatial resolution of coronary CTA allows for evaluation of coronary artery stenosis, remodeling, and characterization of coronary plaque. Just as important, a normal coronary CTA examination can exclude CAD as the cause of a patient's symptoms.

Although there are multiple indications for coronary CTA, one of its main uses is in patients with nonacute chest pain and a low to intermediate pretest probability of having severe obstructive coronary disease. The use of coronary CTA in patients with a high probability of having obstructive CAD is questionable. More recently, the use of coronary CTA in select patients with acute chest pain has become more widely adopted. However, as discussed in more detail below, this test should not be performed in patients having acute coronary syndrome (ACS) with ST elevation or elevated troponin levels.

Coronary Artery Calcification

While coronary artery CTA is not recommended for screening, noncontrast evaluation of the coronary artery calcification (CAC) in asymptomatic patients is recommended in specific populations. This includes low-risk patients with a family history of premature coronary heart disease (male first-degree relative <55 years or female first-degree relative <65 years) and patients with intermediate-risk factors (10-year risk of coronary heart disease of 10% to 20%) and no history of CAD. In addition, asymptomatic adults ≥40 years of age with diabetes can also undergo screening. Per the U.S. Preventative Task Force, screening CAC should not be obtained in low-risk patients (<10% 10-year risk of coronary heart disease). In addition, as CAC is a screening study, it should not be performed in patients who have previously had a MACE.

In the appropriate patient population, coronary artery calcium scoring (CACS) has been a well-validated marker for cardiovascular risk and can provide incremental value to other population-based data, such as the Framingham Risk Score (FRS). Higher CACS is indicative of a greater likelihood of cardiovascular death. Compared to individuals with a 0 CACS, the hazard ratio for having a major coronary event was 3.89, 7.08, and 6.84 in patients with a 1 to 100, 101 to 300, and >300 CACS, respectively. In patients with extremely high scores (Agatston score >1,000), the relative risk was 10.8. A 0 CACS is also of important prognostic value as those without coronary calcium are unlikely to develop a MACE. In a review of 25,903 asymptomatic subjects without coronary calcium, less than 1% had a cardiac event during a 51-month follow-up period.

Currently, CACS is performed using prospective ECG gating with data reconstructed at a 2.5-mm slice thickness. A tube potential of 120 kV is still recommended for CACS as this kV was used for the initial Agatston scoring method, and lowering the kV (70 kV, 80 kV, or 100 kV) would increase the calcium score due to blooming artifact. While older research studies report a radiation dose of around 1.5 mSv for a CACS, modern scanners can perform this at a fraction of this dose.

Once the CACS scan is reconstructed, various software packages automatically highlight areas along the coronary artery territories with an attenuation greater than 130 HU (Fig. 25.29). These areas are then manually selected or rejected by the radiologist or technologist to calculate an Agatston score which takes into account both the size and highest density of the plaque. By entering the Agatston score into a CACS calculator, the patient's score can be compared to those of the same age, gender, and ethnicity. While asymptomatic patients may undergo CACS for screening, many institutions perform CACS as part of their routine protocol for patients undergoing contrast-enhanced coronary CTA.

Coronary Plaque and Remodeling

An advantage of coronary CTA is its ability to characterize coronary atherosclerotic plaque. In general, coronary plaques can be characterized by their composition, pattern of remodeling, and degree of luminal narrowing.

Coronary artery plaques, or fibroatheromas, are classified as calcified, noncalcified, or mixed. While CAC can be either intimal or medial in location, intimal calcifications are the calcifications related to atherosclerotic disease. Intimal calcifications, which occur due to an osteoblastic-like factor released from intimal vascular smooth muscles cells, are associated with hypertension, dyslipidemia, cigarette smoking, and other proinflammatory conditions. The noncalcified portion

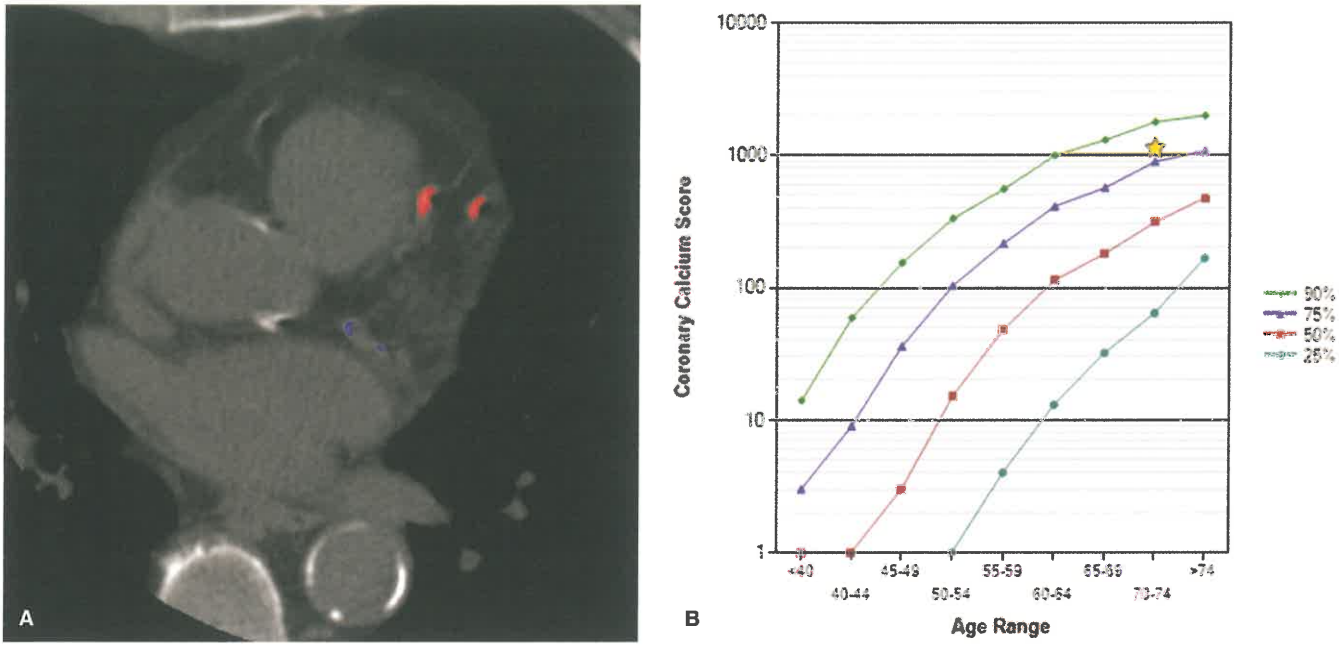

FIGURE 25.29. **Calcium Scoring for Prediction of Future Cardiac Events.** A 73-year-old asymptomatic man with a history of hypertension, smoking, and hyperlipidemia undergoes a calcium score CT. **A:** Axial image from a calcium score CT shows areas of atherosclerotic disease in the LAD distribution and LCx distribution marked as red and blue, respectively. **B:** The patient's total calcium score via the Agatston method was 1,121 which places the patient in the 83rd percentile for patients of the same age, gender, and ethnicity who are free of clinical cardiovascular disease and diabetes.

of a plaque is comprised of two main components within the intima, a fibrous cap which overlies a lipid-rich necrotic core.

Pathologically, plaques can be classified as stable or vulnerable. Atherosclerotic plaques are more vulnerable to rupture with a thinner fibrous cap and larger underlying necrotic core. When the fibrous cap ruptures, the highly thrombogenic necrotic core enters the coronary artery lumen to cause an acute thrombotic event. Plaque rupture is the leading cause of MACEs, and the severity of event will vary depending on the degree of luminal thrombosis. Plaque erosions can also lead to major cardiac events and occur when a portion of the coronary artery endothelium sloughs off. As the endothelium provides a nonthrombogenic surface, the loss of the endothelial layers can precipitate thrombosis formation in the region of the absent endothelium. Since plaque erosion is less common and no current noninvasive imaging techniques are available to predict this process, it will not be discussed.

Imaging manifestations on coronary CTA to help to identify vulnerable plaques include positive remodeling and low-attenuation plaques. Positive remodeling refers to outward growth or expansion of both the coronary artery and associated plaque (Fig. 25.30). The causes of positive remodeling are complex, but it is primarily caused by medial and adventitial inflammation which weakens the underlying framework of the coronary artery and causes its outward expansion. In addition to the medial and adventitial inflammation, intimal inflammation causes thinning of the fibrous cap. As the vessel expands outward, the inflamed and thinned fibrous cap is stretched making it more prone to rupture. In the presence of a large necrotic core, tension and inflammation of the fibrous cap increase making the plaque more vulnerable to rupture. It is important to remember that positive remodeling (outward growth) and negative remodeling (inward growth, stenosis) usually occur together. In cases where positive remodeling is the predominant growth pattern, luminal narrowing may be only mild to moderate, and therefore, the patients will remain asymptomatic. It is also important to remember that positive remodeling can lead to a visual overestimation of stenosis.

The attenuation of the noncalcified plaque can also be assessed to identify vulnerable lesions. In general, a high-attenuation plaque tends to correspond to a fibroatheroma with a larger and thicker fibrous cap and thus has a smaller likelihood of rupture. On the other hand, a low-attenuation plaque, defined as a plaque with attenuation value <30 HU, corresponds to a plaque with a larger lipid-rich necrotic core and thus has a higher propensity to rupture (Fig. 25.30). While either the presence of positive remodeling or low-attenuation plaque on coronary CTA increases the risk of a future acute coronary event, the presence of both findings dramatically increases the risk. In a study by Motoyama et al. assessing plaque characteristics associated with subsequent development of an acute coronary event in 1,059 patients, 22.5% of patients with both findings develop an acute event compared to 3.7% with one finding and 0.5% with neither positive remodeling nor low-attenuation plaque.

An additional coronary CTA finding that may be indicative of a thin-cap atheromatous vulnerable plaque is termed the "napkin-ring" sign (Fig. 25.31). This is visualized as a rim of high attenuation surrounding an area of low attenuation representing the inflamed fibrous cap surrounding the necrotic lipid core, and its presence can be an independent predictor of a future acute coronary event. The presence of these imaging findings should be mentioned in the coronary CTA report, as they may lead to changes in patient therapy.

Coronary Stenosis. Negative remodeling, or inward growth of a plaque, causes coronary artery stenosis. This stenosis can occur rapidly in the setting of an acute coronary thrombosis or plaque rupture. However, in many instances, stenosis occurs slowly due to continued growth of a stable plaque.

As CT technology has continued to improve, there has been increasing sensitivity and negative predictive value for morphologic evaluation of the coronary arteries in comparison to catheter-based angiography. More recent multicenter trials using 64-slice CT have demonstrated even greater efficacy for morphologic evaluation. A 2008 meta-analysis of

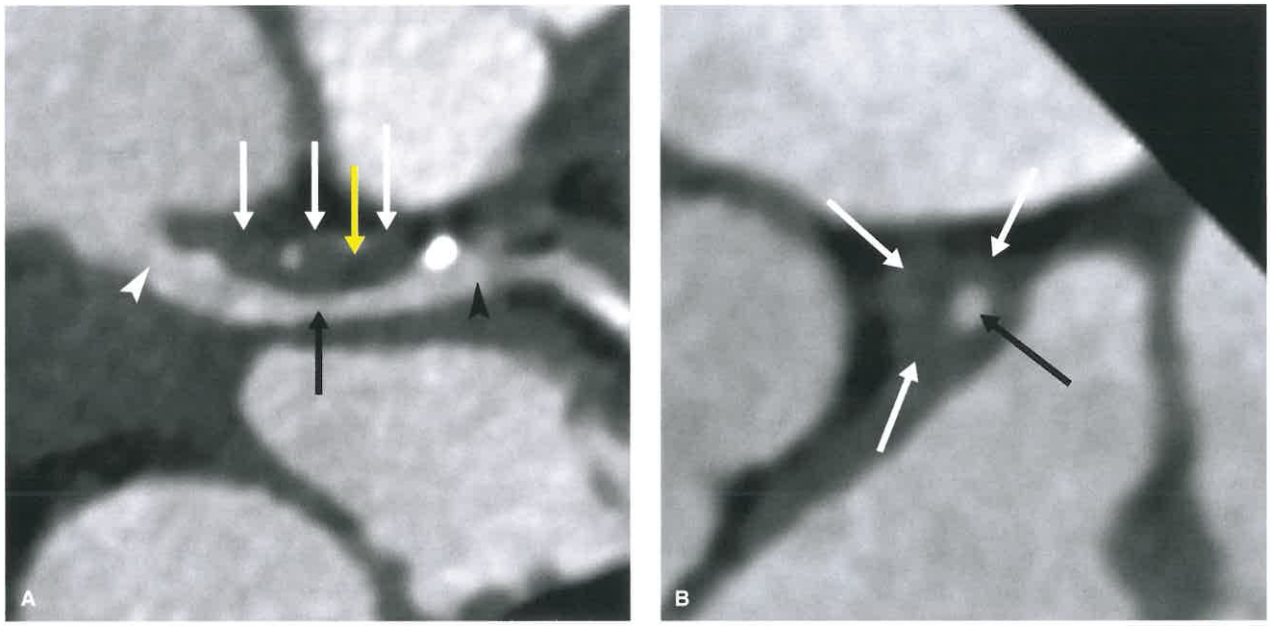

FIGURE 25.30. **Positive Remodeling in a 55-Year-Old Man With Atypical Chest Pain. A, B:** Axial oblique (**A**) and transverse (**B**) images of the left main coronary artery (LM) show exuberant mixed, but predominantly noncalcified, plaque which partially wraps around the vessel (*white arrows*). The plaque leads to outward growth of the vessel, termed positive remodeling. Within the positive remodeling, there is a focus of low-density plaque measuring 10 HU (*yellow arrow*). The presence of both these findings suggests a "vulnerable plaque" with a greater likelihood to rupture and potentially cause an acute myocardial event. Including the plaque, the maximum transverse diameter of the vessel measured in **B** was 8 mm, whereas the proximal and distal LM have a maximal diameter of 6 mm and 4 mm, respectively. This illustrates the outward growth (positive remodeling) of the vessel. The luminal diameters of the proximal (*white arrowhead*, **A**), mid (*black arrow*, **A, B**), and distal (*black arrowhead*, **A**) LM are 5 mm, 3 mm, and 4 mm, respectively, consistent with a 33.3% stenosis. While the positive remodeling is a predominant feature, there is usually a concomitant component of negative remodeling (stenosis) as well.

64-slice coronary CTA among 1,296 patients in 28 studies showed a pooled sensitivity of 98%, specificity of 89%, positive predictive value (PPV) of 93%, and negative predictive value of 100% in comparison with catheter angiography. A more recent meta-analysis using dual-source CT technology demonstrated similarly excellent results even in the setting of higher heart rates. The most recently published multisociety appropriateness guidelines for coronary CTA consider stable symptomatic patients at low to intermediate risk for coronary events suitable for this test.

When reviewing a coronary CTA, it is imperative to use both multiplanar reformatted (MPR) reconstructions and axial images to assess the degree of stenosis. While maximum-intensity projection or volume-rendered images can supplement the use of MPRs, they should not be used for primary diagnosis. Multiple vendors offer software tools beyond MPRs

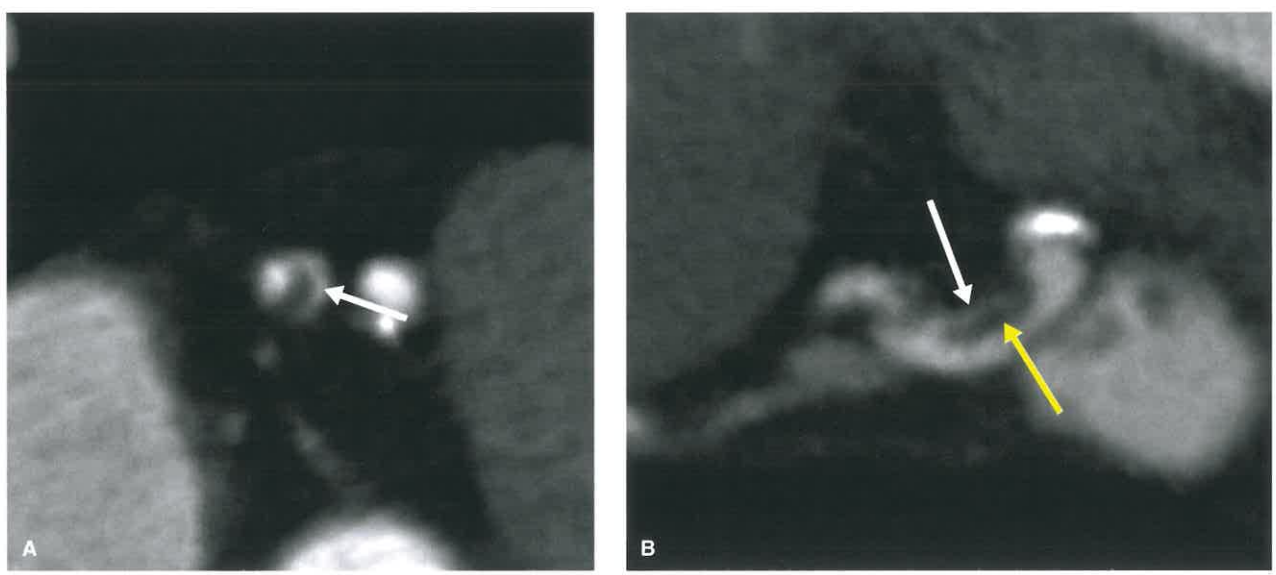

FIGURE 25.31. **Napkin-Ring Sign.** Transverse (**A**) and longitudinal (**B**) images through the mid-LCx show positive remodeling with only a mild stenosis. The positive remodeling demonstrates a few areas of low attenuation plaque (*yellow arrow*). In addition, there is fine linear enhancement along the periphery of the noncalcified plaque, creating a "napkin-ring" sign (*white arrows*, **A, B**). This is another finding suggestive of a "vulnerable plaque."

FIGURE 25.32. **Semi-Automated Stenosis Measurement in a 70-Year-Old Man With a Severe Stenosis in the LCx.** Curved MPR images through the LCx show a focal area of noncalcified plaque leading to a stenosis (*white arrows*). The diameter 1 cm proximal and distal to the stenosis measures 3.3 mm and 2.9 cm, respectively, for a mean diameter of 3.1 cm. The diameter in the areas of stenosis measures 0.44 mm. This corresponds to an 86% stenosis.

which can perform semiautomated stenosis calculations, assess plaque morphology, measure total plaque volume, and create curved MPR images of each vessel (Fig. 25.32).

For all vessels except the left main coronary artery, where a stenosis >50% is considered severe, coronary stenosis is quantified as absent (0%), minimal (1% to 24%), mild (25% to 49%), moderate (50% to 69%), severe (70% to 99%), and occlusive (100%) (Fig. 25.33). In patients with stable chest pain, a coronary artery etiology is highly unlikely in those with absent, minimal, or mild stenosis. Although a 70% or greater stenosis is considered severe, a stenosis ≥50% can potentially lead to hemodynamic compromise and therefore may be significant. Therefore, the presence of a moderate stenosis may require functional assessment with exercise ECG, exercise or pharmacologic nuclear stress testing, or stress echocardiography. In patients with a severe stenosis, functional assessment or an invasive catheter angiography should be considered.

In addition to evaluation of anatomic stenosis, the myocardium should be closely evaluated to assess for subendocardial myocardial perfusion defects (Fig. 25.34). In the presence of a significant stenosis, this usually represents an area of myocardial ischemia or infarct. If a retrospective ECG-gated coronary CTA is performed, at least 10 phases should be reconstructed at uniform intervals to allow for assessment of biventricular function which can be quantified using various software tools. Even with the use of ECG mA modulation, functional data can still be obtained throughout the cardiac cycle. This can be useful to evaluate for regional wall motion abnormalities associated with myocardial ischemia or infarct (Fig. 25.35).

While the negative predictive value of coronary CTA for assessment of coronary stenosis is excellent, the PPV is less optimal. One of the main reasons for this is the presence of moderate and even severe stenosis which is not hemodynamically significant, as determined by functional imaging or invasive catheter angiography. Cardiac CT stress imaging and CT fractional flow reserve (CT-FFR) are two newer techniques that can help provide physiologic data which can further increase the PPV of coronary CTA.

In myocardial perfusion CT, images of the heart and coronary arteries are obtained during the early portion of first-pass circulation, when iodinated contrast is predominantly intravascular. Akin to nuclear medicine stress testing, this is often done both at rest and during pharmacologic stress. A single acquisition, where the heart is scanned once during rest and once during stress, or a dynamic acquisition, where the heart is scanned multiple times during both stress and rest, can be performed. While the dynamic acquisition provides more detailed perfusion data, the radiation dose will be higher albeit similar in range to a ^{99m}Tc and less than a ^{201}Tl and dual-isotope SPECT for viability assessment. Stress and rest attenuation maps of the myocardium can be generated to determine if a coronary stenosis seen on CTA correlates with myocardial hypoperfusion. Similar to MRI stress testing, which is discussed in more detail below, myocardial ischemia on first-pass perfusion will manifest as regional subendocardial hypoperfusion corresponding to a specific vascular territory during stress that should improve or resolve during rest. Infarcted tissue should show persistent perfusion defect(s) during rest imaging. Iodinated contrast will concentrate in infarcted tissue and can be visualized by obtaining a third scan 5 to 10 minutes after the last contrast administration. Although delayed-enhancement CT shows high accuracy for the detection of infarcted tissue, it often underestimates the degree of infarct size when compared to MRI.

The second method is CT-FFR. The concept of CT-FFR is derived from invasive coronary angiography where the differences in pressure across a stenosis are directly measured. An FFR measurement of 1 means that there is no change in pressure across a stenosis, whereas an FFR of 0.7 means that the pressure distal to the stenosis is only 70% of that proximal to the stenosis. In general, a FFR of 0.8 or lower is considered hemodynamically significant. With CT-FFR, the data from a standard coronary CTA undergo computational fluid dynamic modeling and deep machine-based learning algorithms. This allows for both anatomic and hemodynamic information to be obtained from a single acquisition. Multiple studies have shown that the use of CT-FFR in conjunction with coronary CTA improves accuracy and specificity (Fig. 25.36). This can change treatment strategy and avoid unnecessary invasive testing, especially in those with anatomically moderate stenosis.

Coronary CTA in the Setting of Acute Chest Pain. ACS includes myocardial infarction with ST elevation (STEMI), myocardial infarct without ST elevation (NSTEMI), and unstable angina. In patients with acute chest pain and ECG changes or elevated cardiac troponin levels, the first line of therapy is thrombolysis and revascularization. Except in very rare exceptions, noninvasive imaging should not be performed in patients with ACS. However, coronary CTA is an excellent tool to assess patients presenting to the ED with acute chest pain, a low to intermediate risk of CAD, and a negative troponin level. In general, a coronary etiology of the chest pain is unlikely in patients without a significant stenosis on coronary CTA. Multiple prospective trials have been performed to compare the use of coronary CTA to standard

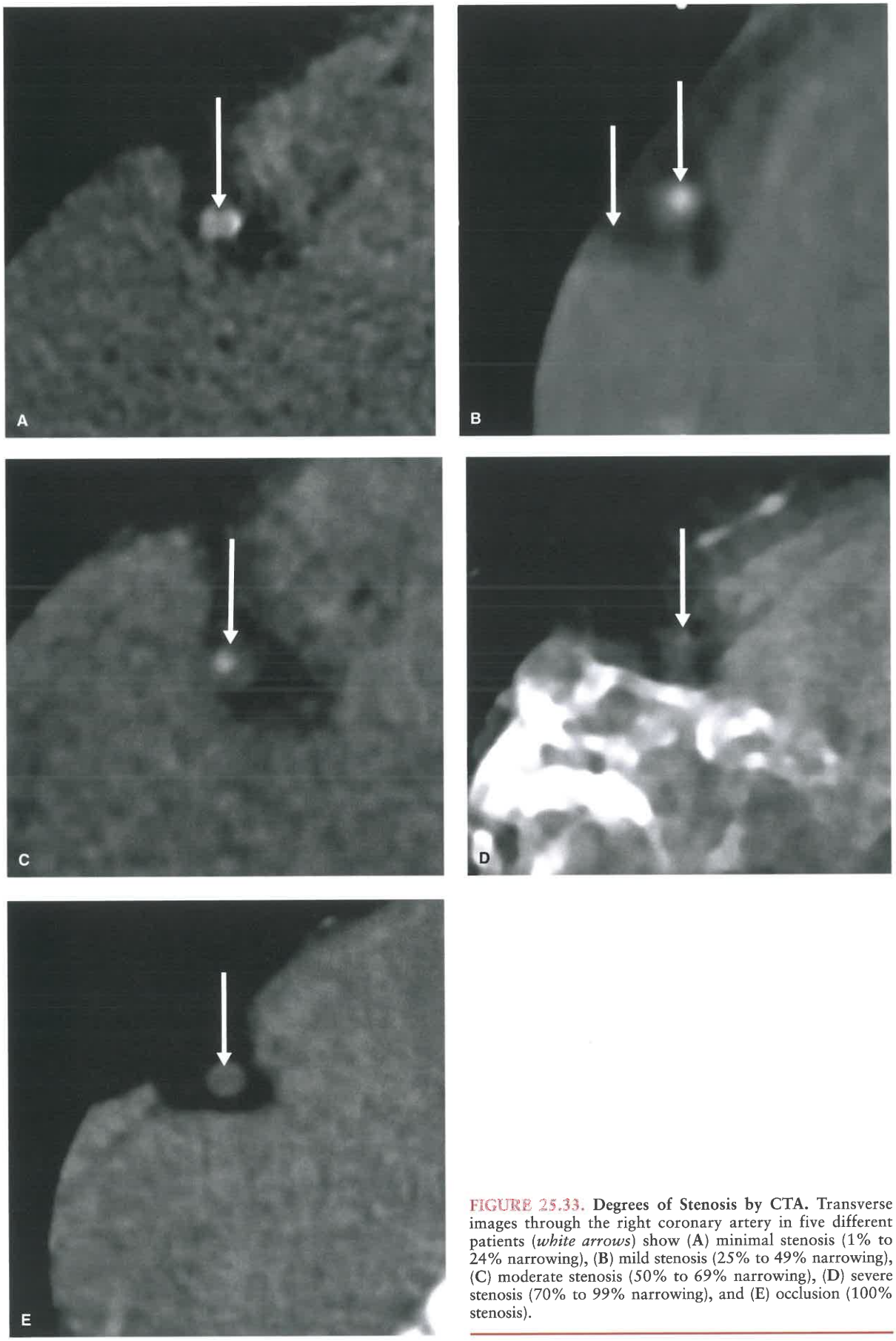

FIGURE 25.33. **Degrees of Stenosis by CTA.** Transverse images through the right coronary artery in five different patients (*white arrows*) show (**A**) minimal stenosis (1% to 24% narrowing), (**B**) mild stenosis (25% to 49% narrowing), (**C**) moderate stenosis (50% to 69% narrowing), (**D**) severe stenosis (70% to 99% narrowing), and (E) occlusion (100% stenosis).

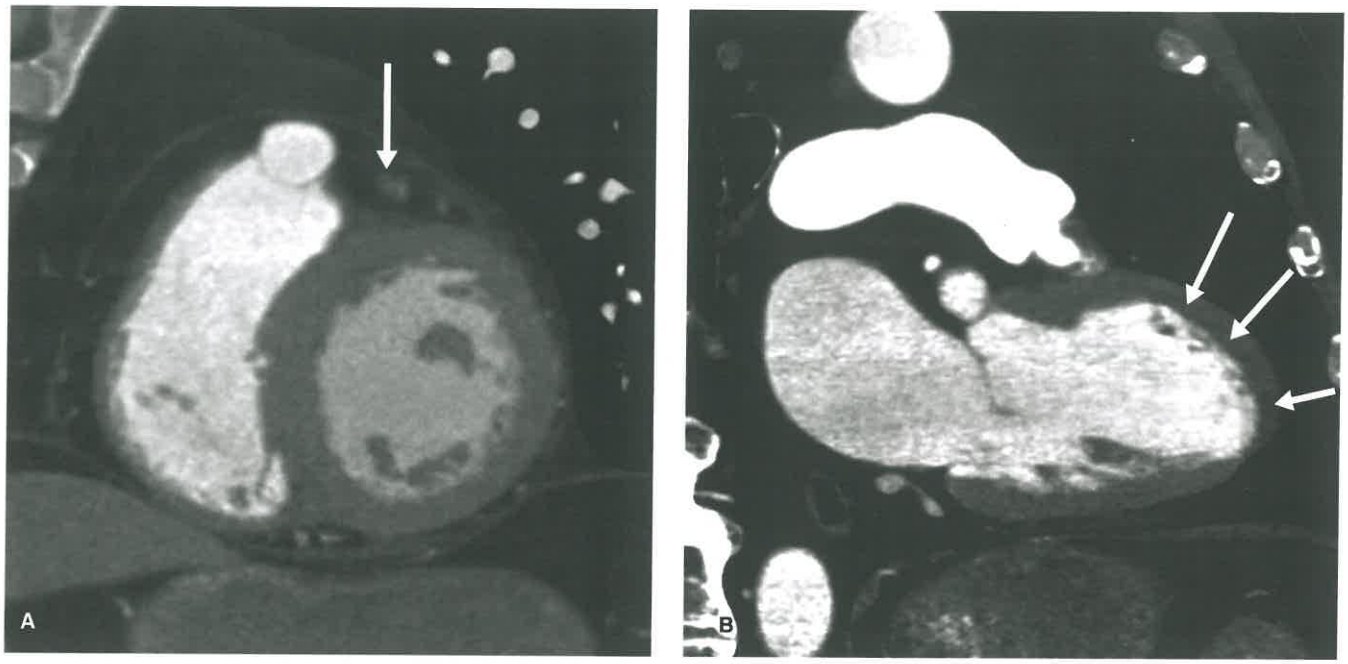

FIGURE 25.34. **Subendocardial Hypoperfusion in a 60-Year-Old Woman With Chest Pain. A:** Short-axis image through the mid-cavity of the left ventricle shows a severe stenosis of the LAD (*white arrow*). **B:** Two-chamber image demonstrates subendocardial hypoperfusion in the LAD distribution (*white arrows*). On CT, the hypoperfused myocardium could represent ischemic or infarcted tissue.

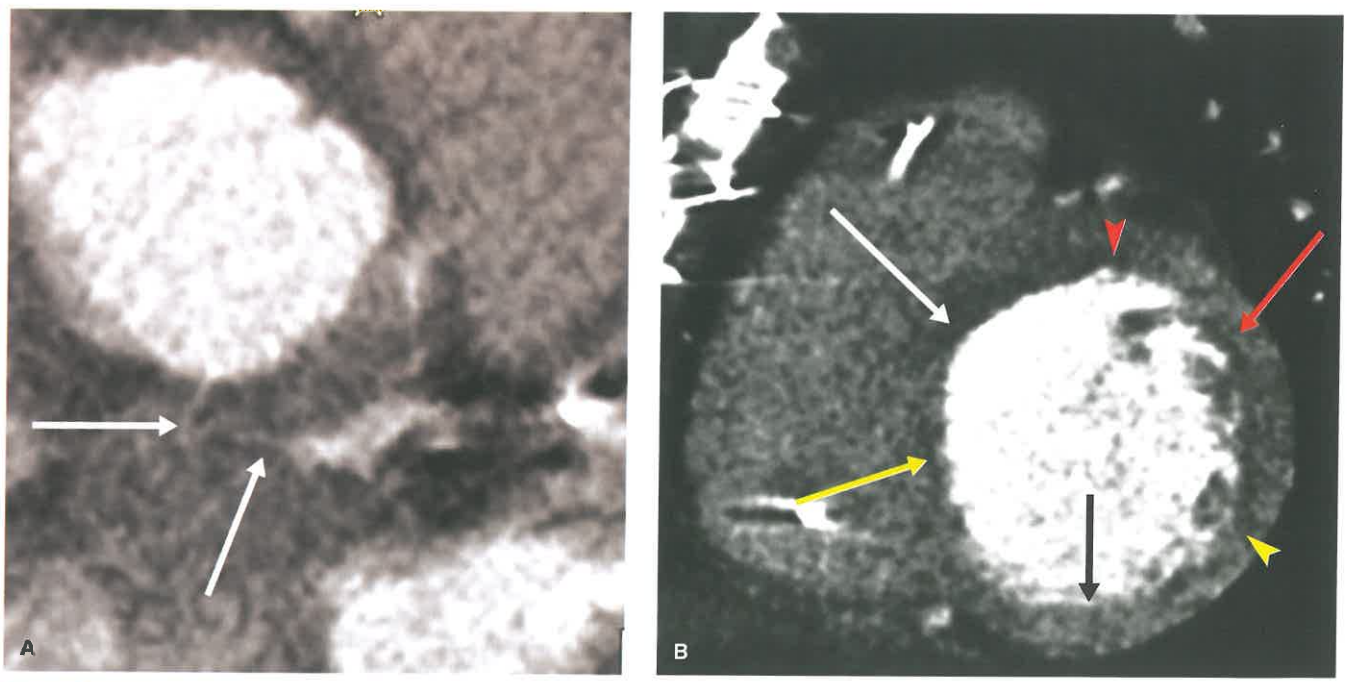

FIGURE 25.35. **Left Main Coronary Artery Territory Myocardial Infarct in a 60-Year-Old Man in Disseminated Intravascular Coagulation (DIC), Platelet Count of 2,950/mL, Troponin I of 57.7 ng/mL, and a Heart Rate of 122 bpm. A:** Axial oblique image from a retrospectively gated coronary CTA shows near-complete occlusion of the LM (*white arrows*). **B:** Short-axis image through the base shows subendocardial hypoperfusion involving the anteroseptal (*white arrow*), anterior (*red arrowhead*), anterolateral (*red arrow*), and portions of the inferolateral (*yellow arrowhead*) and inferoseptal (*yellow arrow*) segments. These findings are consistent with infarcts in both the LAD and LCx distributions. The inferior segment (*black arrow*) and portion of the inferolateral and inferoseptal segment are supplied by the RCA which was normal.

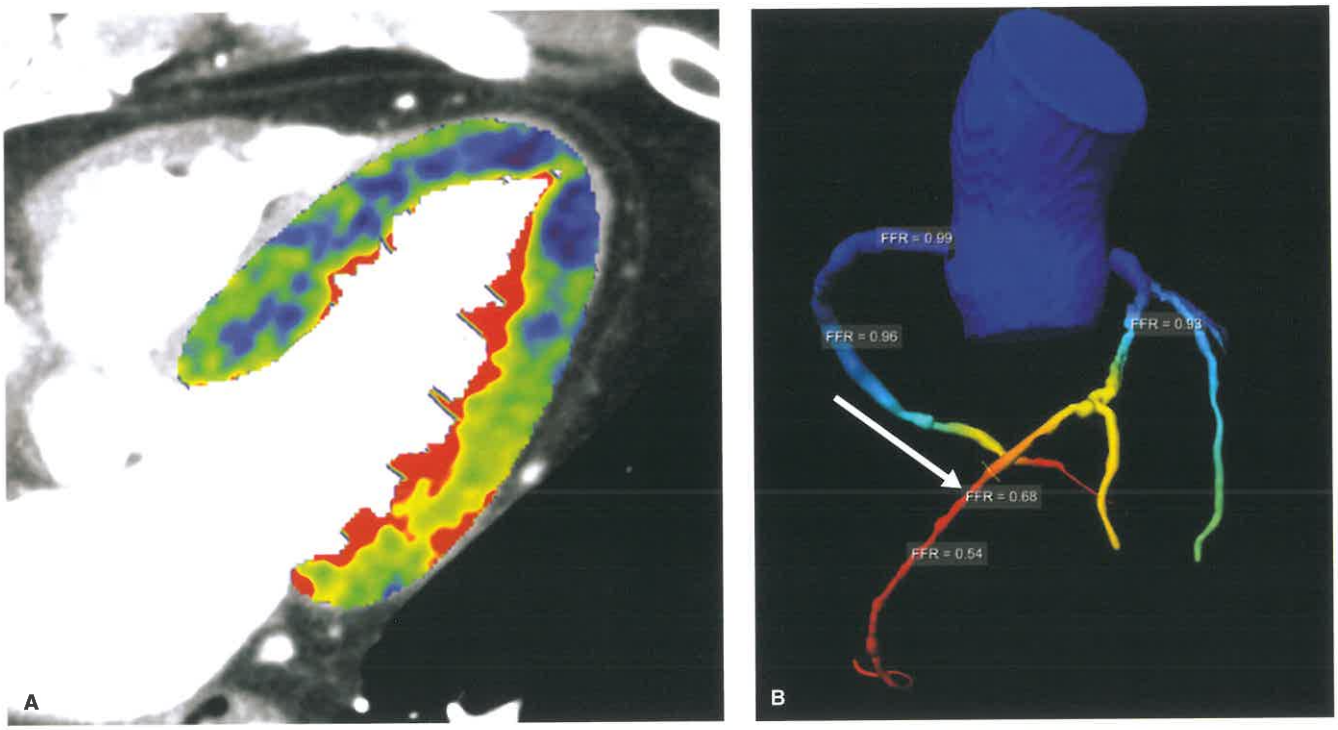

FIGURE 25.36. **Myocardial Perfusion Imaging and CT-FFR in a 75-Year-Old Man With Episodic Chest Pain. A:** Four-chamber image from a stress perfusion CT shows hypoperfusion (*blue pixels*) in the septum and apex consistent with LAD territory ischemia. The rest perfusion study was normal. **B:** CT-FFR image from the same patient shows significantly reduced flow in the mid and distal LAD (*white arrow*), with CT-FFR values less than 0.8. Flow in the LCx and RCA territories is normal. The patient underwent stenting of his LAD. (Images courtesy of Joseph Schoepf, MD.)

of care therapy, such as functional stress test, in the emergency department setting. Each showed that coronary CTA, compared to the standard of care, allows for earlier discharge without a significant difference in adverse cardiac events. Similar to patients with stable chest pain, those with a moderate stenosis may still have hemodynamic compromise and may need to undergo functional testing or invasive coronary angiography (Fig. 25.37).

MRI IN CORONARY ARTERY DISEASE

MR Imaging of the Coronary Arteries

While coronary CTA is the primary noninvasive technique for evaluating the coronary arteries, coronary MR angiography (cMRA) has demonstrated value as a potential alternative technique. Coronary MRA has some distinct advantages as studies can be performed without intravenous contrast and patients are not exposed to ionizing radiation. However, compared to coronary CTA, cMRA is limited due to its reduced spatial resolution, longer exam times, and operator dependency. Although there are advocates for using this technology in the assessment of CAD, cMRA is not currently used for the assessment of CAD in most institutions. Coronary MRA is accepted as a tool to assess for anomalous coronary arteries and coronary artery aneurysms, especially in the pediatric population or those with severe contrast allergies (Fig. 25.38). At 1.5 T, cMRA is performed using a whole-heart, free-breathing, 3D steady–state free precession (SSFP) sequence. Blood appears bright on SSFP sequences due its inherent T2/T1 weighting, obviating the need for contrast. At 3 T, gadolinium contrast agents are recommended due to the different sequences used.

MR Assessment of the Myocardium in Coronary Artery Disease

MRI is one of the strongest tools in the noninvasive evaluation of cardiomyopathies. It is considered the gold standard for evaluating cardiac function and can differentiate between ischemic and nonischemic etiologies of myocardial injury and dysfunction. The below section will concentrate on the use of cardiac MRI for ischemic cardiomyopathies, as its use in the assessment of nonischemic cardiomyopathies is presented in a different chapter.

When a patient undergoes a cardiac MRI with a known or suspected ischemic cardiomyopathy, the radiologist has four main goals: confirm (or refute) the suspected diagnosis, evaluate cardiac function and morphology, assess for myocardial viability, and look for any complications. Functional evaluation is performed using an SSFP sequence at 1.5 T and either a GRE of SSFP sequence at 3 T. To acquire a single slice along a prespecified cardiac plane, an expiratory breath-held, retrospectively gated, segmented sequence is obtained over multiple heart beats. Depending on the patient-related factors, such as heart rate, rhythm, and breath-hold ability, as well as technical factors, such as use of parallel imaging, k-space filling techniques, and TR optimization, this breath hold can last between 5 and 12 seconds. Although protocols vary by institution, in most instances, a single SSFP (or GRE) cine sequence is obtained in the two-, three-, and four-chamber planes. However, the mainstay for functional evaluation is the short-axis plane. Using a 6- to 8-mm slice thickness, sometimes with a 2-mm gap between slices, a short-axis stack of cine SSFP (or GRE) sequences are obtained through the entire cardiac axis from the mitral valve plane to the cardiac apex.

When placed in a cine viewer, SSFP imaging allows detailed assessment of wall motion and thickness. Due to the territorial

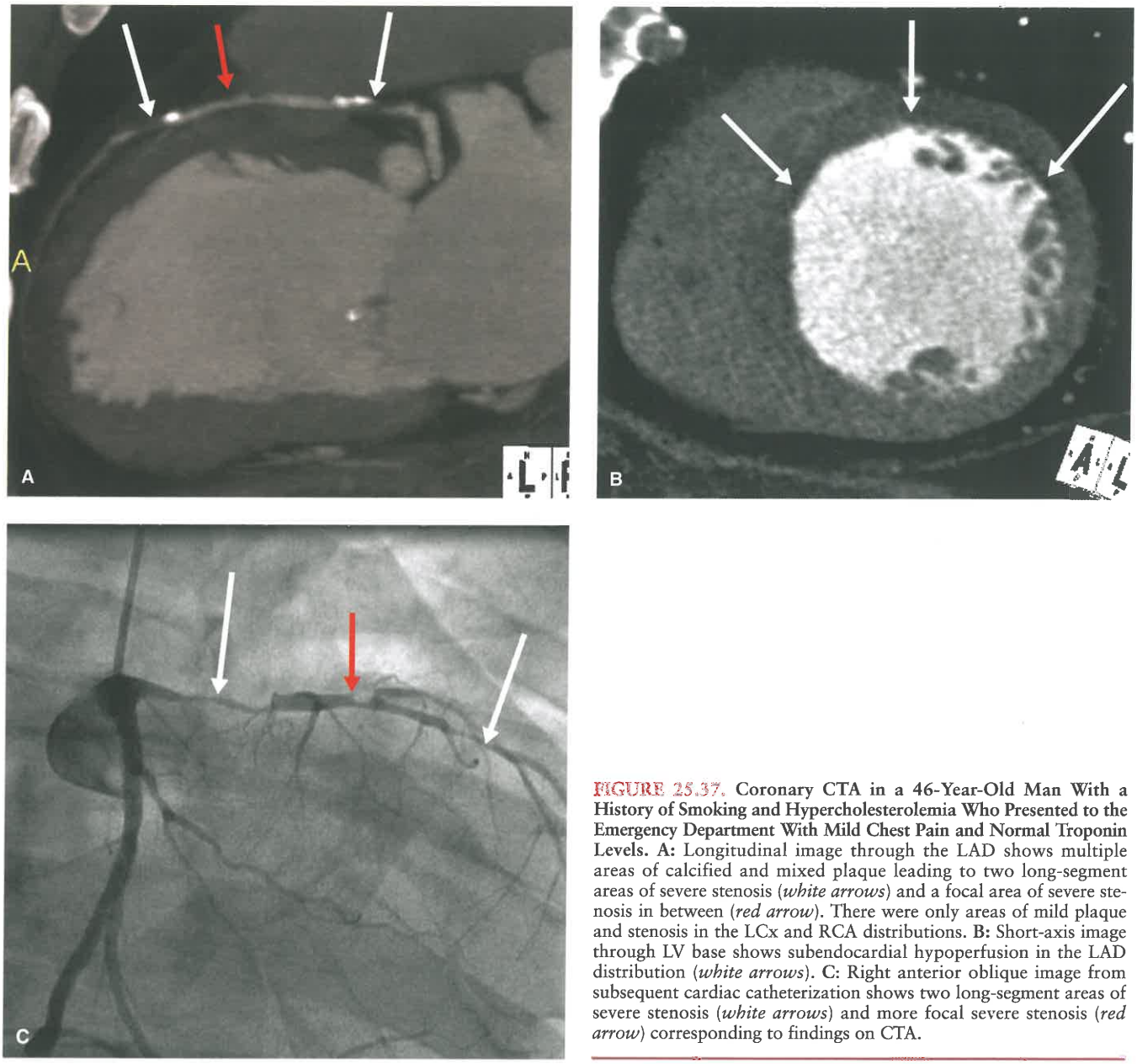

FIGURE 25.37. Coronary CTA in a 46-Year-Old Man With a History of Smoking and Hypercholesterolemia Who Presented to the Emergency Department With Mild Chest Pain and Normal Troponin Levels. A: Longitudinal image through the LAD shows multiple areas of calcified and mixed plaque leading to two long-segment areas of severe stenosis (*white arrows*) and a focal area of severe stenosis in between (*red arrow*). There were only areas of mild plaque and stenosis in the LCx and RCA distributions. **B:** Short-axis image through LV base shows subendocardial hypoperfusion in the LAD distribution (*white arrows*). **C:** Right anterior oblique image from subsequent cardiac catheterization shows two long-segment areas of severe stenosis (*white arrows*) and more focal severe stenosis (*red arrow*) corresponding to findings on CTA.

distribution of the coronary arteries, myocardial infarct or ischemia will manifest as a wall motion abnormality localized to a specific vascular territory (Figs. 25.39 to 25.41). Depending on the severity of injury, the wall motion can be described as hypokinetic (reduced contractility), akinetic (no contractility), or dyskinetic (paradoxical movement). This distribution of motion abnormality due to infarct can significantly vary given the heterogeneity of coronary artery distribution and location of obstruction. In most patients, the anterior and anteroseptal segments at the base and mid-cavity levels are supplied by the LAD and its branches (Fig. 25.39). Portions of the anterolateral segments can be supplied by diagonal branches from the LAD depending on a patient's anatomy. The LCx and its OM branches will often supply the inferolateral segment but can also supply portions of the anterolateral and/or inferior segments depending on size and dominance (Fig. 25.40). At the apical level, in many patients, the anterior, lateral, and septal segments are supplied by the LAD distribution and the inferior segment is supplied by the PDA. The cardiac apex (segment 17) is usually supplied by the LAD. If the left main is involved, myocardium in both the LAD and LCx distributions will be affected. If a patient is right dominant, the RCA and its PDA and PLV branches will supply the inferoseptal, inferior, and possibly portions of the inferolateral segments at the base and mid-cavity levels, depending on the size and extent of the PLV branch (Figs. 25.41 and 25.42). Wall motion abnormalities corresponding to one of these vascular distributions is a good clue that the underlying etiology is coronary in origin. Even in multivessel disease where wall motion abnormalities may involve multiple territories, the degree of dysfunction and extent of myocardial injury often varies between territories allowing for diagnosis.

Other signs of myocardial injury due to infarct depend on the acuity of the injury. In the setting of a recent MI, there may be increased subendocardial signal intensity in the myocardium on T2-weighted sequences secondary to myocardial edema. These T2-weighted sequences are usually performed using a double inversion recovery, "black blood," preparation used to null the signal in the blood pool or a triple inversion recovery preparation to null both the signal in blood

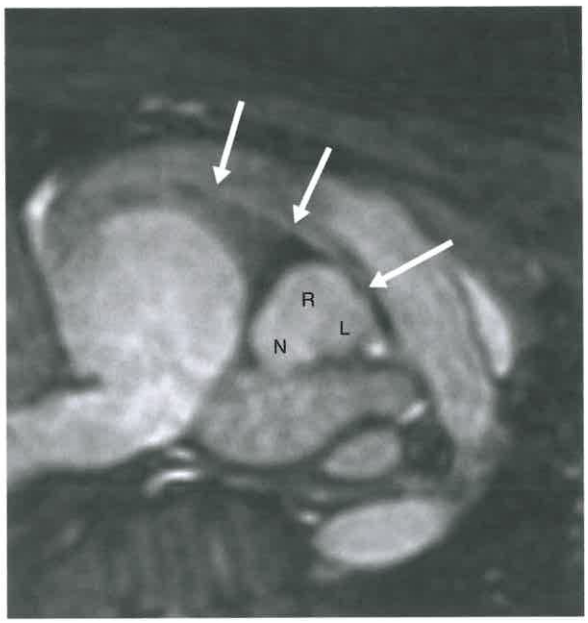

FIGURE 25.38. A 3D SSFP MRA of the coronary arteries in a 15-year-old boy with chest pain and an abnormal echocardiogram show an inter-arterial course of the RCA which is narrowed proximally (*white arrows*). Although there are advocates for using coronary MRA to assess for atherosclerotic coronary artery disease, most institutions use cMRA to assess for anomalous coronary arteries and coronary artery aneurysms, especially in the pediatric population or those with severe contrast allergies (*R, L, N* = right, left, and noncoronary sinuses, respectively).

and fat (Fig. 25.41; Video 25.4). It should also be mentioned that myocardial edema can sometimes be seen on an SSFP sequence due to its T2/T1 weighting (Fig. 25.42). Microvascular obstruction (MO), another sign of an acute or subacute infarct, is discussed below.

As the myocardium remodels after an infarct, the affected segments can become thinned depending on the severity of injury. This thinning is often associated with worsening function as the affected segments may become akinetic or dyskinetic (Figs. 25.39, Videos 25.2 and 25.3; 25.40 and 25.42). While myocardial thinning often suggests scarring, it does not necessarily indicate nonviable myocardium, which is assessed using delayed enhancement imaging.

First-pass myocardial perfusion imaging is performed during the administration of intravenous gadolinium, which is a contrast medium that shortens T1 relaxation. In areas of ischemia and infarct, subendocardial predominant hypoperfusion is often seen corresponding to the region(s) of wall motion abnormality identified in cine imaging (Fig. 25.41).

Ten to 15 minutes after the injection of gadolinium, delayed images are usually acquired. Although gadolinium is an extracellular agent, it can accumulate in areas where there has been acute myocyte injury secondary to cell membrane disruption seen in acute or subacute infarct (Figs. 25.41 and 25.42) or it can accumulate in areas with an increased interstitial space, such as in an area of scarring as seen in chronic infarct (Figs. 25.39 and 25.40). This retained gadolinium leads to T1 shortening in the affected areas. To highlight the effects of gadolinium, the delayed enhancement sequences are performed at a set inversion time which is used to null the signal of the normal myocardium. As myocardial injury from an infarct starts in the subendocardial region of the ventricle and extends outward, subendocardial late gadolinium enhancement corresponding to a coronary artery segmental territory is indicative of myocardial infarction. The extent of LGE is directly related to the likelihood of successful revascularization with bypass grafting or percutaneous coronary intervention. Subendocardial enhancement measuring <50% of the regional myocardial thickness is associated with functional recovery after revascularization (Fig. 25.41), while areas of >50% transmural LGE extent are much less likely to respond to revascularization (Figs. 25.39, 25.40, and 25.42). If the infarct involves the entire thickness of the myocardium, it is called a transmural infarct. Large transmural infarcts, especially those in the LAD distribution, are more likely to cause left ventricular aneurysms (Fig. 25.39). Due to alterations of blood flow, anterior left ventricular aneurysms have a propensity to develop thrombus which can subsequently embolize.

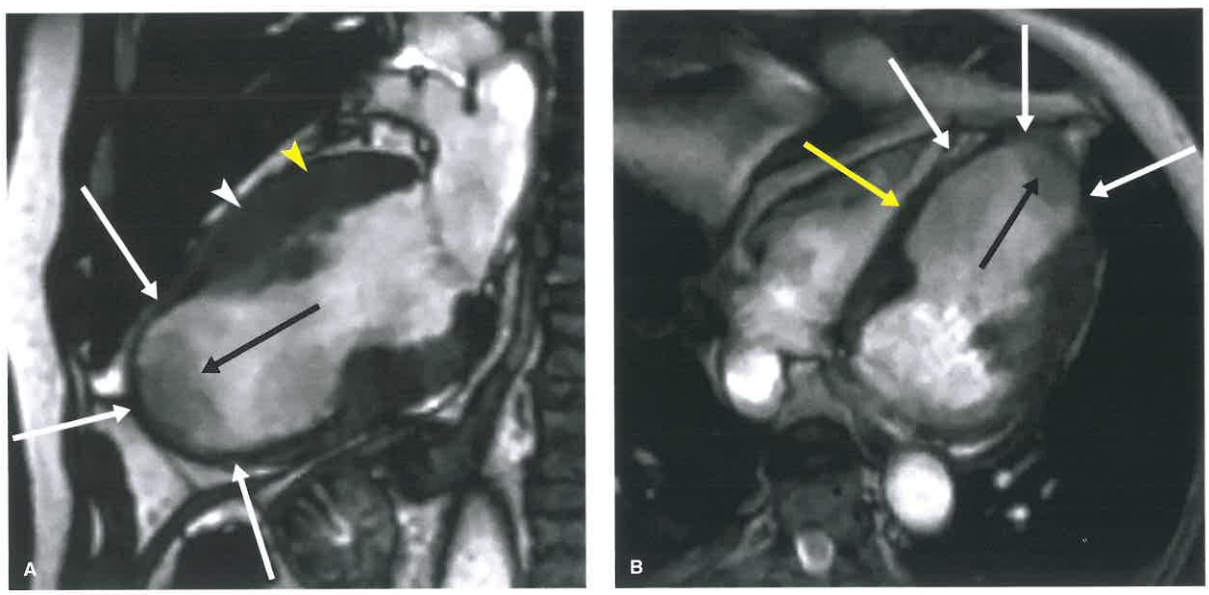

FIGURE 25.39. **Transmural LAD Territory Infarct With Apical Aneurysm and Thrombus in a 77-Year-Old Man. A, B:** 2-chamber (A) and 4-chamber (B) images from a cine SSFP sequences demonstrate thinning of all the apical segments of the left ventricle (*white arrows*) which were also dyskinetic. The anteroseptal segment at the mid-cavity level was also thinned and akinetic (*yellow arrow*). The anterior segments at the mid-cavity level (*white arrowhead*, A) and base (*yellow arrowhead*) were hypokinetic. There is a low-signal mass in the left ventricular apex consistent with a thrombus (*black arrows*).

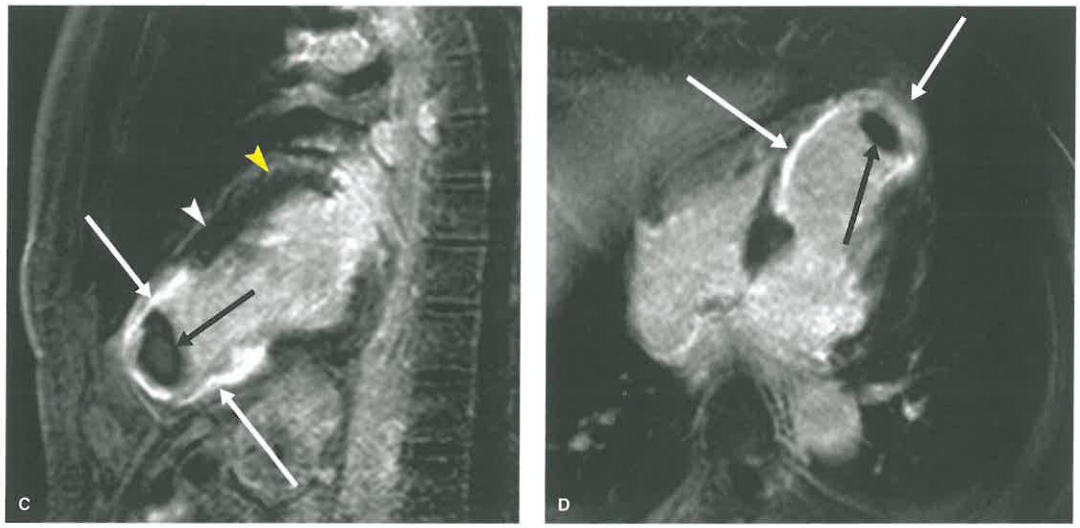

FIGURE 25.39. (*Continued*) **C, D:** 2-chamber (C) and 4-chamber (D) gadolinium delayed enhancement images shows transmural enhancement of the dyskinetic to akinetic segments (*white arrows*) consistent with non-viable myocardium. However, the hypokinetic anterior segments at the mid-cavity (*white arrowhead*) and base (*yellow arrowhead*) show no enhancement and could improve function with revascularization. The apical thrombus (*black arrows*) is devoid of signal.

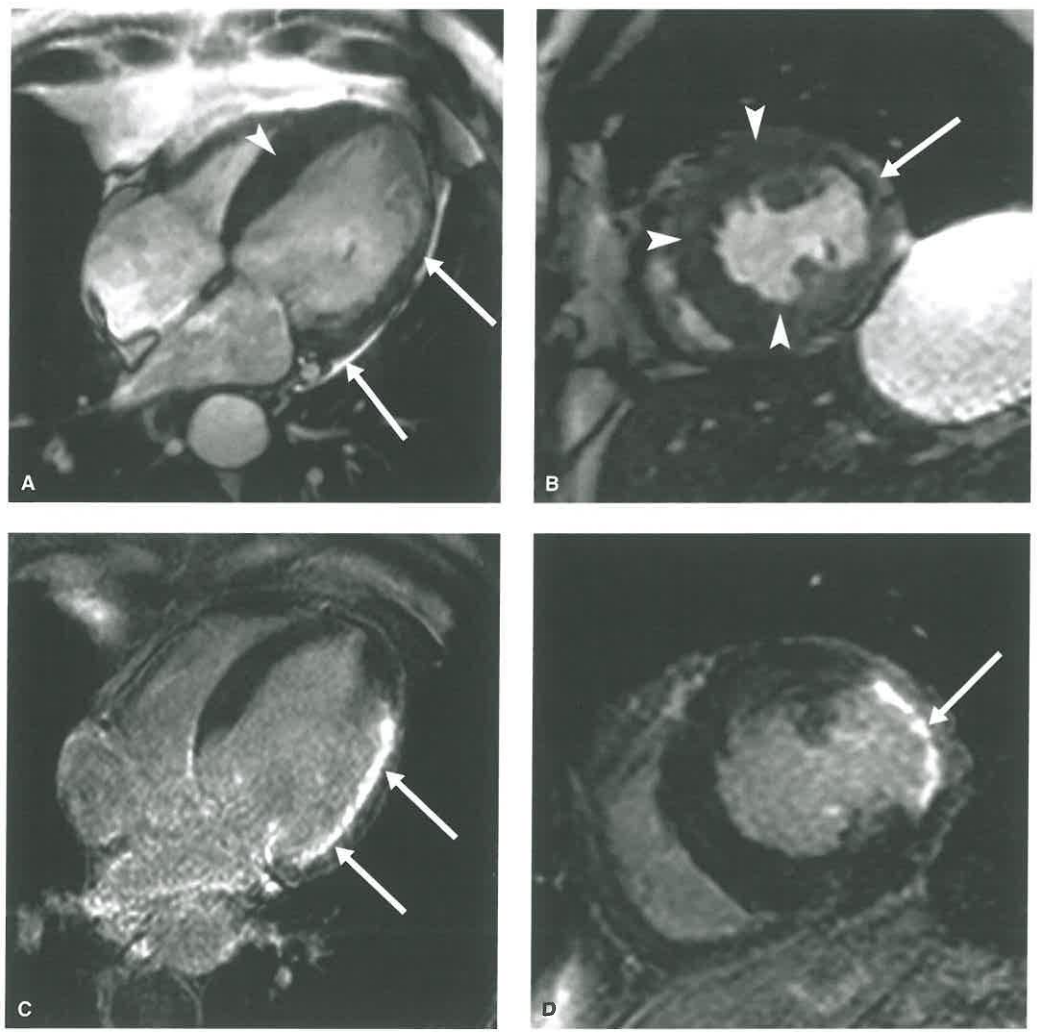

FIGURE 25.40. **Left Circumflex Territory Infarct (LCx) in a 67-Year-Old Patient With History of Myocardial Infarction. A, B:** 4-chamber (A) and mid-cavity short axis (B) images from SSFP cine sequences show thinning of the anterolateral segments and portions of the inferolateral segments of the left ventricle at the base and mid-cavity levels (*white arrows*). These segments were also akinetic. **C, D:** 4-chamber (C) and mid-cavity short-axis (D) LGE images show transmural enhancement in the akinetic segments (*white arrows*) consistent with non-viable myocardium. Although this territory could potentially be supplied by a large diagonal branch from the LAD, cardiac catheterization confirmed a proximal LCx occlusion in this right coronary artery dominant patient.

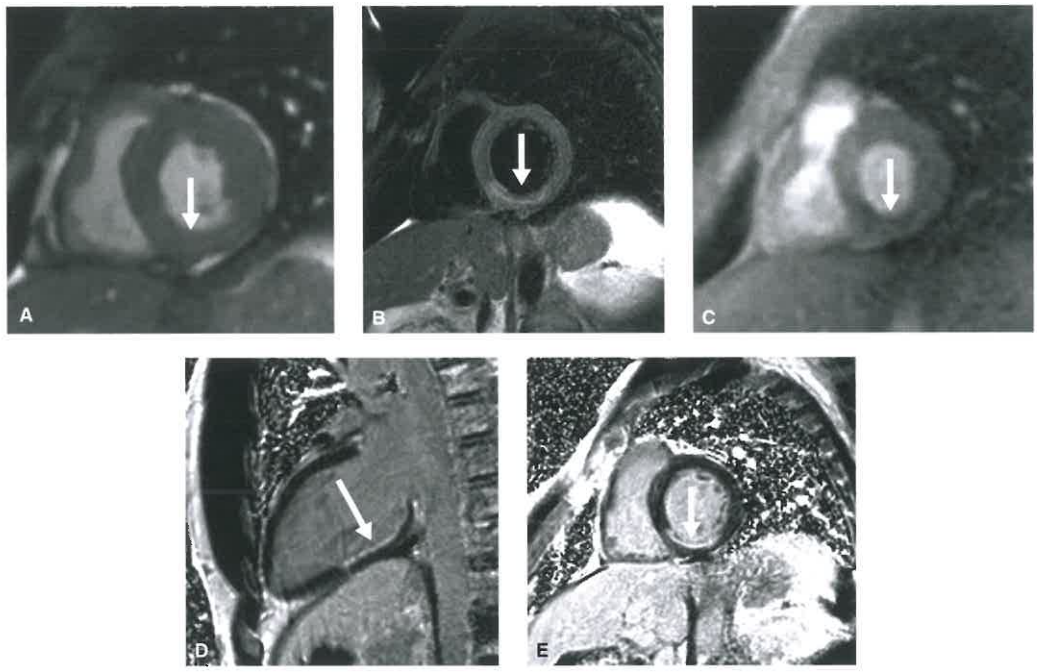

FIGURE 25.41. **Subacute Myocardial Infarct in the RCA Distribution in a Patient With Right Coronary Artery Dominance but a Relatively Small Posterior Left Ventricular Branch. A:** Short axis image through the base of the left ventricle from a cine SSFP sequence shows mild thinning of the inferior segment which was hypokinetic (*white arrow*). **B:** T2-weighted triple inversion recovery image through the base shows subendocardial high signal due to edema from recent infarct (*white arrow*). **C:** Short-axis perfusion image at the base shows subendocardial hypoperfusion which can be seen with ischemia or infarct (*white arrow*). **D, E:** Short-axis (D) and two-chamber (E) LGE images show thin subendocardial delayed enhancement (*white arrows*) involving the inferior segment at the base and mid-cavity level consistent with infarct. Given that the enhancement is less than 50% of the myocardial thickness, the underlying myocardium is considered viable, and the patient is likely to recover function after reperfusion.

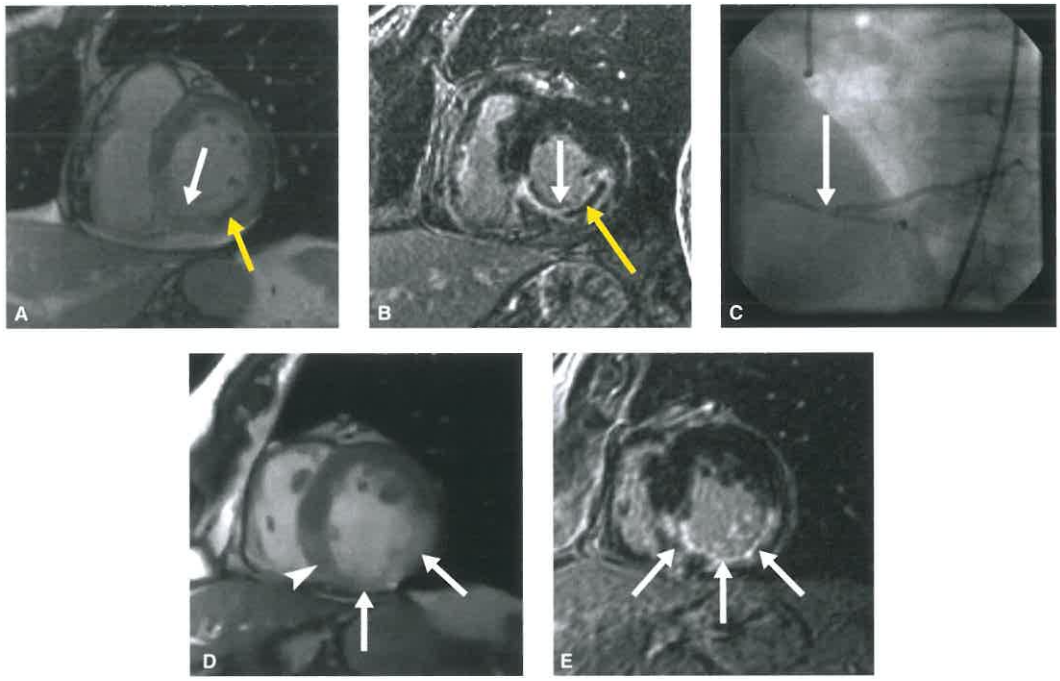

FIGURE 25.42. **Subacute Myocardial Infarct in the RCA Distribution in a Patient With Right Coronary Artery Dominance and a Large Posterior Lateral Ventricular Branch. A:** Short axis image from a SSFP cine sequence at the mid-cavity level obtained after intravenous contrast injection shows severe edema and early enhancement of the inferoseptal, inferior, and inferolateral segments (*white arrows*). An areas of low signal within these segments represents a focus of microvascular obstruction (MVO, *yellow arrow*). **B:** Short axis LGE image at the same level shows near transmural infarct (*white arrow*) with a large focus of MVO (*yellow arrow*). **C:** Right anterior oblique image from a cardiac catheterization performed one week earlier shows the severe stenosis in the distal RCA (*white arrow*). The PLV is a large branch which explain the extent of injury to the inferolateral segment. **D:** Image from a cine SSFP sequence 6 months later at the same level as (**A**) shows thinning the inferior and inferolateral segments (*white arrows*) which were akinetic. Although the inferoseptal segment appears thicker, it was also akinetic (*white arrowhead*). **E:** Short axis LGE image 6-months later at the same level as (C) shows thinning and near transmural enhancement of the affected segments (*white arrow*) with associated functional decline consistent with abnormal left ventricular remodeling. The MVO has resolved.

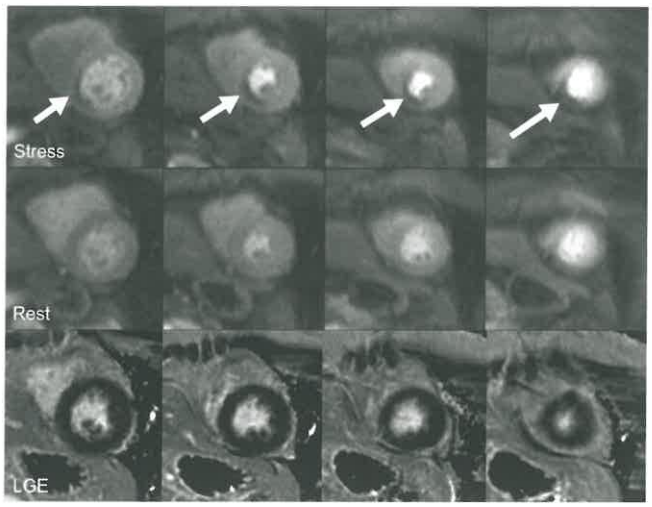

FIGURE 25.43. **Cardiac MRI Stress Test.** Stress imaging (first row) shows hypoperfusion of the inferior segments from the base to the apex (*white arrows*) which resolves on rest imaging (middle row). Delayed-enhancement imaging demonstrates no evidence of infarct. Subsequent cardiac catheterization showed a severe PDA stenosis requiring stent placement.

Microvascular obstruction (MO) is a specific form of myocardial reperfusion injury that occurs after therapy for an acute MI. The cause of MO is multifactorial and is thought to be caused by the release of cytotoxic mediators that cause local vasoconstriction, capillary endothelial swelling, myocardial edema, hemorrhage, and microembolization of atherosclerotic debris. The exact timing of MO is unclear, but it occurs nearly immediately after reperfusion, can increase in size and extent up to 48 hours after injury, and can be seen up to 1 month after reperfusion. Given severity of the injury, gadolinium cannot diffuse into the areas of MO. Therefore, on LGE imaging, the areas of MO appear as dark, nonenhanced areas surrounded by enhancing infarct (Fig. 25.42). When present, MO is an indicator of severe myocardial injury that often leads to adverse left ventricular remodeling and is an independent predictor of worse patient outcomes.

MRI in the Assessment of Ischemia. Stress MR imaging using SSFP and perfusion imaging can be used to distinguish ischemia from prior myocardial infarction. Rest followed by stress MR imaging is often performed using pharmacologic agents such as adenosine because of the challenges of introducing MR-compatible equipment into the MR imaging suite to perform physiologic stress testing. Similar to other imaging-based stress techniques, segmental, subendocardial hypoperfusion on stress imaging which returns to normal on rest imaging suggests myocardial ischemia (Fig. 25.43). Since LGE is performed, stress MRI can also assess for areas of scarring from infarct. Although not as widely used, recent studies of stress MR imaging demonstrate sensitivity of 0.82 to 0.92 and specificity of 0.75 to 0.94, suggesting that stress MR imaging is as good as conventional approaches of stress imaging.

TREATMENT OF CORONARY ARTERY DISEASE

Coronary Stents

Compared to coronary angioplasty alone, coronary stents create a larger residual diameter and reduce the rate of restenosis. In-stent restenosis occurs in up to 35% of patients with bare-metal stents and up to 10% of patients with drug-eluting stents. In addition to restenosis, stent thrombosis, sometimes fatal, can occur.

Coronary CTA can be used to evaluate for stent occlusion and restenosis (Fig. 25.44). In general, stents ≥3 mm in diameter are more likely to be evaluable. However, evaluation can

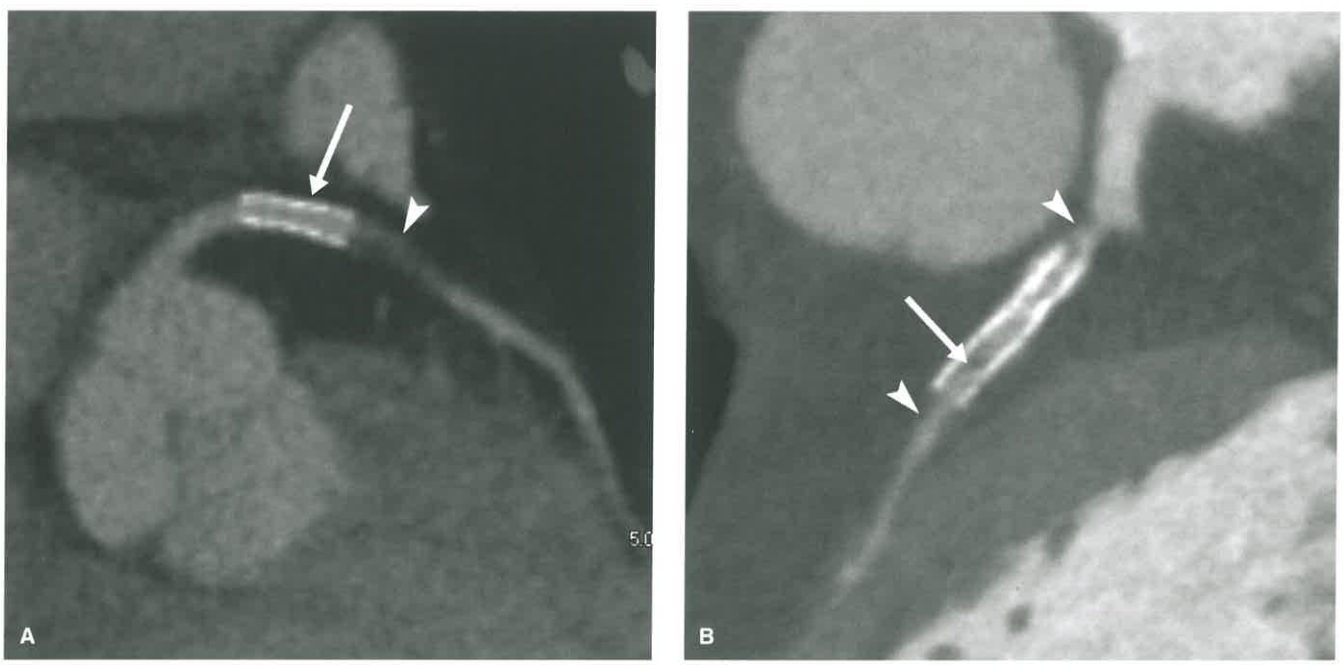

FIGURE 25.44. **Stent Evaluation Using Coronary CTA. A:** Curved MPR image through the LAD in a 59-year-old woman with chest pain shows a patent stent (*white arrow*) with no in-stent restenosis. However, there is a severe stenosis distal to the stent (*white arrowhead*). **B:** Curved MPR through the LAD in a 66-year-old man demonstrates an area of hypoattenuation in the distal aspect of the stent due to in-stent restenosis (*white arrow*). In addition, there are moderate stenoses in the LAD proximal and distal to the stent (*white arrowheads*). While the negative predictive value for CTA in assessing in-stent restenosis is high, the positive predictive value is low.

be difficult given the metal artifact created by the struts of the stent. In one large meta-analysis using 64-slice CT, the overall NPV of CT was high at 97% but the PPV was very low at 53%. In general, thin-slice image reconstruction with a sharp kernel, small field of view, and use of wide windows is recommended to optimize stent visualization. Low-kV imaging, which will often reduce contrast dose and increase the attenuation of contrast, will increase the metallic artifact associated with stents.

Coronary Artery Bypass Grafts

Since its introduction in 1962, coronary artery bypass grafting (CABG) has remained the definitive treatment for advanced CAD. Patency of the coronary grafts is critical for long-term survival and depends on the type of graft that is used. In the VA Cooperative Study, internal mammary grafts had a patency rate of 85% after 10 years, as compared to 61% for saphenous vein grafts (SVG). ECG-gated CTA is an excellent tool for assessing the patency of coronary artery bypass grafts. Since internal mammary artery grafts originate from the subclavian artery, it is important to perform an ECG-gated evaluation of the entire chest. In most instances, the left internal mammary artery (LIMA) is used due to its proximity to the left ventricular apex. This vessel is dissected from the parasternal region and anastomosed to the LAD due to its higher patency rate (Fig. 25.45). Due to its high patency rate, the LIMA graft usually appears as a well-opacified, small-caliber vessel coursing inferiorly through the anterior mediastinum and eventually into the epicardial fat where it will anastomose with the distal LAD. Although stenosis is most common near the distal anastomosis, it can occur anywhere along the vessel.

SVG are harvested from the legs and attached as a free graft to the ascending aorta and coronary artery distal to the site of obstruction. A rightward-directed SVG usually is directed toward the RCA distribution and will anastomose with the PDA. Leftward-directed SVG can anastomose with various vessels including the LAD, diagonal, OM, and LCx arteries (Fig. 25.46). While an SVG can supply a single vessel, in some instances a sequential or "jump graft" will be used where a single vein is anastomosed to multiple adjacent vessels, such as a diagonal and OM vessel. When evaluating a SVG, it is important to evaluate the entire graft for patency and signs of opacification distal to the graft, which suggests graft patency. When an SVG does thrombose, all that may be visible is a small vascular outpouching from the ascending aorta, a finding that is sometimes referred to as the "nubbin sign" (Fig. 25.46).

It is also important to evaluate for complications such as SVG aneurysm (SVGA) (Fig. 25.47). Aneurysms of saphenous venous grafts after coronary artery bypass are not uncommon, but the exact incidence is unknown. Nearly 70% of SVGA occur more than 10 years after initial CABG, while approximately 10% occur within the first 5 years. The size widely varies, but in case reports, the average SVGA exceeded 6 cm in diameter and SVG-to-RCA distribution grafts are most common. The pathophysiology leading to SVGA is primarily due to accelerated atherosclerosis. While most cases are asymptomatic, SVGAs can become symptomatic due to thrombosis, rupture, fistulization with adjacent structures, or compression of adjacent structures. Both surgical and percutaneous approaches have been used to treat aneurysms with variable success.

Pseudoaneurysms of either internal mammary or saphenous vein bypass grafts are a rare complication. They most commonly occur due to graft breakdown and dehiscence (Fig. 25.48). Compared to SVGAs, they tend to occur at the proximal or distal anastomotic sites and within the first weeks to months after surgery. Treatment is usually surgical.

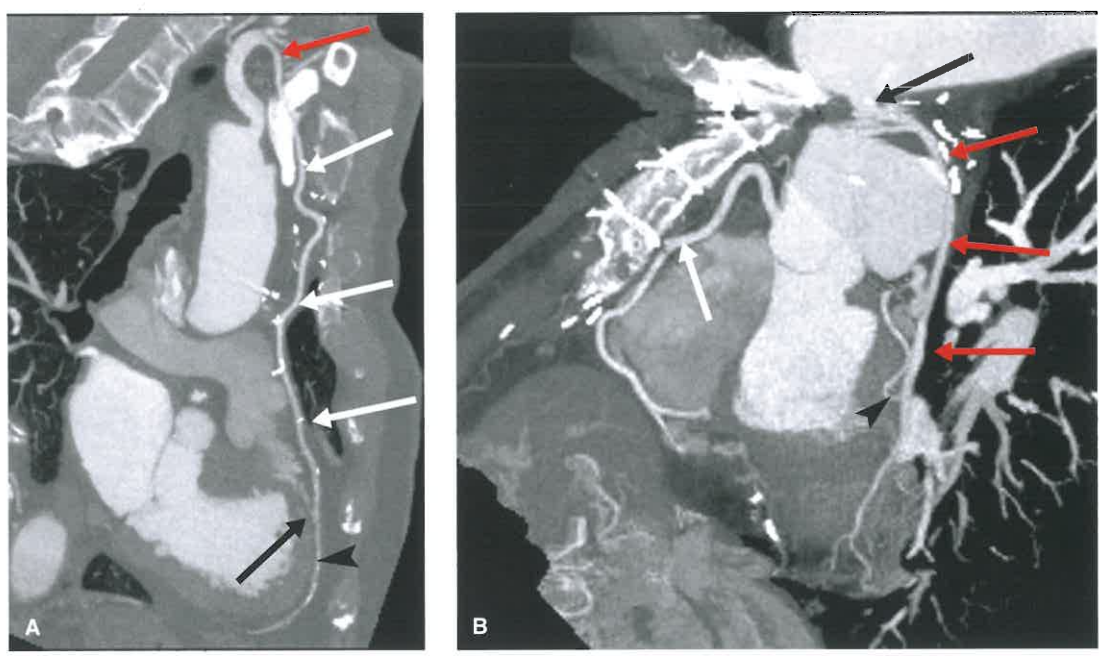

FIGURE 25.45. **Bypass Graft Assessment in a 60-Year-Old Man Status Post Coronary Artery Bypass. A:** Curved parasagittal maximum-intensity projection (MIP) image from a gated CTA of the chest shows a patent left internal mammary artery (LIMA) bypass graft (*white arrows*) arising from the left subclavian artery (*red arrow*) and anastomosing with the distal LAD (*black arrow*). There is good opacification of the LAD distal to the anastomosis (*black arrowhead*). **B:** Curved MIP shows a patent saphenous vein graft (*red arrows*) arising from the aorta (*black arrow*) and anastomosing with the second obtuse marginal artery (*black arrowhead*). The RCA (*white arrow*) is without significant disease. ECG-gated CTA of the thorax is an excellent tool for assessing the patency of coronary artery bypass grafts.

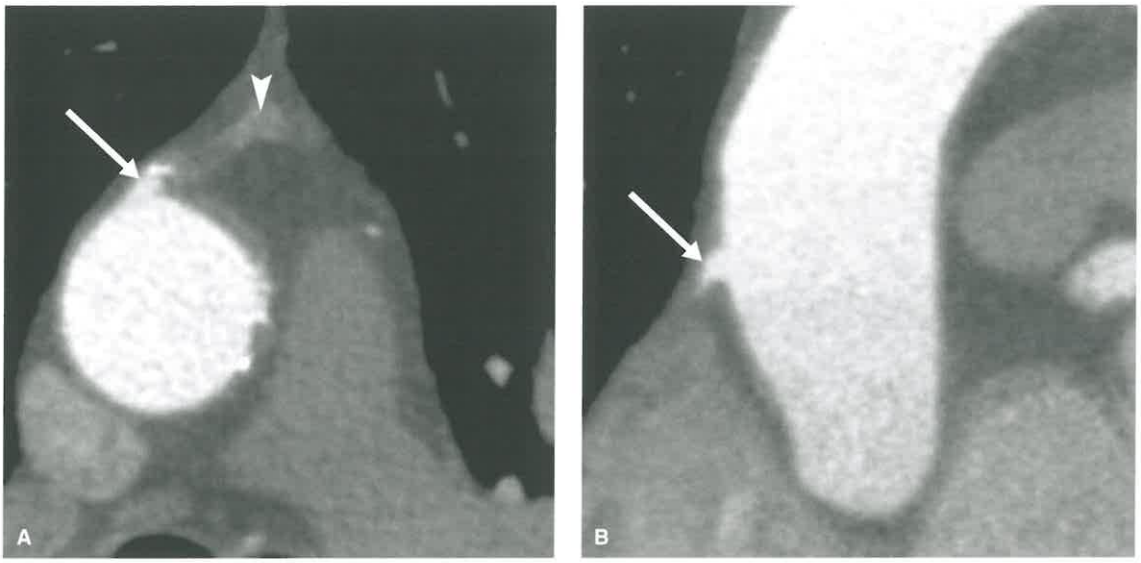

FIGURE 25.46. **Saphenous Vein Graft (SVG) Occlusions on Coronary CTA in a 64-Year-Old Woman With a History of CABG. A:** Axial oblique image through the ascending aorta shows a small outpouching from the aorta (*white arrow*) with a subtle thrombosed saphenous vein to diagonal bypass graft (*white arrowhead*). **B:** The patient's saphenous vein to posterior descending artery bypass graft (*white arrow*) was also thrombosed. The appearance of these small outpouchings from the aorta has been referred to as the "nubbin sign."

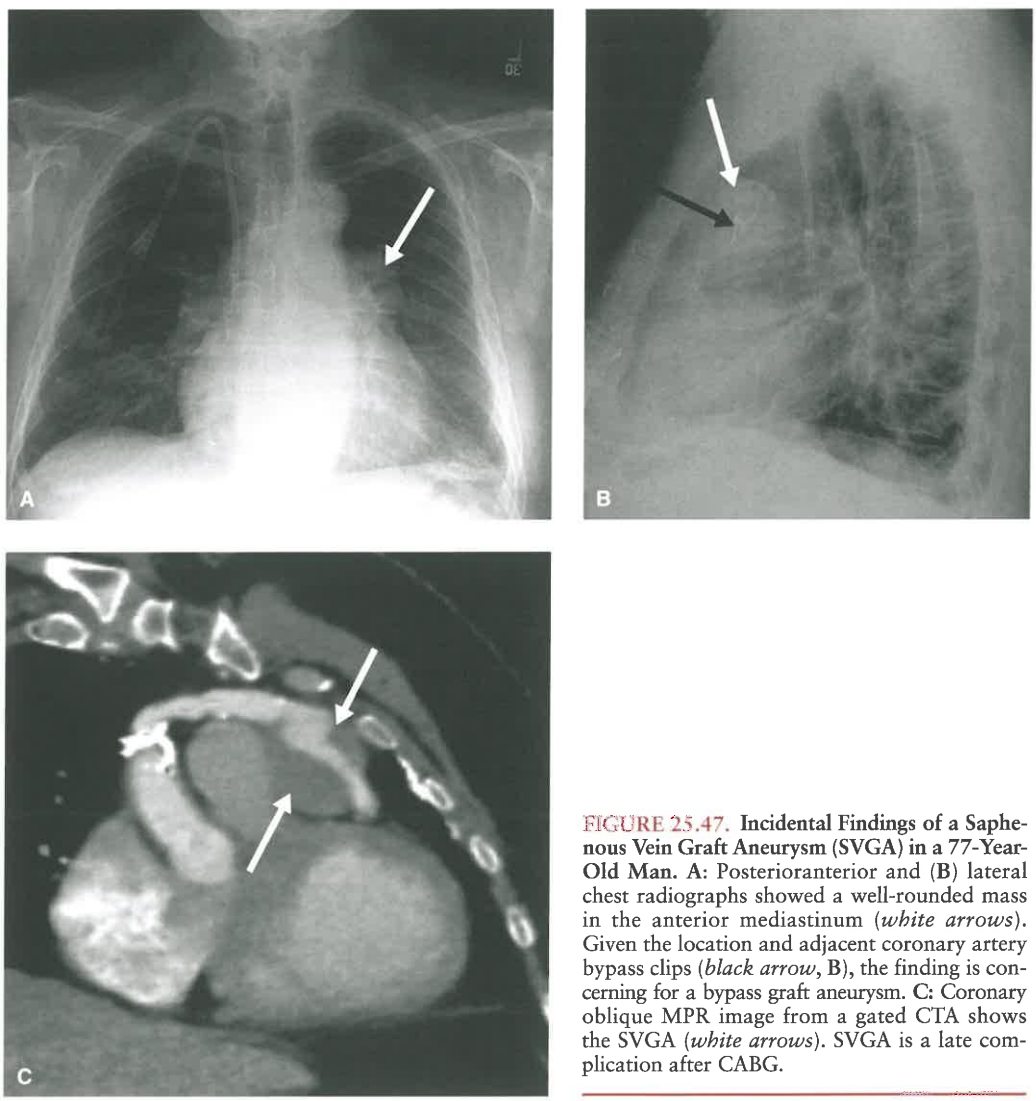

FIGURE 25.47. **Incidental Findings of a Saphenous Vein Graft Aneurysm (SVGA) in a 77-Year-Old Man. A:** Posterioranterior and (**B**) lateral chest radiographs showed a well-rounded mass in the anterior mediastinum (*white arrows*). Given the location and adjacent coronary artery bypass clips (*black arrow*, **B**), the finding is concerning for a bypass graft aneurysm. **C:** Coronary oblique MPR image from a gated CTA shows the SVGA (*white arrows*). SVGA is a late complication after CABG.

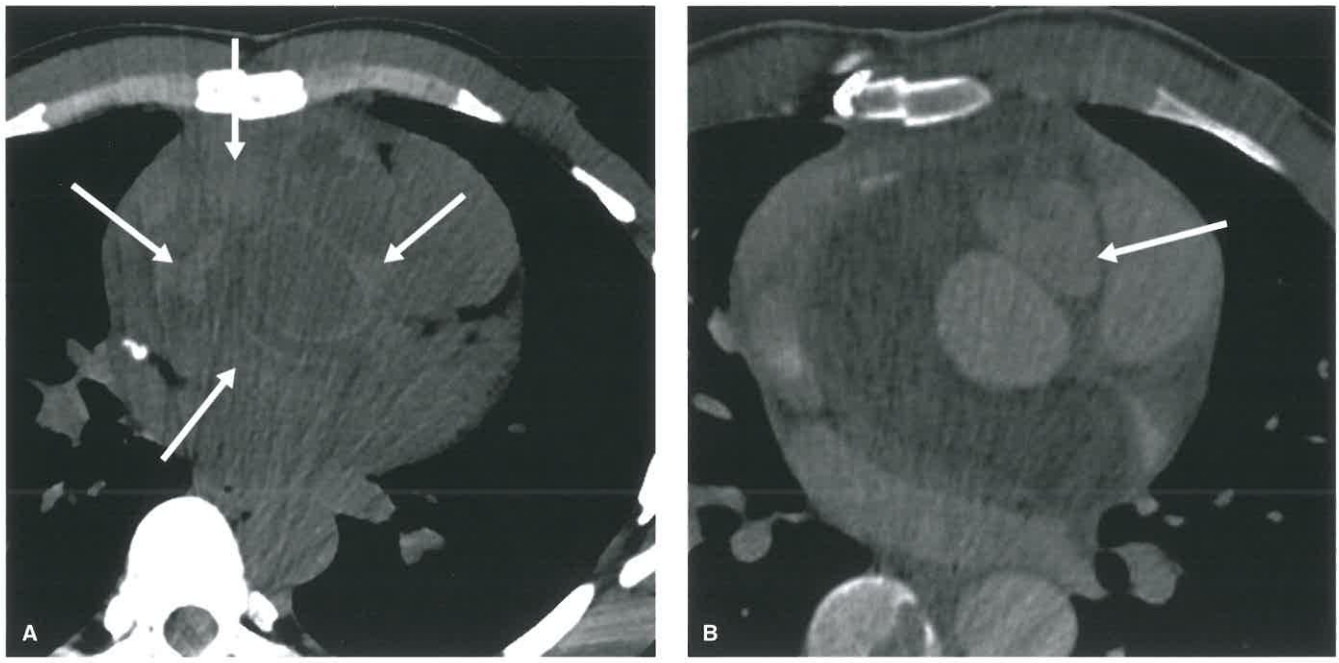

FIGURE 25.48. **Saphenous Venous Graft Pseudoaneurysm in a 40-Year-Old Man With Worsening Chest Pain 2 Days After Surgery. A:** Axial noncontrast image from a gated CTA shows heterogeneous fluid collection surrounding the aortic root with areas of high attenuation suggestive of blood products (*white arrows*). **B:** Axial image at the same level after administration of contrast shows contrast extravasation near the right sinus of Valsalva (*white arrow*). The patient underwent redo sternotomy which showed that the RCA saphenous venous graft had dehisced from its aortic anastomosis. Bypass graft pseudoaneurysms are uncommon and usually occur at the anastomotic sites.

CORONARY ARTERY ANEURYSM AND PSEUDOANEURYSM

Coronary artery aneurysm is defined as a segment of the coronary artery that measures more than 1.5 times the adjacent normal coronary artery. Of all of the different etiologies of coronary artery aneurysms, atherosclerotic disease is the most common, accounting for approximately 50% of coronary artery aneurysms diagnosed in adults (Fig. 25.49). The exact incidence is unknown as many atherosclerotic coronary artery aneurysms (ACAA) are detected incidentally.

The most common cause of aneurysms in the pediatric population is Kawasaki disease (KD), which is a systemic small- and medium-vessel vasculitis which occurs in infants and young children (Fig. 25.49). It is the leading cause of acquired childhood heart disease in the United States, and coronary artery aneurysms are a major cause of morbidity in this population. Smaller coronary artery aneurysms may decrease in size or resolve in patients with KD, but giant aneurysms (>8 mm) do not regress and can lead to myocardial infarct or death due to rupture or stenosis/thrombosis. In addition to atherosclerosis and KD, there are many additional causes of coronary artery aneurysms including other vasculitides, connective tissue disease, inflammatory conditions, and fistulas.

Coronary artery pseudoaneurysms are rare and usually iatrogenic due to coronary catheterization (Fig. 25.50). They can also occur from infection, trauma, or even be idiopathic. Due to their risk of rupture, treatments include stenting, coil embolization, or surgical repair with or without bypass grafting.

CORONARY ARTERY DISSECTION

There are three main causes of coronary artery dissection. The most common cause is percutaneous interventions such as angioplasty, where coronary dissections occur in less than 1% of cases. In most cases, these dissections are limited and can be successfully treated with stent placement. Retrograde extension into the aorta can occur but is uncommon.

Type A aortic dissections involve the ascending aorta and can extend into the aortic root. When the aortic root is involved, obstruction of coronary blood flow can occur via two mechanisms. First, the intimal flap can directly cover the ostium of a coronary artery. Second, the dissection can extend from the aorta into the coronary artery (Fig. 25.51). Both causes can lead to coronary occlusion. When there is suspicion for a type A dissection, ECG gating should be used so the aortic root and coronary arteries can be evaluated in detail.

Spontaneous coronary artery dissections (SCAD) are the third main cause of coronary dissection. This process usually affects younger women and although considered rare, in one institution, SCAD was the cause of MI in 24% of women less than 50 years of age undergoing cardiac catheterization. The occurrence of SCAD is most commonly associated with pregnant or postpartum patients and in patients undergoing intense exercise (Fig. 25.52). However, other etiologies include fibromuscular dysplasia, connective tissue disorders, systemic inflammatory conditions, hormonal therapy, and even intense emotional stress. Almost all patients present with ACS, and treatment depends on the extent of the dissection and can range from conservative therapy to CABG.

MECHANICAL COMPLICATIONS OF MYOCARDIAL INFARCTION

Left ventricular free wall rupture, ventricular septal rupture (VSR), and papillary muscle rupture are three catastrophic mechanical complications after acute myocardial infarction. Although timing can vary, these entities usually occur within the

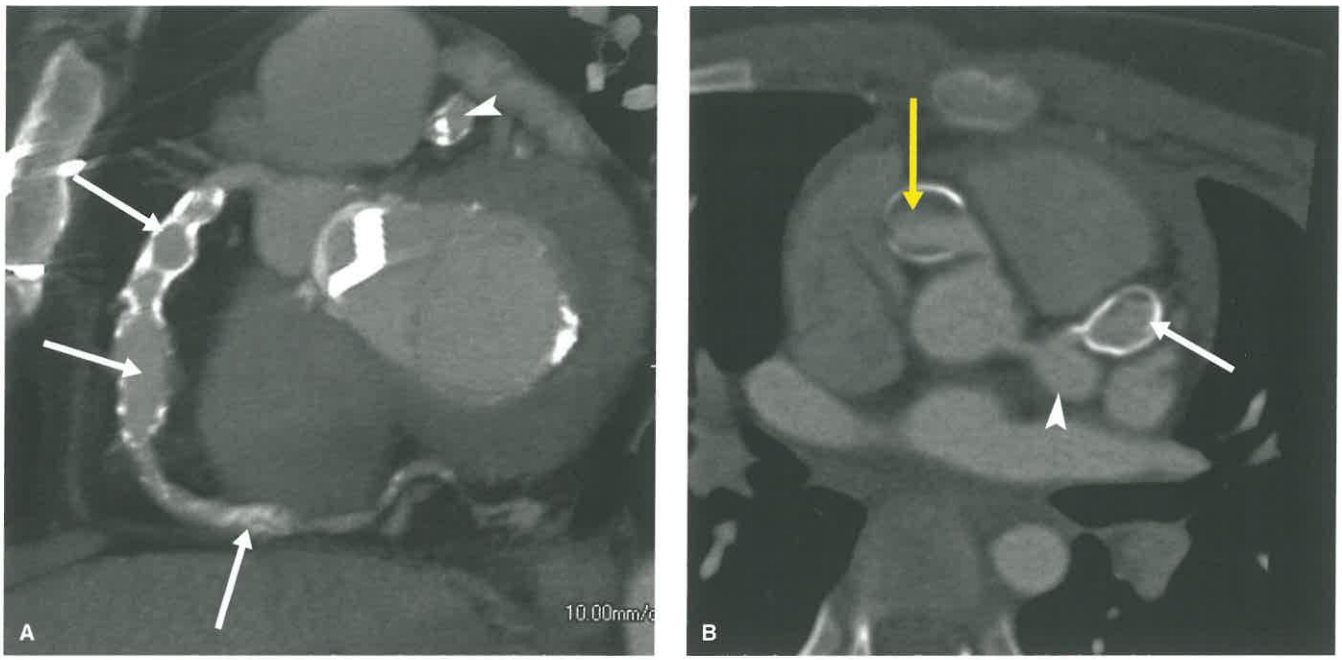

FIGURE 25.49. **Coronary Artery Aneurysms. A:** Sagittal oblique MPR image through the RCA in an 81-year-old man shows extensive atherosclerotic disease with multiple RCA aneurysms (*white arrows*). The partially visualized LAD is also aneurysmal (*white arrowhead*). **B:** Axial oblique image in a 5-year-old girl with a history of Kawasaki disease shows large aneurysms of the proximal LAD (*white arrow*), LCx (*white arrowhead*), and RCA (*yellow arrow*). Atherosclerotic disease is the most common cause of coronary artery aneurysms in adults, while Kawasaki disease is the most common cause in children.

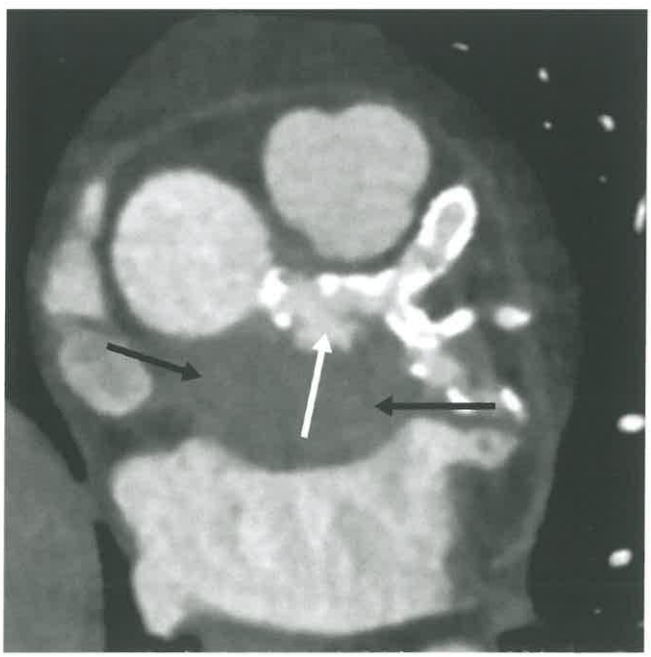

FIGURE 25.50. Axial oblique MPR in a 68-year-old man with diffusely aneurysmal and calcified coronary arteries shows a defect in the posterior wall of the left main coronary artery (LM, *white arrow*) with surrounding hematoma (*black arrows*). The patient had undergone cardiac catheterization the day prior, and the injury was thought to be iatrogenic. However, a large hole in the LM was confirmed during surgery which required repair.

first week after infarction and may be lethal if not quickly recognized and treated. These entities may be lethal if not quickly recognized and treatment usually involves surgical repair.

A left ventricular pseudoaneurysm, also referred to as left ventricular free wall rupture, occurs when there is a tear through the myocardium which is contained by adjacent pericardium or scar tissue (Fig. 25.53). Myocardial infarct is the most common cause, but other etiologies include cardiac surgery, trauma, and infection. Although many patients die immediately after the rupture, a patient can survive if the rupture is contained. It is important to differentiate true aneurysms and pseudoaneurysm due to different treatments and outcomes. Although most pseudoaneurysms involve the inferior and inferolateral walls and most true aneurysms occur in the anterior walls, both pathologies can occur in both regions and thus location alone does not make the diagnosis. In general, true aneurysms have a broad neck (Fig. 25.54). Pseudoaneurysms usually have a narrow neck that has a diameter less than 50% of that of the maximal diameter of the distal outpouching.

Although quite rare, a VSR occurs in 0.17% to 0.31% of patients 1 to 5 days after an acute MI. Septal rupture can develop after transmural infarct and leads to a left-to-right shunt which can lead to complete hemodynamic collapse (Fig. 25.55). Even with surgical intervention, overall operative mortality is 42.9%.

While the left ventricular anteromedial papillary muscle has a dual blood supply, the posteromedial papillary muscle of the LV is usually supplied only by the PDA. Therefore, the posteromedial papillary muscle is 6 to 12 times more likely to rupture after MI. Rupture usually occurs 2 to 7 days after an acute MI, and if left untreated, up to 50% of patients can die within 24 hours and 94% at 2 months. If this muscle ruptures, the posterior leaflet of the mitral valve becomes incompetent causing severe mitral regurgitation which is often directed rightward, more notably toward the right superior pulmonary vein (RSPV). As pressures in the RSPV increase, there is decreased pulmonary venous return causing asymmetric right-sided edema, which is most pronounced in the right upper lung (Fig. 25.56).

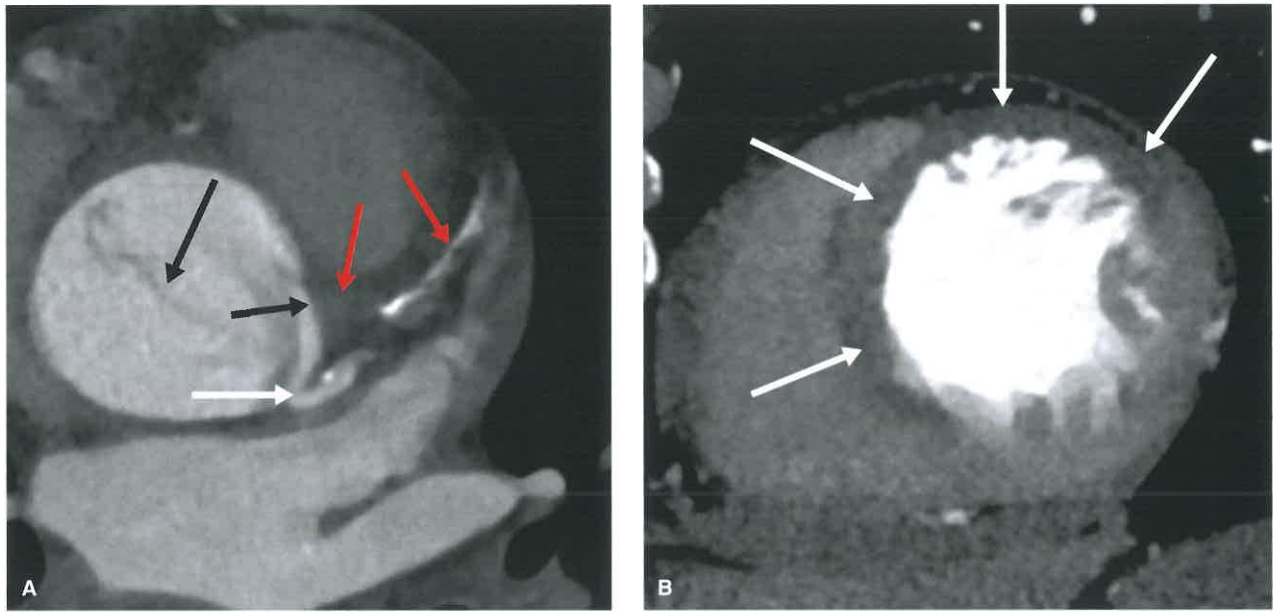

FIGURE 25.51. **Type A Aortic Dissection Extending Into the LAD in a 55-Year-Old Man With Hypertension. A:** Axial oblique image through the aortic root shows the type A dissection. The dissection flap (*black arrows*) extended into and occluded the left anterior descending coronary artery (*red arrows*). Fortunately for the patient, he had an uncommon coronary artery variant where the LAD and LCx have separate ostia from the left sinus of Valsalva (absent left main). Because of this, the LCx remained patent (*white arrow*). **B:** Short-axis image through the base of the heart shows transmural infarction of the anterior, anteroseptal, and inferoseptal segments due to LAD occlusion (*white arrows*). The LCx and RCA territories show normal perfusion.

ADDITIONAL CONSIDERATIONS

As modern scanners continue to improve their spatial and temporal resolution, aspects of cardiac pathology can be assessed on nearly any routine chest or abdomen CT (Fig. 25.57). While ECG gating is necessary to assess the coronary arteries in detail, in many instances, the coronary ostia can be visualized on routine scans, even those that are performed without intravenous contrast. Similarly, myocardial perfusion defects or other sequelae of infarct, such as fatty metaplasia or calcification of the myocardium, left ventricular aneurysm, and thrombus are often visible. Therefore, routine evaluation of the heart should be added to one's search pattern as part of the assessment on any chest or abdomen CT.

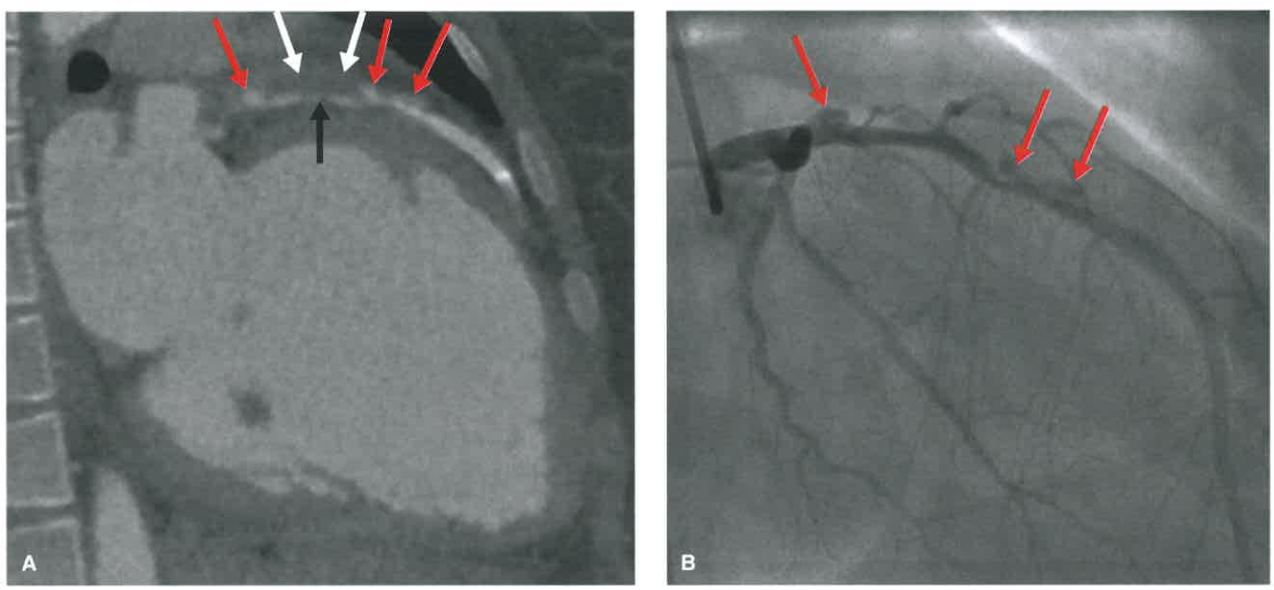

FIGURE 25.52. **A 24-Year-Old Woman With a History of Spontaneous Coronary Artery Dissection (SCAD) With Subsequent Stenting After Giving Birth to Her Second Child. A:** Longitudinal image through the proximal LAD shows soft tissue attenuation surrounding the vessel corresponding to the thrombosed false lumen (*white arrows*) which compresses true lumen (*black arrow*). There are a few areas of contrast outpouchings that represent persistent filling of the false lumen (*red arrows*). The left ventricle is severely dilated and the patient's ejection fraction was 31%. **B:** Right anterior oblique image from a coronary catheterization shows areas of persistent filling of the false lumen (*red arrows*) corresponding to the findings on CTA.

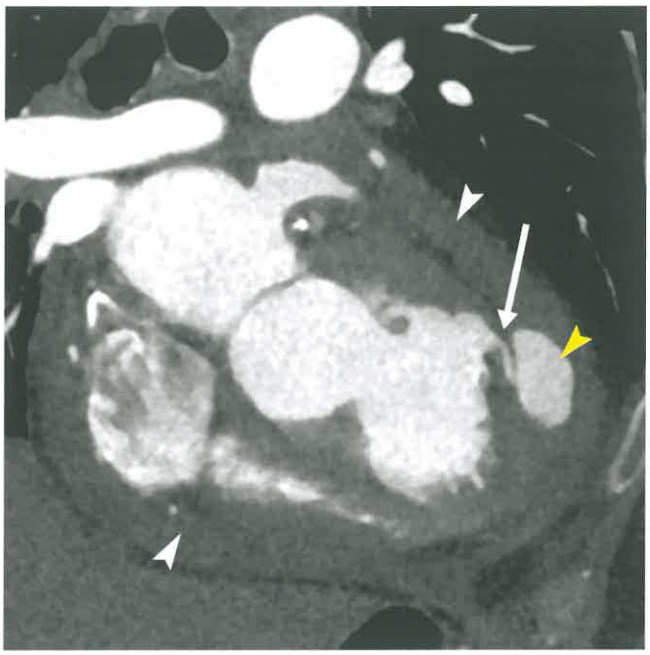

FIGURE 25.53. **Retrospectively Gated Coronary CTA in a 61-Year-Old Man With Recent LAD Territory Infarct.** Coronal oblique reformat shows the narrow-necked tear through the left ventricular myocardium (*white arrow*) with distal pseudoaneurysm (*yellow arrowhead*) and surrounding hemopericardium (*white arrowheads*). Pseudoaneurysm formation represents a myocardial rupture contained by surrounding pericardium or scarring. Although most common in the inferior segments, they can occur anteriorly as well.

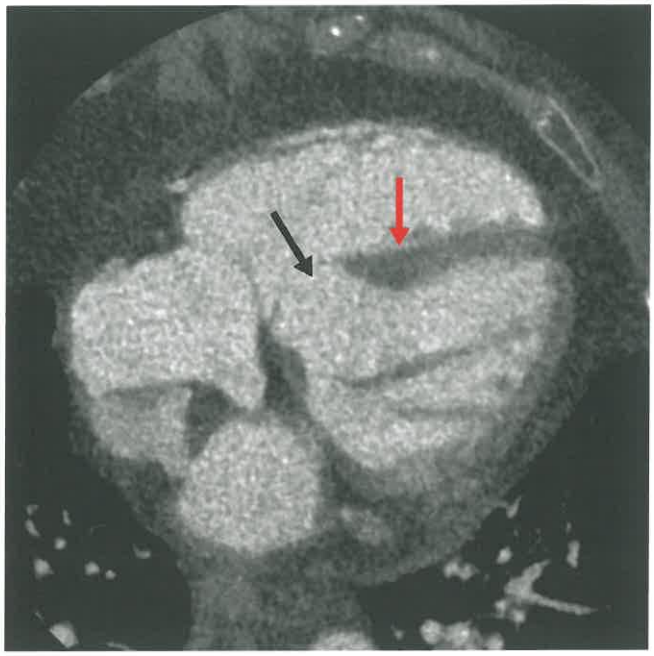

FIGURE 25.55. Four-chamber image from a cardiac CTA in a 78-year-old woman who developed worsening shortness of breath 4 days after LAD territory infarct shows a large defect in the anteroseptal segment at the base (*black arrow*) consistent with a postinfarct ventricular septal rupture. The edges of the myocardium adjacent to the rupture are hypoattenuating due to the infarct (*red arrow*). The patient died 1 day later.

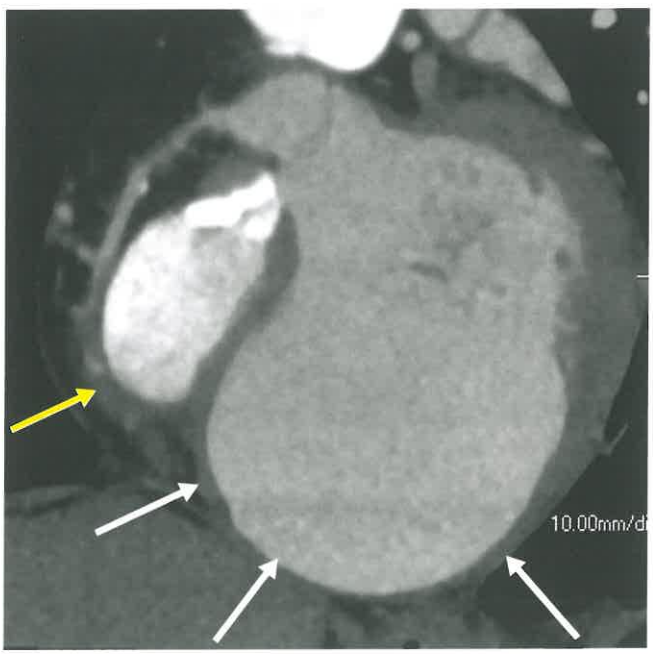

FIGURE 25.54. Coronal oblique image through the base of the heart in a 61-year-old man shows a large wide-mouthed true aneurysm of the inferior wall which is surrounded by thin myocardium (*white arrows*). The RCA is chronically occluded (*yellow arrow*). Due to its large size, the patient underwent surgery with mesh repair of the inferior wall. Pathology confirmed the imaging diagnosis of an aneurysm. Although aneurysms are more common in the anterior segments, they can occur inferiorly as well.

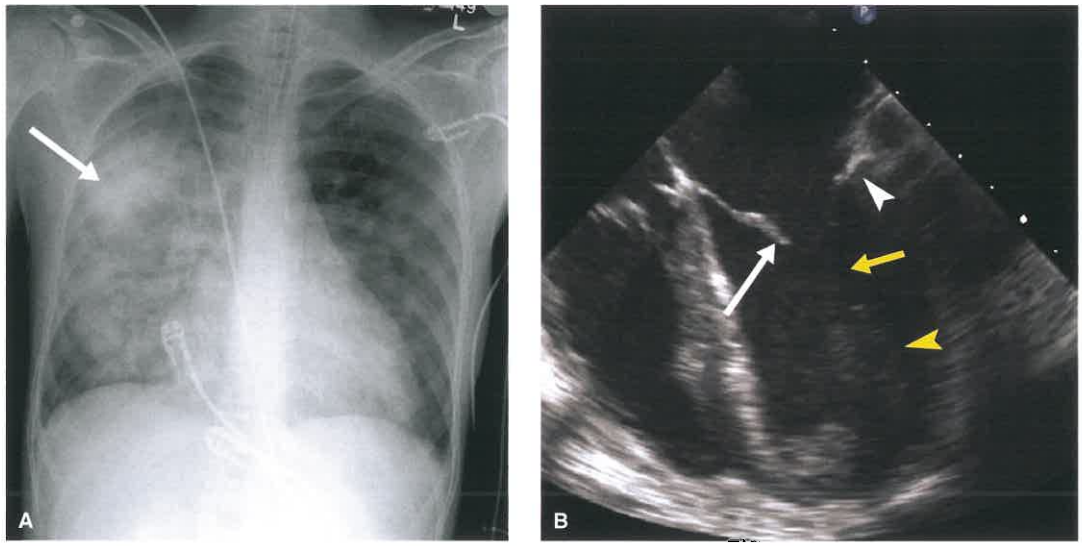

FIGURE 25.56. **A:** AP radiograph in a 49-year-old woman with severely worsening dyspnea 7 days after RCA territory infarct shows asymmetric edema most notably in the right upper lung (*white arrow*). **B:** Four-chamber view from a bedside echocardiogram shows a flair posterior leaflet (*white arrow*) leading to severe acute mitral regurgitation. The anterior leaflet (*white arrow*) is still attached to its chordae (*yellow arrow*) and papillary muscle (*yellow arrowhead*). The rightward and superior direction of the jet causes this characteristic finding. The patient underwent emergent surgery to repair the valve.

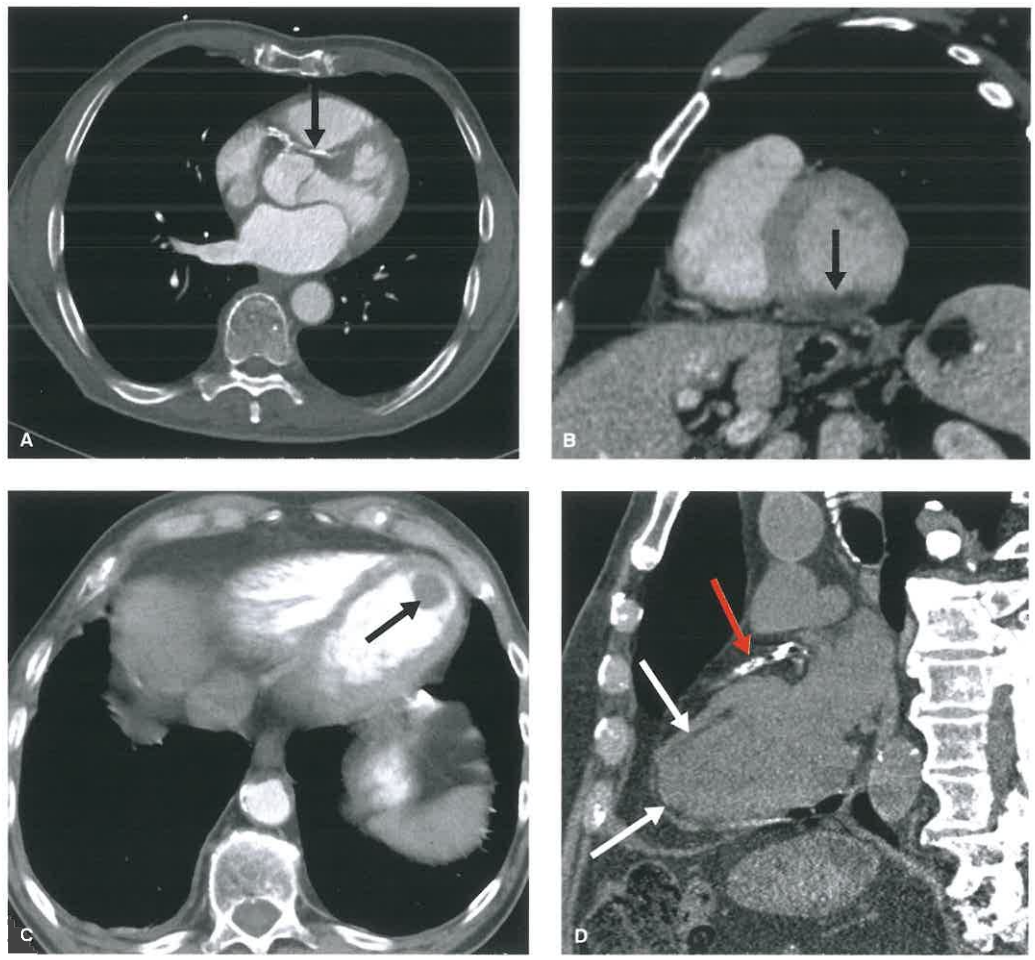

FIGURE 25.57. **Cardiac Findings on Nongated CT Examinations. A:** Axial image from a contrast-enhanced CT of the chest in a 71 year old shows an anomalous septal course of the left anterior descending coronary artery (*black arrow*). **B:** Short-axis reconstruction from a routine chest CT in a 59-year-old man shows subendocardial hypoperfusion in the inferior wall (*black arrow*). The patient had an acute MI 2 days prior. **C:** Axial image from an abdominal CT in a 63-year-old woman shows a left ventricular apical aneurysm with a 2-cm thrombus (*black arrow*). The finding was unknown to the primary team. **D:** Sagittal oblique MPR in an 85-year-old woman shows extensive calcification in the LAD territory (*red arrow*) with subendocardial fatty metaplasia of the associated myocardium due to old infarct (*white arrows*). Fatty metaplasia is a common finding and can be visualized with or without contrast.

Suggested Readings

Abdel-Aty H, Zagrosek A, Schulz-Menger J, et al. Delayed enhancement and T2-weighted cardiovascular magnetic resonance imaging differentiate acute from chronic myocardial infarction. *Circulation* 2004;109(20):2411–2416.

Achenbach S, Giesler T, Ropers D, et al. Detection of coronary artery stenoses by contrast-enhanced, retrospectively electrocardiographically-gated, multislice spiral computed tomography. *Circulation* 2001;103(21):2535–2538.

Alford WC Jr, Stoney WS, Burrus GR, Frist RA, Thomas CS Jr. Recognition and operative management of patients with arteriosclerotic coronary artery aneurysms. *Ann Thorac Surg* 1976;22(4):317–321.

Angelini P. Coronary artery anomalies: an entity in search of an identity. *Circulation* 2007;115(10):1296–1305.

Arnaoutakis GJ, Zhao Y, George TJ, Sciortino CM, McCarthy PM, Conte JV. Surgical repair of ventricular septal defect after myocardial infarction: outcomes from the Society of Thoracic Surgeons National Database. *Ann Thorac Surg* 2012;94(2):436–443; discussion 443–444.

Bastarrika G, Lee YS, Huda W, Ruzsics B, Costello P, Schoepf UJ. CT of coronary artery disease. *Radiology* 2009;253(2):317–338.

Bazzocchi G, Romagnoli A, Sperandio M, Simonetti G. Evaluation with 64-slice CT of the prevalence of coronary artery variants and congenital anomalies: a retrospective study of 3,236 patients. *Radiol Med* 2011;116(5):675–689.

Bourassa MG, Butnaru A, Lesperance J, Tardif JC. Symptomatic myocardial bridges: overview of ischemic mechanisms and current diagnostic and treatment strategies. *J Am Coll Cardiol* 2003;41(3):351–359.

Budoff MJ, Dowe D, Jollis JG, et al. Diagnostic performance of 64-multidetector row coronary computed tomographic angiography for evaluation of coronary artery stenosis in individuals without known coronary artery disease: results from the prospective multicenter ACCURACY (Assessment by Coronary Computed Tomographic Angiography of Individuals Undergoing Invasive Coronary Angiography) trial. *J Am Coll Cardiol* 2008;52(21):1724–1732.

Burke AP, Kolodgie FD, Farb A, Weber D, Virmani R. Morphological predictors of arterial remodeling in coronary atherosclerosis. *Circulation* 2002;105(3):297–303.

Cademartiri F, La Grutta L, Malago R, et al. Prevalence of anatomical variants and coronary anomalies in 543 consecutive patients studied with 64-slice CT coronary angiography. *Eur Radiol* 2008;18(4):781–791.

Chen YF, Chien TM, Chen CW, Lin CC, Lee CS. Double right coronary artery or split right coronary artery? *Int J Cardiol* 2012;154(3):243–245.

Coelho-Filho OR, Rickers C, Kwong RY, Jerosch-Herold M. MR myocardial perfusion imaging. *Radiology* 2013;266(3):701–715.

Cook CM, Petraco R, Shun-Shin MJ, et al. Diagnostic accuracy of computed tomography-derived fractional flow reserve: a systematic review. *JAMA Cardiol* 2017;2(7):803–810.

Cowles RA, Berdon WE. Bland-White-Garland syndrome of anomalous left coronary artery arising from the pulmonary artery (ALCAPA): a historical review. *Pediatr Radiol* 2007;37(9):890–895.

Cury RC, Abbara S, Achenbach S, et al. CAD-RADS: Coronary Artery Disease – Reporting and Data System. An expert consensus document of the Society of Cardiovascular Computed Tomography (SCCT), the American College of Radiology (ACR) and the North American Society for Cardiovascular Imaging (NASCI). Endorsed by the American College of Cardiology. *J Am Coll Radiol* 2016;13(12 Pt A):1458–1466. e9.

Daoud AS, Pankin D, Tulgan H, Florentin RA. Aneurysms of the coronary artery. Report of ten cases and review of literature. *Am J Cardiol* 1963;11:228–237.

Dash D. Complications of coronary intervention: abrupt closure, dissection, perforation. *Heart Asia* 2013;5(1):61–65.

de Agustin JA, Marcos-Alberca P, Hernandez-Antolin R, et al. Collateral circulation from the conus coronary artery to the anterior descending coronary artery: assessment using multislice coronary computed tomography. *Rev Esp Cardiol* 2010;63(3):347–351.

Detrano R, Guerci AD, Carr JJ, et al. Coronary calcium as a predictor of coronary events in four racial or ethnic groups. *N Engl J Med* 2008;358(13):1336–1345.

Dodge JT Jr, Brown BG, Bolson EL, Dodge HT. Lumen diameter of normal human coronary arteries. Influence of age, sex, anatomic variation, and left ventricular hypertrophy or dilation. *Circulation* 1992;86(1):232–246.

Duarte R, Cisneros S, Fernandez G, et al. Kawasaki disease: a review with emphasis on cardiovascular complications. *Insights Imaging* 2010;1(4):223–231.

Eckart RE, Scoville SL, Campbell CL, et al. Sudden death in young adults: a 25-year review of autopsies in military recruits. *Ann Intern Med* 2004;141(11):829–834.

Erol C, Seker M. The prevalence of coronary artery variations on coronary computed tomography angiography. *Acta Radiol* 2012;53(3):278–284.

Farb A, Burke AP, Tang AL, et al. Coronary plaque erosion without rupture into a lipid core. A frequent cause of coronary thrombosis in sudden coronary death. *Circulation* 1996;93(7):1354–1363.

Ferencik M, Ropers D, Abbara S, et al. Diagnostic accuracy of image postprocessing methods for the detection of coronary artery stenoses by using multidetector CT. *Radiology* 2007;243(3):696–702.

Fischman DL, Leon MB, Baim DS, et al. A randomized comparison of coronary-stent placement and balloon angioplasty in the treatment of coronary artery disease. Stent Restenosis Study Investigators. *N Engl J Med* 1994;331(8):496–501.

Frances C, Romero A, Grady D. Left ventricular pseudoaneurysm. *J Am Coll Cardiol* 1998;32(3):557–561.

Frazier AA, Qureshi F, Read KM, Gilkeson RC, Poston RS, White CS. Coronary artery bypass grafts: assessment with multidetector CT in the early and late postoperative settings. *Radiographics* 2005;25(4):881–896.

Friedman BM, Dunn MI. Postinfarction ventricular aneurysms. *Clin Cardiol* 1995;18(9):505–511.

Galli A, Lombardi F. Postinfarct left ventricular remodelling: a prevailing cause of heart failure. *Cardiol Res Pract* 2016;2016:2579832.

Garcia MJ, Lessick J, Hoffmann MH; CATSCAN Study Investigators. Accuracy of 16-row multidetector computed tomography for the assessment of coronary artery stenosis. *JAMA* 2006;296(4):403–411.

Goetti R, Feuchtner G, Stolzmann P, et al. Delayed enhancement imaging of myocardial viability: low-dose high-pitch CT versus MRI. *Eur Radiol* 2011;21(10):2091–2099.

Goldman S, Zadina K, Moritz T, et al. Long-term patency of saphenous vein and left internal mammary artery grafts after coronary artery bypass surgery: results from a Department of Veterans Affairs Cooperative Study. *J Am Coll Cardiol* 2004;44(11):2149–2156.

Goldstein JA, Chinnaiyan KM, Abidov A, et al. The CT-STAT (Coronary Computed Tomographic Angiography for Systematic Triage of Acute Chest Pain Patients to Treatment) trial. *J Am Coll Cardiol* 2011;58(14):1414–1422.

Greenland P, Bonow RO, Brundage BH, et al. ACCF/AHA 2007 clinical expert consensus document on coronary artery calcium scoring by computed tomography in global cardiovascular risk assessment and in evaluation of patients with chest pain: a report of the American College of Cardiology Foundation Clinical Expert Consensus Task Force (ACCF/AHA Writing Committee to Update the 2000 Expert Consensus Document on Electron Beam Computed Tomography) developed in collaboration with the Society of Atherosclerosis Imaging and Prevention and the Society of Cardiovascular Computed Tomography. *J Am Coll Cardiol* 2007;49(3):378–402.

Hamirani YS, Wong A, Kramer CM, Salerno M. Effect of microvascular obstruction and intramyocardial hemorrhage by CMR on LV remodeling and outcomes after myocardial infarction: a systematic review and meta-analysis. *JACC Cardiovasc Imaging* 2014;7(9):940–952.

Harris PJ, Behar VS, Conley MJ, et al. The prognostic significance of 50% coronary stenosis in medically treated patients with coronary artery disease. *Circulation* 1980;62(2):240–248.

Hecht HS, Budoff MJ, Berman DS, Ehrlich J, Rumberger JA. Coronary artery calcium scanning: clinical paradigms for cardiac risk assessment and treatment. *Am Heart J* 2006;151(6):1139–1146.

Hobbs RE, Millit HD, Raghavan PV, Moodie DS, Sheldon WC. Coronary artery fistulae: a 10-year review. *Cleve Clin Q* 1982;49(4):191–197.

Hoffmann U, Truong QA, Schoenfeld DA, et al. Coronary CT angiography versus standard evaluation in acute chest pain. *N Engl J Med* 2012;367(4):299–308.

Holmes DR Jr, Leon MB, Moses JW, et al. Analysis of 1-year clinical outcomes in the SIRIUS trial: a randomized trial of a sirolimus-eluting stent versus a standard stent in patients at high risk for coronary restenosis. *Circulation* 2004;109(5):634–640.

Hulten EA, Blankstein R. Pseudoaneurysms of the heart. *Circulation* 2012;125(15):1920–1925.

Hwang JH, Ko SM, Roh HG, et al. Myocardial bridging of the left anterior descending coronary artery: depiction rate and morphologic features by dual-source CT coronary angiography. *Korean J Radiol* 2010;11(5):514–521.

Iemura J, Oku H, Shirotani H. Right coronary artery pseudoaneurysm after blunt injury to the chest. *Heart* 1996;76(1):86.

Ilia R, Rosenshtein G, Weinstein J, Cafri C, Abu-Ful A, Gueron M. Left anterior descending artery length in left and right coronary artery dominance. *Coron Artery Dis* 2001;12(1):77–78.

Javadi MS, Lautamaki R, Merrill J, et al. Definition of vascular territories on myocardial perfusion images by integration with true coronary anatomy: a hybrid PET/CT analysis. *J Nucl Med* 2010;51(2):198–203.

Jeudy J, White CS, Kligerman SJ, et al. Spectrum of coronary artery aneurysms: from the radiologic pathology archives. *Radiographics* 2018;38(1):11–36.

Jones BM, Kapadia SR, Smedira NG, et al. Ventricular septal rupture complicating acute myocardial infarction: a contemporary review. *Eur Heart J* 2014;35(31):2060–2068.

Joshi SD, Joshi SS, Athavale SA. Origins of the coronary arteries and their significance. *Clinics (Sao Paulo)* 2010;65(1):79–84.

Kanza RE, Allard C, Berube M. Cardiac findings on non-gated chest computed tomography: a clinical and pictorial review. *Eur J Radiol* 2016;85(2):435–451.

Kar S, Webel RR. Diagnosis and treatment of spontaneous coronary artery pseudoaneurysm: rare anomaly with potentially significant clinical implications. *Catheter Cardiovasc Interv* 2017;90(4):589–597.

Kashiwagi M, Tanaka A, Kitabata H, et al. Feasibility of noninvasive assessment of thin-cap fibroatheroma by multidetector computed tomography. *JACC Cardiovasc Imaging* 2009;2(12):1412–1419.

Kim PJ, Hur G, Kim SY, et al. Frequency of myocardial bridges and dynamic compression of epicardial coronary arteries: a comparison between computed tomography and invasive coronary angiography. *Circulation* 2009;119(10):1408–1416.

Kim SY, Seo JB, Do KH, et al. Coronary artery anomalies: classification and ECG-gated multi-detector row CT findings with angiographic correlation. *Radiographics* 2006;26(2):317–333; discussion 333–334.

Kim RJ, Wu E, Rafael A, et al. The use of contrast-enhanced magnetic resonance imaging to identify reversible myocardial dysfunction. *N Engl J Med* 2000;343(20):1445–1453.

Kishi S, Giannopoulos AA, Tang A, et al. Fractional flow reserve estimated at coronary CT angiography in intermediate lesions: comparison of diagnostic accuracy of different methods to determine coronary flow distribution. *Radiology* 2018;287(1):76–84.

Kitagawa T, Yamamoto H, Horiguchi J, et al. Characterization of noncalcified coronary plaques and identification of culprit lesions in patients with acute coronary syndrome by 64-slice computed tomography. *JACC Cardiovasc Imaging* 2009;2(2):153–160.

Knaapen M, Koch AH, Koch C, et al. Prevalence of left and balanced coronary arterial dominance decreases with increasing age of patients at autopsy. A postmortem coronary angiograms study. *Cardiovasc Pathol* 2013;22(1):49–53.

Kosar P, Ergun E, Ozturk C, Kosar U. Anatomic variations and anomalies of the coronary arteries: 64-slice CT angiographic appearance. *Diagn Interv Radiol* 2009;15(4):275–283.

Krasuski RA, Magyar D, Hart S, et al. Long-term outcome and impact of surgery on adults with coronary arteries originating from the opposite coronary cusp. *Circulation* 2011;123(2):154–162.

Krishnan B, Cross C, Dykoski R, et al. Intra-atrial right coronary artery and its ablation implications. *JACC Clin Electrophysiol* 2017;3(9):1037–1045.

Kumar A, Beohar N, Arumana JM, et al. CMR imaging of edema in myocardial infarction using cine balanced steady-state free precession. *JACC Cardiovasc Imaging* 2011;4(12):1265–1273.

Kumbhani DJ, Ingelmo CP, Schoenhagen P, Curtin RJ, Flamm SD, Desai MY. Meta-analysis of diagnostic efficacy of 64-slice computed tomography in the evaluation of coronary in-stent restenosis. *Am J Cardiol* 2009;103(12):1675–1681.

Kutty RS, Jones N, Moorjani N. Mechanical complications of acute myocardial infarction. *Cardiol Clin* 2013;31(4):519–531, vii–viii.

Le Breton H, Pavin D, Langanay T, et al. Aneurysms and pseudoaneurysms of saphenous vein coronary artery bypass grafts. *Heart* 1998;79(5):505–508.

Lee BY. Anomalous right coronary artery from the left coronary sinus with an interarterial course: is it really dangerous? *Korean Circ J* 2009;39(5):175–179.

Lee HJ, Hong YJ, Kim HY, et al. Anomalous origin of the right coronary artery from the left coronary sinus with an interarterial course: subtypes and clinical importance. *Radiology* 2012;262(1):101–108.

Lempel JK, Jeudy J, Kligerman SJ, White CS. The nubbin sign. *J Thorac Imaging* 2013;28(3):W42.

Litt HI, Gatsonis C, Snyder B, et al. CT angiography for safe discharge of patients with possible acute coronary syndromes. *N Engl J Med* 2012;366(15):1393–1403.

Lowe JE, Oldham HN Jr, Sabiston DC Jr. Surgical management of congenital coronary artery fistulas. *Ann Surg* 1981;194(4):373–380.

Madhavan MV, Tarigopula M, Mintz GS, Maehara A, Stone GW, Genereux P. Coronary artery calcification: pathogenesis and prognostic implications. *J Am Coll Cardiol* 2014;63(17):1703–1714.

Malagutti P, Nieman K, Meijboom WB, et al. Use of 64-slice CT in symptomatic patients after coronary bypass surgery: evaluation of grafts and coronary arteries. *Eur Heart J* 2007;28(15):1879–1885.

Mandal S, Tadros SS, Soni S, Madan S. Single coronary artery anomaly: classification and evaluation using multidetector computed tomography and magnetic resonance angiography. *Pediatr Cardiol* 2014;35(3):441–449.

Masci PG, Bogaert J. Post myocardial infarction of the left ventricle: the course ahead seen by cardiac MRI. *Cardiovasc Diagn Ther* 2012;2(2):113–127.

Miller JA, Anavekar NS, El Yaman MM, Burkhart HM, Miller AJ, Julsrud PR. Computed tomographic angiography identification of intramural segments in anomalous coronary arteries with interarterial course. *Int J Cardiovasc Imaging* 2012;28(6):1525–1532.

Miller JM, Rochitte CE, Dewey M, et al. Diagnostic performance of coronary angiography by 64-row CT. *N Engl J Med* 2008;359(22):2324–2336.

Min JK, Leipsic J, Pencina MJ, et al. Diagnostic accuracy of fractional flow reserve from anatomic CT angiography. *JAMA* 2012;308(12):1237–1245.

Mohara J, Konishi H, Kato M, Misawa Y, Kamisawa O, Fuse K. Saphenous vein graft pseudoaneurysm rupture after coronary artery bypass grafting. *Ann Thorac Surg* 1998;65(3):831–832.

Mohlenkamp S, Hort W, Ge J, Erbel R. Update on myocardial bridging. *Circulation* 2002;106(20):2616–2622.

Motoyama S, Kondo T, Sarai M, et al. Multislice computed tomographic characteristics of coronary lesions in acute coronary syndromes. *J Am Coll Cardiol* 2007;50(4):319–326.

Motoyama S, Sarai M, Harigaya H, et al. Computed tomographic angiography characteristics of atherosclerotic plaques subsequently resulting in acute coronary syndrome. *J Am Coll Cardiol* 2009;54(1):49–57.

Mowatt G, Cook JA, Hillis GS, et al. 64-Slice computed tomography angiography in the diagnosis and assessment of coronary artery disease: systematic review and meta-analysis. *Heart* 2008;94(11):1386–1393.

Musiani A, Cernigliaro C, Sansa M, Maselli D, De Gasperis C. Left main coronary artery atresia: literature review and therapeutical considerations. *Eur J Cardiothorac Surg* 1997;11(3):505–514.

Narula J, Achenbach S. Napkin-ring necrotic cores: defining circumferential extent of necrotic cores in unstable plaques. *JACC Cardiovasc Imaging* 2009;2(12):1436–1438.

Opolski MP, Pregowski J, Kruk M, et al. The prevalence and characteristics of intra-atrial right coronary artery anomaly in 9,284 patients referred for coronary computed tomography angiography. *Eur J Radiol* 2014;83(7):1129–1134.

Pejkovic B, Krajnc I, Anderhuber F, Kosutic D. Anatomical aspects of the arterial blood supply to the sinoatrial and atrioventricular nodes of the human heart. *J Int Med Res* 2008;36(4):691–698.

Pena E, Nguyen ET, Merchant N, Dennie C. ALCAPA syndrome: not just a pediatric disease. *Radiographics* 2009;29(2):553–565.

Polacek P, Kralove H. Relation of myocardial bridges and loops on the coronary arteries to coronary occulsions. *Am Heart J* 1961;61:44–52.

Raff GL, Abidov A, Achenbach S, et al. SCCT guidelines for the interpretation and reporting of coronary computed tomographic angiography. *J Cardiovasc Comput Tomogr* 2009;3(2):122–136.

Ramirez FD, Hibbert B, Simard T, et al. Natural history and management of aortocoronary saphenous vein graft aneurysms: a systematic review of published cases. *Circulation* 2012;126(18):2248–2256.

Renapurkar R, Desai MY, Curtin RJ. Intracavitary course of the right coronary artery: an increasingly recognized anomaly by coronary computed tomography angiography. *J Thorac Imaging* 2010;25(3):W77–W78.

Ropers D, Pohle FK, Kuettner A, et al. Diagnostic accuracy of noninvasive coronary angiography in patients after bypass surgery using 64-slice spiral computed tomography with 330-ms gantry rotation. *Circulation* 2006;114(22):2334–2341; quiz 2334.

Rossi A, Merkus D, Klotz E, Mollet N, de Feyter PJ, Krestin GP. Stress myocardial perfusion: imaging with multidetector CT. *Radiology* 2014;270(1):25–46.

Said SA, van der Werf T. Dutch survey of coronary artery fistulas in adults: congenital solitary fistulas. *Int J Cardiol* 2006;106(3):323–332.

Sakuma H. Coronary CT versus MR angiography: the role of MR angiography. *Radiology* 2011;258(2):340–349.

Salavati A, Radmanesh F, Heidari K, Dwamena BA, Kelly AM, Cronin P. Dual-source computed tomography angiography for diagnosis and assessment of coronary artery disease: systematic review and meta-analysis. *J Cardiovasc Comput Tomogr* 2012;6(2):78–90.

Saremi F, Goodman G, Wilcox A, Salibian R, Vorobiof G. Coronary artery ostial atresia: diagnosis of conotruncal anastomotic collateral rings using CT angiography. *JACC Cardiovasc Imaging* 2011;4(12):1320–1323.

Sari I, Kizilkan N, Sucu M, et al. Double right coronary artery: report of two cases and review of the literature. *Int J Cardiol* 2008;130(2):e74–e77.

Sarwar A, Shaw LJ, Shapiro MD, et al. Diagnostic and prognostic value of absence of coronary artery calcification. *JACC Cardiovasc Imaging* 2009;2(6):675–688.

Saw J, Aymong E, Sedlak T, et al. Spontaneous coronary artery dissection: association with predisposing arteriopathies and precipitating stressors and cardiovascular outcomes. *Circ Cardiovasc Interv* 2014;7(5):645–655.

Serruys PW, de Jaegere P, Kiemeneij F, et al. A comparison of balloon-expandable-stent implantation with balloon angioplasty in patients with coronary artery disease. Benestent Study Group. *N Engl J Med* 1994;331(8):489–495.

Shah DJ, Kim HW, James O, et al. Prevalence of regional myocardial thinning and relationship with myocardial scarring in patients with coronary artery disease. *JAMA* 2013;309(9):909–918.

Shen WF, Tribouilloy C, Mirode A, Dufosse H, Lesbre JP. Left ventricular aneurysm and prognosis in patients with first acute transmural anterior myocardial infarction and isolated left anterior descending artery disease. *Eur Heart J* 1992;13(1):39–44.

Stone GW, Moses JW, Ellis SG, et al. Safety and efficacy of sirolimus- and paclitaxel-eluting coronary stents. *N Engl J Med* 2007;356(10):998–1008.

Syed M, Lesch M. Coronary artery aneurysm: a review. *Prog Cardiovasc Dis* 1997;40(1):77–84.

Taylor AJ, Cerqueira M, Hodgson JM, et al. ACCF/SCCT/ACR/AHA/ASE/ASNC/NASCI/SCAI/SCMR 2010 appropriate use criteria for cardiac computed tomography. A Report of the American College of Cardiology Foundation Appropriate Use Criteria Task Force, the Society of Cardiovascular Computed Tomography, the American College of Radiology, the American Heart Association, the American Society of Echocardiography, the American Society of Nuclear Cardiology, the North American Society for Cardiovascular Imaging, the Society for Cardiovascular Angiography and Interventions, and the Society for Cardiovascular Magnetic Resonance. *Circulation* 2010;122(21):e525–e555.

Tesche C, De Cecco CN, Albrecht MH, et al. Coronary CT angiography-derived fractional flow reserve. *Radiology* 2017;285(1):17–33.

Topaz O, DiSciascio G, Cowley MJ, et al. Absent left main coronary artery: angiographic findings in 83 patients with separate ostia of the left anterior descending and circumflex arteries at the left aortic sinus. *Am Heart J* 1991;122(2):447–452.

Tunick PA, Slater J, Kronzon I, Glassman E. Discrete atherosclerotic coronary artery aneurysms: a study of 20 patients. *J Am Coll Cardiol* 1990;15(2):279–282.

Varga-Szemes A, Meinel FG, De Cecco CN, Fuller SR, Bayer RR, 2nd, Schoepf UJ. CT myocardial perfusion imaging. *AJR Am J Roentgenol* 2015;204(3):487–497.

Veltman CE, de Graaf FR, Schuijf JD, et al. Prognostic value of coronary vessel dominance in relation to significant coronary artery disease determined

with non-invasive computed tomography coronary angiography. *Eur Heart J* 2012;33(11):1367–1377.
Virmani R, Burke AP, Farb A. Plaque rupture and plaque erosion. *Thromb Haemost* 1999;82 Suppl 1:1–3.
Virmani R, Burke AP, Farb A, Kolodgie FD. Pathology of the vulnerable plaque. *J Am Coll Cardiol* 2006;47(8 Suppl):C13–C18.
Virmani R, Burke AP, Kolodgie FD, Farb A. Vulnerable plaque: the pathology of unstable coronary lesions. *J Interv Cardiol* 2002;15(6):439–446.
Virmani R, Burke AP, Kolodgie FD, Farb A. Pathology of the thin-cap fibroatheroma: a type of vulnerable plaque. *J Interv Cardiol* 2003;16(3):267–272.
Vliegenthart R, Henzler T, Moscariello A, et al. CT of coronary heart disease: part 1, CT of myocardial infarction, ischemia, and viability. *AJR Am J Roentgenol* 2012;198(3):531–547.
Warnes CA, Williams RG, Bashore TM, et al. ACC/AHA 2008 guidelines for the management of adults with congenital heart disease: a report of the American College of Cardiology/American Heart Association Task Force on Practice Guidelines (writing committee to develop guidelines on the management of adults with congenital heart disease). *Circulation* 2008;118(23):e714–e833.
Weustink AC, Nieman K, Pugliese F, et al. Diagnostic accuracy of computed tomography angiography in patients after bypass grafting: comparison with invasive coronary angiography. *JACC Cardiovasc Imaging* 2009;2(7):816–824.
Yamagishi M, Terashima M, Awano K, et al. Morphology of vulnerable coronary plaque: insights from follow-up of patients examined by intravascular ultrasound before an acute coronary syndrome. *J Am Coll Cardiol* 2000; 35(1):106–111.
Yamamoto H, Kitagawa T, Ohashi N, et al. Noncalcified atherosclerotic lesions with vulnerable characteristics detected by coronary CT angiography and future coronary events. *J Cardiovasc Comput Tomogr* 2013;7(3): 192–199.
Yamanaka O, Hobbs RE. Coronary artery anomalies in 126,595 patients undergoing coronary arteriography. *Cathet Cardiovasc Diagn* 1990;21(1):28–40.
Yau JM, Singh R, Halpern EJ, Fischman D. Anomalous origin of the left coronary artery from the pulmonary artery in adults: a comprehensive review of 151 adult cases and a new diagnosis in a 53-year-old woman. *Clin Cardiol* 2011;34(4):204–210.
Yoshida S, Sakuma K, Ueda O. Acute mitral regurgitation due to total rupture in the anterior papillary muscle after acute myocardial infarction successfully treated by emergency surgery. *Jpn J Thorac Cardiovasc Surg* 2003;51(5):208–210.
Zarins CK, Taylor CA, Min JK. Computed fractional flow reserve (FFTCT) derived from coronary CT angiography. *J Cardiovasc Transl Res* 2013;6(5): 708–714.
Zeina AR, Odeh M, Blinder J, Rosenschein U, Barmeir E. Myocardial bridge: evaluation on MDCT. *AJR Am J Roentgenol* 2007;188(4):1069–1073.
Zenooz NA, Habibi R, Mammen L, Finn JP, Gilkeson RC. Coronary artery fistulas: CT findings. *Radiographics* 2009;29(3):781–789.